

THE ROLE OF HEAVY MINERALS IN THE THERMAL MATURATION OF THE
WOODFORD SHALE, ANADARKO BASIN, OKLAHOMA

by

KACEE CODDINGTON

B.S., Kansas State University, 2012

A THESIS

submitted in partial fulfillment of the requirements for the degree

MASTER OF SCIENCE

Department of Geology
College of Arts and Sciences

KANSAS STATE UNIVERSITY
Manhattan, Kansas

2013

Approved by:

Major Professor
Dr. Matthew W. Totten

Copyright

KACEE CODDINGTON

2013

Abstract

Shales are generally regarded as organic rich source and seal rocks that are unworthy of the amount of research that has been given to their coarser-grained counterparts, even though shales comprise nearly two-thirds of Earth's sedimentary record (Potter et al., 1980). The Woodford Shale is acknowledged as a prolific source rock across much of Oklahoma and the midcontinent (Lambert, 1990). Up to 8% world's original hydrocarbon reserves are estimated to have been sourced by the Woodford and its equivalents (Fritz et al., 1991).

Study of the heavy-mineral fraction in sedimentary rocks is important because it can indicate provenance and some of the diagenetic changes that occur in sedimentary rocks. This goal of this study is to describe the heavy-mineral fraction of eight Woodford Shale samples from the Greater Anadarko Basin of Oklahoma, and determine whether or not the constituents that make up the heavy-mineral fraction have any impact on the process of thermal maturity within source rocks. This study utilizes a method designed to efficiently separate the heavy-mineral fraction of shale samples. Scanning electron microscope (SEM) and Energy Dispersive X-ray Spectroscopy (EDS) are used in this study to identify mineralogy, grain size, composition and shape. Mineral distributions in the samples have been determined from point counting.

The weight percent of the heavy mineral fraction was calculated for each of the samples. This was then compared to their location within the basin, depth, vitrinite reflectance and total organic carbon (TOC). We found that as the thermal maturity increase, the weight percent of heavy minerals also increases. Pyrite (FeS_2) was the most abundant heavy mineral found in the Woodford samples used in this study. From analyzing the different forms of pyrite, it was found that as thermal maturity increases, framboidal pyrite alters to euhedral pyrite.

Table of Contents

List of Figures	vi
List of Tables	viii
Acknowledgements.....	ix
Dedication	x
Chapter 1 - Introduction.....	1
Significance	2
Study Area	3
Regional Geology	5
Tectonic History of the Southern Oklahoma Aulacogen	8
The Woodford Shale.....	9
Previous Work	12
Chapter 2 - Heavy Minerals in Shales	15
Chapter 3 - Methods.....	16
Materials	17
Sample Preparation	18
Procedure	19
Heavy Mineral Separation	19
Mineral Identification and Size Analysis.....	20
Chapter 4 - Results.....	20
EDS Spectra.....	22
WF#6 (Cement Ord)	22
WF#8 (Curtis)	27
WF#10 (Hannah)	31
Point-Counting Results.....	35
Chapter 5 - Discussion	41
Other Heavy Mineral Studies	41
Pyrite in the Heavy Mineral Fraction of the Woodford Shale	43
The Sulfur Cycle.....	50

Heavy minerals as an Indicator of Thermal Maturity	52
Chapter 6 - Conclusions.....	55
References.....	56
Appendix A - Photomicrographs and EDS Spectra	61
Appendix B - Heavy Mineral Distribution	82

List of Figures

Figure 1. U.S. Shale gas plays of the lower 48 states from EIA, 2011.....	2
Figure 2. South-north cross section A-A' through the Anadarko Basin (Sorenson, 2005).	4
Figure 3. Distribution of Devonian Black Shales in the USA (The Anadarko Basin is indicated by a red box), modified from Comer, 2008.	5
Figure 4. Map of the North American southern mid-continent during the early to middle Paleozoic showing the Oklahoma basin (green) and Ouachita trough (blue) depositional provinces as well as the southern Oklahoma Aulacogen (yellow) tectonic province. Modified from Johnson et al., 1989.	6
Figure 5. Map of Oklahoma showing the present day tectonic and depositional provinces (Northcutt and Campbell, 1995).	8
Figure 6. Woodford Shale thickness map of Oklahoma and Western Arkansas. From Comer, 2008b; in Miceli, 2010.	10
Figure 7. Woodford Shale organic maturity map of Oklahoma based on vitrinite reflectance (%R _o) data. Modified from Comer, 1992 and Comer, 2008a.	12
Figure 8. Generalized stratigraphic column for the Anadarko Basin, south-central Oklahoma (http://aapgbull.geoscienceworld.org/content/96/3/493/F1.expansion.html).	14
Figure 9. Location of Woodford Shale Samples are indicated by black dots.	16
Figure 11. Photomicrograph showing the heavy minerals in WF#6 (Cement Ord). Pyrite framboids are clearly visible throughout this sample and appear as raspberry-like spheres.	22
Figure 12. Heavy minerals in sample WF#6 Cement Ord. In this photomicrograph a few euhedral pyrite grains are present, along with scheelite crystals that are less than 1 μm in size. A grain of Fe-mica is visible in the center of the right side.	23
Figure 13. Locations for the EDS spectra shown in Figure 14. Spectrum 1 is located on a framboid, spectrum 2 is located on fine-grained Fe-Mica, Spectrum 3 is located on a grain of scheelite, and Spectrum 4 is located on cubic pyrite.	24
Figure 14. EDS spectra for WF#6 Cement Ord sample locations.	25
Figure 15. Elemental, weight percent and atomic percent data for WF#6 Cement Ord.	26
Figure 16. Heavy minerals in sample WF#8 Curtis. BSE image shows W-bearing mineral artifacts as bright grains (arrow).	27

Figure 17. Heavy minerals in sample WF#8 Curtis. W-bearing mineral artifacts are euhedral, bright grains.	28
Figure 18. Locations for the EDS spectra shown in figure 19.	29
Figure 19. Elemental, weight percent and atomic percent data for WF#8 Curtis.	29
Figure 20. Elemental, weight percent and atomic percent data for WF#8 Curtis.	30
Figure 21. Heavy minerals in sample WF#10 Hannah. This sample is very pyrite rich and has many different forms of pyrite present to include: octahedral pyrite, pyritohedrons, cubic pyrite, framboidal pyrite, as well as euhedral grains of Ankerite.	31
Figure 22. Heavy minerals in sample WF#10 Hannah. In this zoomed in view of WF#10 we can see octahedral and cubic pyrite, a few framboids, some euhedral pyrite and a piece of Ankerite.	32
Figure 23. Locations for the EDS spectra shown in figure 24.	33
Figure 24. Elemental, weight percent and atomic percent data for WF#10 Hannah.	33
Figure 25. Elemental, weight percent and atomic percent data for WF#10 Hannah.	34
Figure 26. Mineral abundances in sample WF#7 (Amerada-Chenoweth).	38
Figure 27. Example of Fe-Mica found in Woodford Shale Samples (WF#3 Lela Rahm).	39
Figure 28. An example of the Ankerite found in the Woodford Shale samples (WF#10 Hannah).	40
Figure 29. An example of the fossil fragments found in the Woodford Shale samples (WF#3 Lela Rahm).	41
Figure 30. Average distribution of heavy minerals within the Average Stanley Shale (black) and the average Cenozoic Gulf of Mexico Shale (gray) From Totten and Hannan 1998.	42
Figure 31. Heavy mineral distribution in the average Woodford Shale.	43
Figure 32. Pyrite distributions for four Woodford samples are shown in the smaller of the two pie charts.	44

List of Tables

Table 1. Properties of LMT.	18
Table 2. Masses of disaggregated mudrock samples, centrifuge tube, and sample and LMT.....	19
Table 3. Percentage of heavy minerals in the Woodford Shale samples.	21
Table 4. Depth, vitrinite reflectance values and Toc data for the Woodford Shale samples.....	21
Table 5. Point-counting results for WF#1 McCalla Ranch.....	35
Table 6. Point-counting results for WF#3 Lela Rahm.....	35
Table 7. Point-counting results for WF#5 Dwyer.....	36
Table 8. Point-counting results for WF#6 Cement Ord.....	36
Table 9. Point-counting results for WF#7 Chenoweth.	36
Table 10. Point-counting results for WF#8 Curtis.....	37
Table 11. Point counting results for WF#9 Jones and Pellow.	37
Table 12. Point-counting results for WF#10 Hannah.	37
Table 13. TOC values for the Woodford Shale samples.	54

Acknowledgements

I would like to thank Dr. Matt Totten for taking me on as a graduate student and for always being available to talk about my thesis. I would also like to thank Dr. Sambhudas Chaudhuri and Dr. George Clark for being on my committee. I would like to thank Dr. Lambert for sharing his knowledge of the Woodford with me. I need to thank my brother, Dustin Coddington, and my best friend, Samantha Ramirez, for helping me get through grad school. I couldn't have done this without you two. To my mother, thank you for always believing in me, I miss you so much. Lastly, I need to thank all the faculty and graduate students at K-State.

Dedication

I dedicate this work to my beautiful little Zoe-Bee and my mother Marilyn Baldwin. I love you both so much.

Chapter 1 - Introduction

Historically, shales have been regarded almost exclusively as organic-rich source and seal mudstones that were less interesting than coarser-grained sedimentary rocks received (Potter et al. 1980). The utilization of modern hydraulic fracture and horizontal drilling techniques, has expanded interest in shales with active research focusing on characterizing these highly variable and complex fine-grained rocks (Totten, 2011).

Shales comprise nearly two-thirds of Earth's sedimentary record (Potter et al. 1980). This means that there is an enormous economic potential for unconventional gas discoveries. Industry activity in the continental United States reflects this trend of increased economic potential: in 2010 there was 4.87 Tcf of shale gas production (23% of the total U.S. natural gas production), while in 2000 there was just 0.39 Tcf (EIA, 2011). After the success of the Barnett Shale (Mississippian) gas wells in Texas, Kuuskaraa (2011) recognized the Woodford Shale as one of the "Magnificent Seven" gas shale plays in North America. The Barnett, Fayetteville, Haynesville, Marcellus, Horn River and Monterey Shales (Figure 1) make up the rest of the Magnificent Seven. The Woodford Shale is acknowledged as a prolific source rock across much of Oklahoma and the midcontinent (Lambert, 1990). Up to 8% world's original hydrocarbon reserves are estimated to have been sourced by the Woodford and its equivalents (Fritz et al, 1991). In the Oklahoma Woodford Shale gas plays, the application of advanced completion technologies resulted in an increase in wells from an average of only two completions per year between 1934 to 2003, to 501 horizontal completions for the year 2009 (Cardott, 2009).

This goal of this study is to describe the heavy-mineral fraction of the Woodford Shale in the Anadarko Basin of Oklahoma. This study utilizes a method designed to efficiently separate the heavy-mineral fraction of shale samples. The heavy-mineral separation is then used to make

grain mounts that are analyzed by scanning electron microscopy in order to identify the heavy-mineralogy of the Woodford samples.

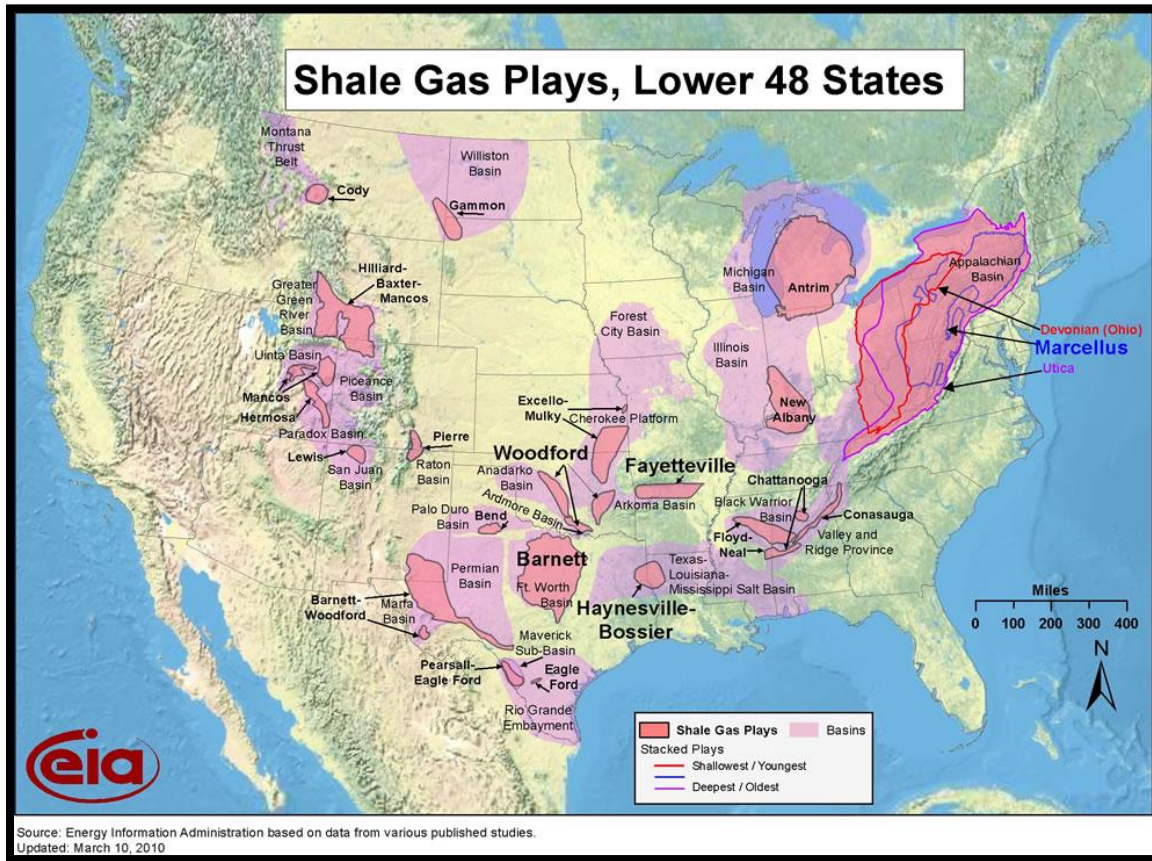


Figure 1. U.S. Shale gas plays of the lower 48 states from EIA, 2011.

Significance

The significance of this work lies in the fact that the analyses of heavy minerals within mudrocks has largely been ignored. In 1908 Sorby stated: “Possibly many may think that the deposition and consolidation of fine-grained mud must be a very simple matter, and the results of little interest. However, when carefully studied... it is soon found to be dependent on so many variable conditions, that one might feel inclined to abandon the inquiry, were it not that so much of the history of our rocks appear to be written in this language.” Goldschmidt predicted that the

immobile trace-element geochemistry of mudrocks would reflect the evolution of the upper continental crust (1933). Analyzing the heavy minerals within the Woodford has the potential to help us better understand the diagenetic changes that the Woodford underwent after deposition, and how these events might affect the generation of hydrocarbons.

Study Area

The study area lies within the Anadarko Basin of Oklahoma. The Anadarko Basin is important in terms of both oil and gas production. The Anadarko Basin is bordered on the south by the Amarillo-Wichita uplift and the Marietta Basin. On the southeast it is bounded by the Ardmore Basin and the Arbuckle uplift, on the east by the Nemaha ridge and on the north and west by the northern shelf areas. The Anadarko Basin is part of a much larger geologic province called the southern Oklahoma aulacogen (Hoffman et al 1974). The basin is a northwest-southeast trending sedimentary structural basin that is axially asymmetric and of Paleozoic age in western Oklahoma and the Texas Panhandle (Cardott and Lambert, 1982). A cross section of the Anadarko Basin is shown in Figure 2 and the location of the Anadarko Basin, the Woodford shale and the other major black shales are shown in Figure 3.

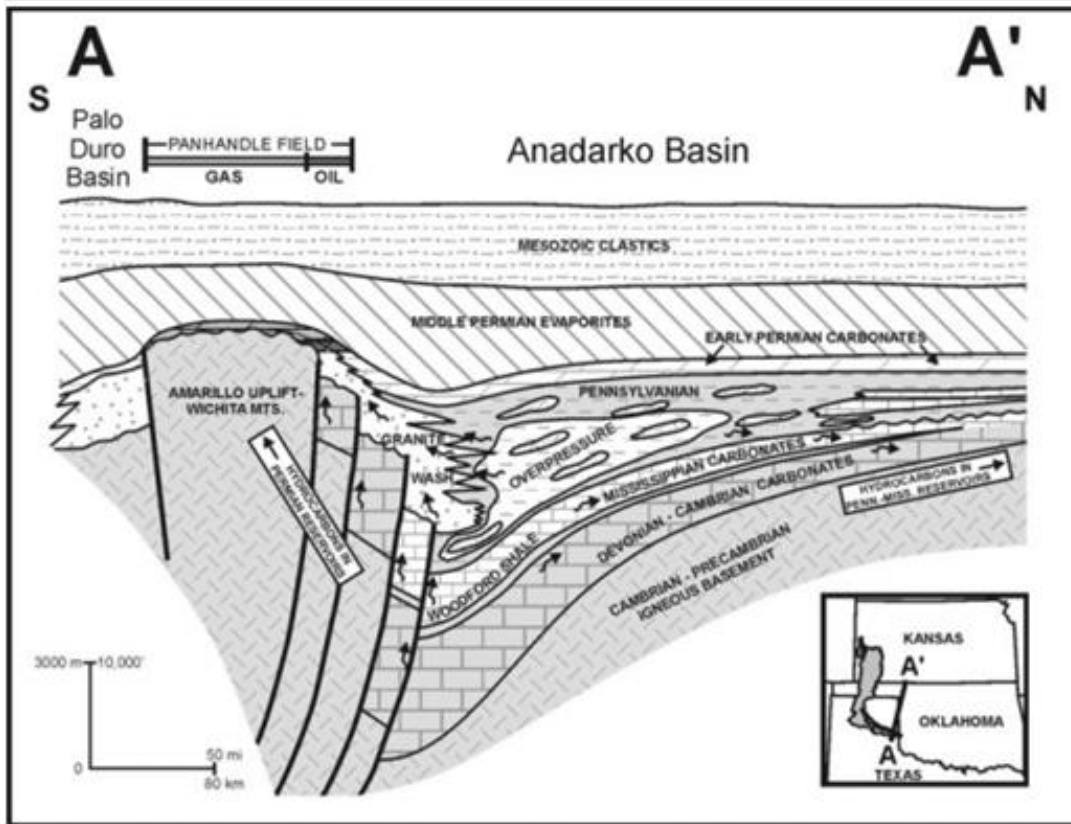


Figure 2. South-north cross section A-A' through the Anadarko Basin (Sorenson, 2005).

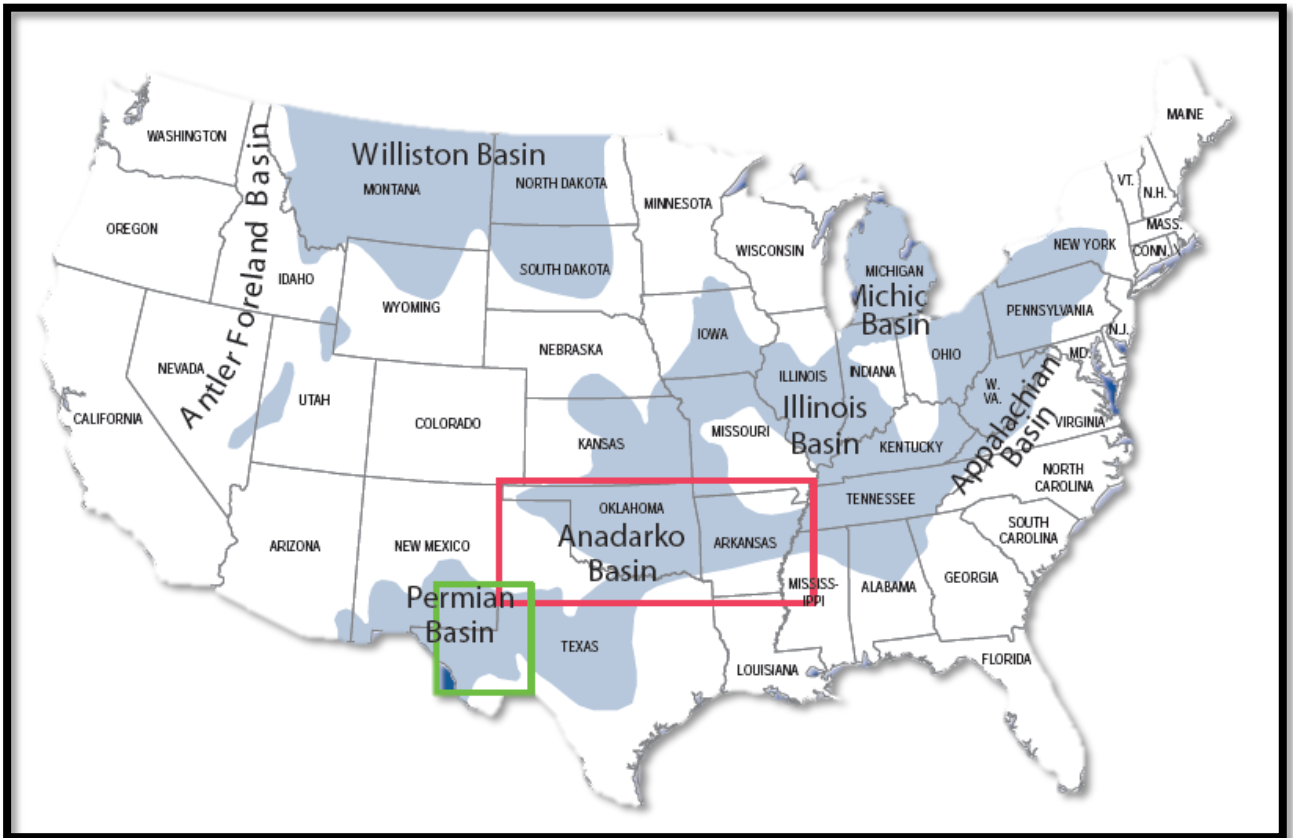


Figure 3. Distribution of Devonian Black Shales in the USA, modified from Comer, 2008.

Regional Geology

The major early Paleozoic tectonic and depositional provinces of Oklahoma include: 1) the Oklahoma Basin, 2) the Southern Oklahoma Aulacogen, and 3) the Ouachita trough (Figure 4). The Oklahoma Basin is an expansive thick shallow marine carbonate shelf that is interbedded with marine sandstones that cover majority of Oklahoma and extend into northwest Arkansas, southeast Nebraska, southern Kansas and north to northwest Texas (Johnson et al., 1989; Johnson and Cardott, 1992; Northcutt et. al., 2005).

Deposition of the Hunton Group, a shallow marine limestone, occurred during the Silurian through Early Devonian (Johnson and Cardott, 1992). This Hunton Group ranges from a clean-washed fossiliferous limestone at its base, to argillaceous and silty carbonates in the middle section, then back to clean-washed limestone at the top (Johnson and Cardott, 1992). Significant epirogenic uplift and erosion occurred after the deposition of the Hunton, which

resulted in what is now known as the pre-Late Devonian (pre-Woodford-Chattanooga) unconformity (Johnson et al., 1989).

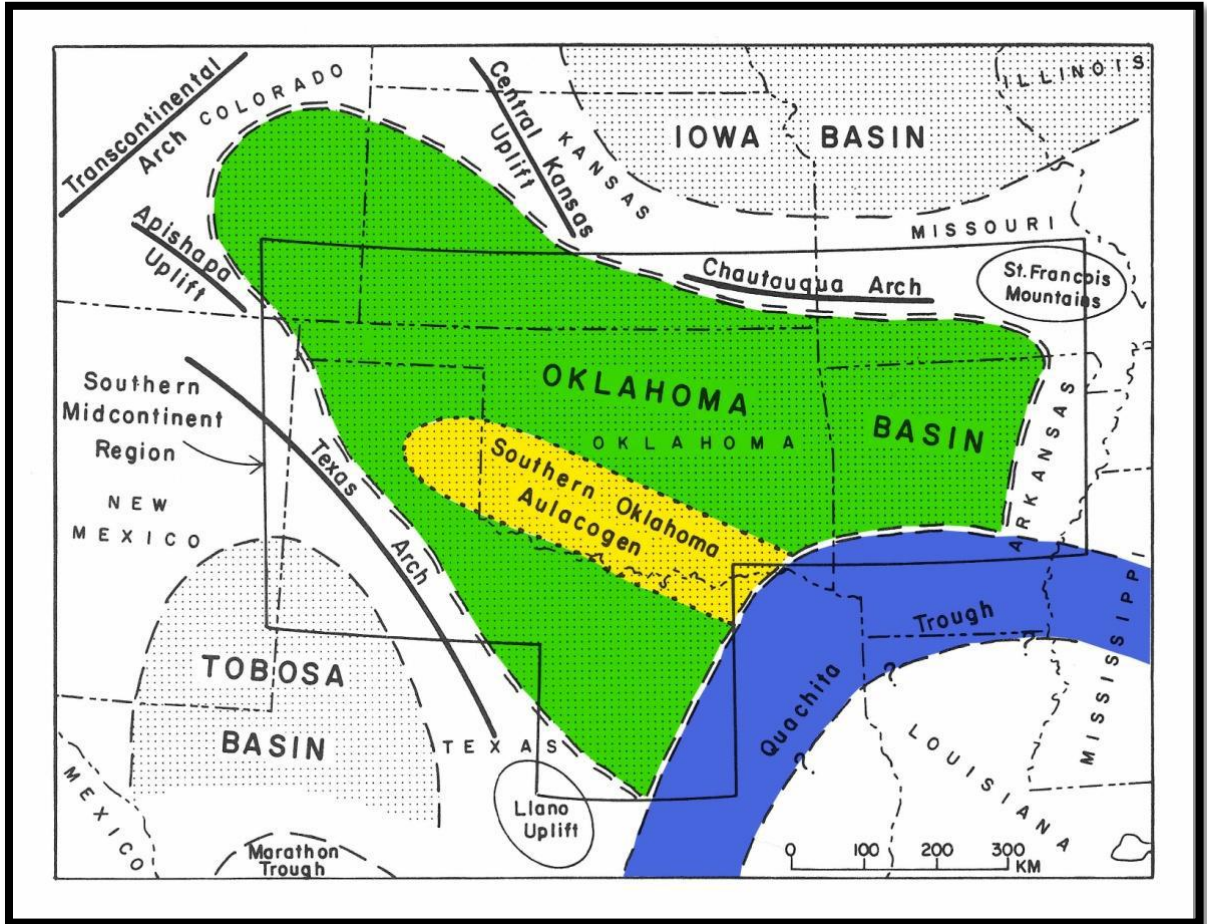


Figure 4. Map of the North American southern mid-continent during the early to middle Paleozoic showing the Oklahoma basin (green) and Ouachita trough (blue) depositional provinces as well as the southern Oklahoma Aulacogen (yellow) tectonic province. Modified from Johnson et al., 1989.

The late Middle Devonian to early Late Devonian saw the transgression of a euxinic ocean from the south–southeast (Kirkland et al., 1992). This resulted in the deposition of dark-gray or black, fine-silt to clay-sized organic rich sediments that comprise the Woodford Shale

(Johnson et al., 1989). Much of the exposed Hunton Group debris and sands were incorporated within initial Woodford deposition into thin basal conglomerate or sandstone units that are referred to as the Misener-Sycamore Sandstones (Johnson et al., 1989). Deposition of the Woodford continued until the early Mississippian, when a warm and shallow oxygenated ocean prevailed, supporting a variety of different benthic organisms that resulted in a conformable limestone layer above the Woodford (Johnson and Cardott, 1992).

In the late Mississippian to early Pennsylvanian, Oklahoma experienced further epeirogenic uplift and erosion, followed by periods of orogenesis due to the collision of Laurentia and Gondwana during the early, middle and late Pennsylvanian (Johnson and Cardott, 1992). This produced the present day depositional and tectonic provinces which include: (1) The Ouachita foldbelt, (2) the Wichita Criner, Arbuckle, Nemaha, and Ozark uplifts, and (3) the Anadarko, Hollis, Marietta, Ardmore and Arkoma basins (Johnson et al., 1989). The present day geologic provinces of Oklahoma are shown in Figure 5.

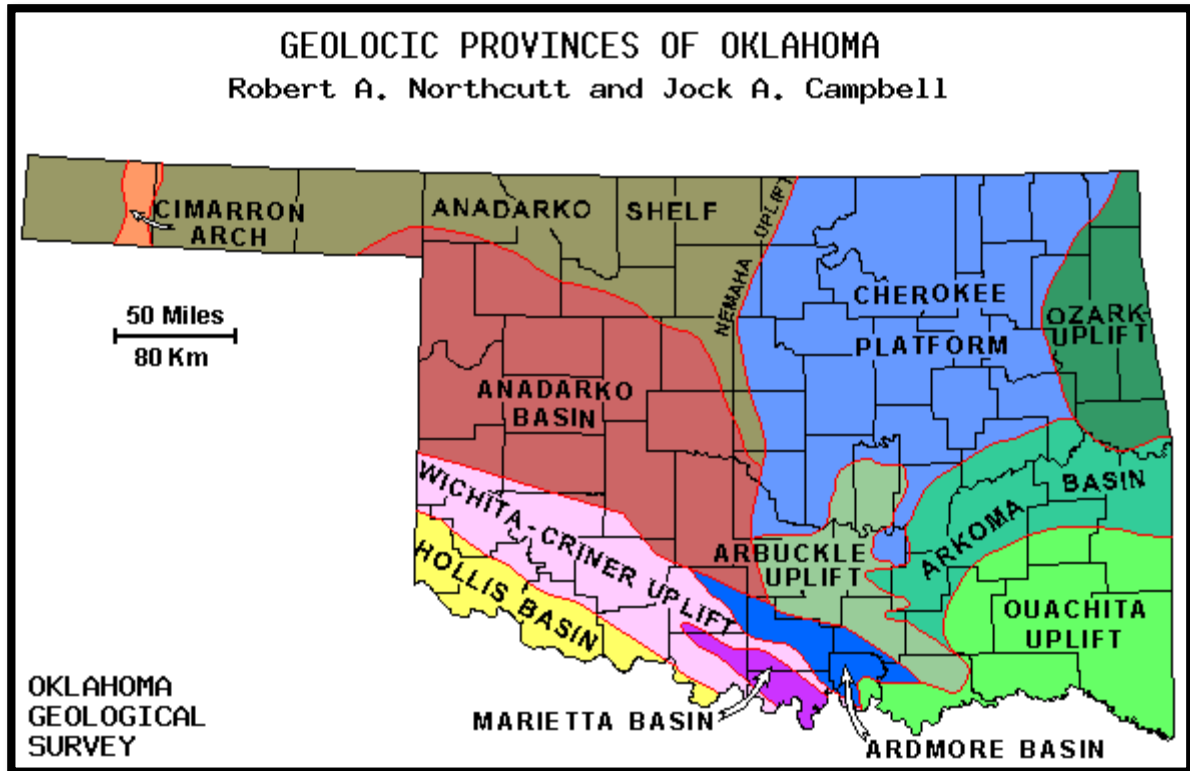


Figure 5. Map of Oklahoma showing the present day tectonic and depositional provinces (Northcutt and Campbell, 1995).

Tectonic History of the Southern Oklahoma Aulacogen

An aulacogen is a thick sedimentary sequence that extends at high angles from an orogenic belt. They are considered favorable locations for oil and gas accumulations (Walper, 1976; Webster, 1977, and Robert, 1980). Crustal extension occurred in the Cambrian in the southern Oklahoma aulacogen, most likely as a failed rift arm of the opening Iapetus ocean (Burke, 1973; Keller et al, 1983). This emplaced igneous rocks in the deepest part of the present day Anadarko Basin. By the middle Cambrian, igneous activity ceased. The Wichita fault zone was active during the early stages of rifting (Ham et al. 1964) but inactive during the stable-shelf carbonate phase in the early Paleozoic (Amsden 1975, 1983).

There were several phases of subsidence, beginning in the late Cambrian and continuing into the early Mississippian. In 1984, Garner and Turcotte proposed crustal and lithospheric thinning as a model to explain accelerated isostatic subsidence during the late Mississippian. This implies that the upper crustal extension and faulting were accompanied by a rise in heat flow during the late Mississippian.

During the Wichita Orogeny (early Pennsylvanian) the region saw intense crustal shortening. This shortening was most likely associated with the late Paleozoic collision involving the Ouachita orogenic belt, raised vertical blocks in the Amarillo-Wichita uplift and reactivated zones of weakness associated with the initial graben stage (Ham et al, 1964; Walper, 1977; Brewer et al, 1983; Keller et al, 1983). Reverse faults produced in the frontal Wichita fault zone and the adjacent deep Anadarko Basin typically had throws of more than 30,000 feet. Deep-water sediments accumulated in the Ouachita through due to earlier rifting of the North American Craton (Johnson and Cardott, 1992; Northcutt et al., 2001). The present day basins in Oklahoma formed due to down-warping and were thus differentiated from earlier Paleozoic basins in Oklahoma (Johnson and Cardott, 1992).

The Woodford Shale

The Woodford Shale is a late Devonian to early Mississippian organic-rich black shale that was deposited over Oklahoma, southern Kansas, and western Arkansas (Johnson et al., 1989). It has a thickness that ranges from 200 to 900 ft in the Southern Oklahoma Aulacogen, and from 50 to 100 ft on the shallower shelf areas in northern Oklahoma (Johnson and Cardott, 1992). Time-stratigraphic equivalents of the Woodford include the New Albany, Chattanooga, Ohio, Millboro, Burket, Geneseo, and Antrim shales, as well as the Arkansas Novaculite (Conant

and Swanson, 1961; Ham and Wilson, 1967, p. 362). Figure 6 shows the thinning trend of the Woodford from the southern Oklahoma Aulacogen onto the Cherokee Platform.

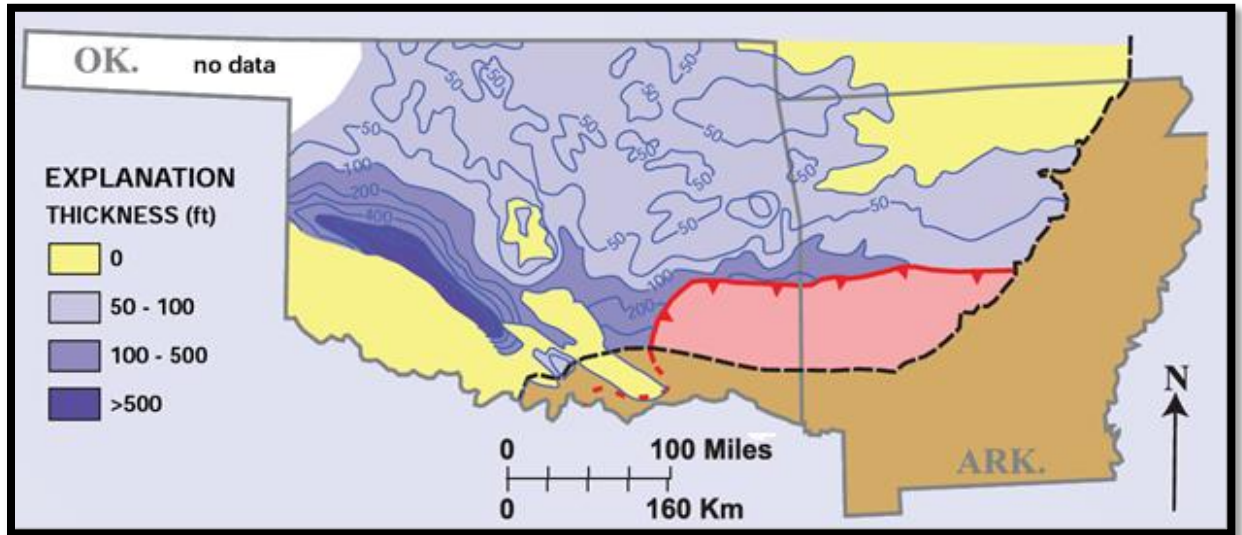


Figure 6. Woodford Shale thickness map of Oklahoma and Western Arkansas. From Comer, 2008b; in Miceli, 2010.

The Woodford is informally subdivided into three members (Lower, Middle and Upper) based on composition, log signatures, geomechanical response, and geochemistry (Cardot, 2007; Portas, 2009; Miceli, 2010; Slatt et al., 2010). Chert, siltstones, sandstone, dolostone and light-colored shale are common lithological variations (Comer, 2005). Examination of phosphate nodules, pyrite concretions and calcite concretions throughout various stratigraphic intervals of the Woodford have documented the presence of conodonts, planktonic remains, and lenses of silica. Ammonoid and crustacean fossil remains are restricted to the upper one-seventh of the Woodford (Kirkland et al., 1992).

After the deposition of the Hunton Group, significant epeirogenic uplift and erosion occurred. The Woodford was deposited unconformably above the carbonates of the Hunton Group. The calm, anoxic and highly saline waters of the Woodford- Chattanooga Sea allowed

for the deposition and preservation of organic particles without dilution from excessive clastic deposition (Kirkland et al., 1992; Comer, 2005). The Woodford shale kerogen is predominately type II (marine origin) with TOC values ranging from 1 to 17% (Kirkland et al., 1992; Miceli, 2010). An important division of the Lower, Middle, and Upper Woodford is the variation in TOC content. The Middle Woodford has the highest TOC values, and the Upper Woodford has the lowest (Kirkland et al., 1992; Miceli, 2010; Slatt et al., 2010). Figure 6 shows a generalized stratigraphic column of the Anadarko Basin.

Vitrinite reflectance data shows that the Woodford Shale in Oklahoma ranges from low oil generation values ($<0.5\% R_o$) along the Nemaha uplift and throughout central Oklahoma, to high, dry gas generation values ($>2.0\% R_o$) in the deeper portions of the Anadarko basins (Comer and Hinch, 1987; Comer, 2008a). This data is supported by Miceli (2010) who obtained vitrinite reflectance values from core and cutting samples throughout south central Oklahoma. Figure 7 shows a map of organic maturity in the Woodford Shale throughout Oklahoma.

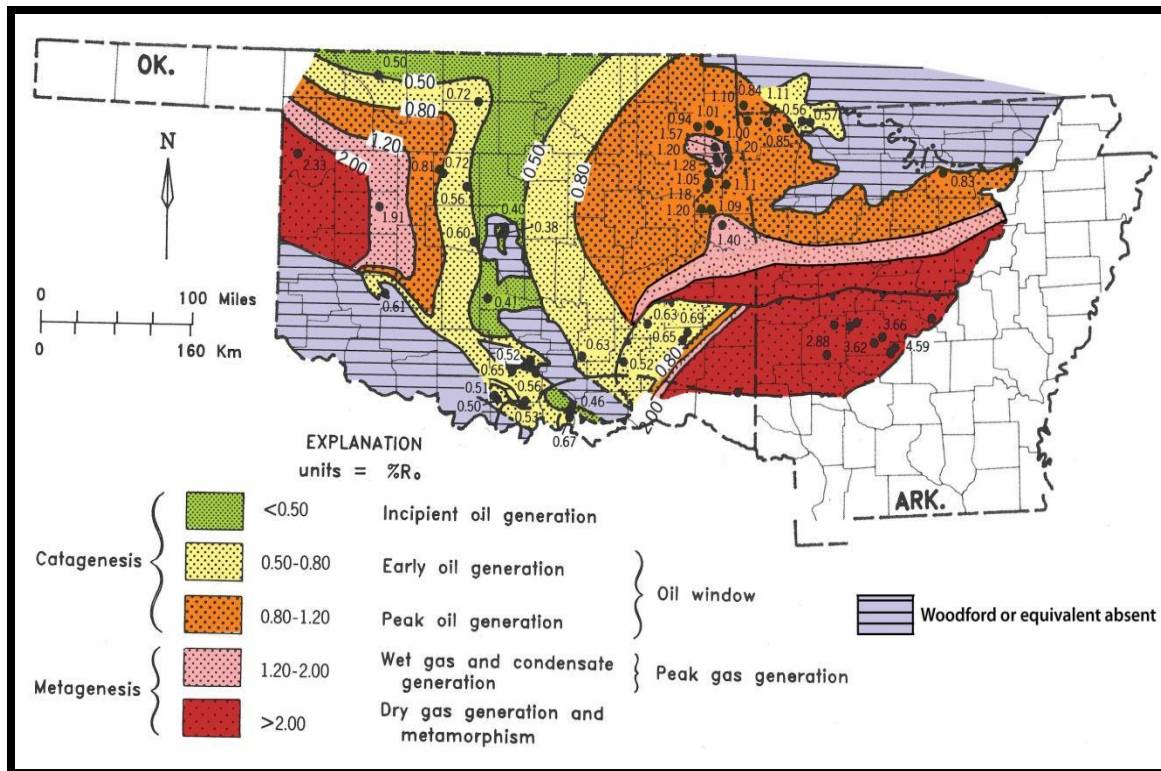


Figure 7. Woodford Shale organic maturity map of Oklahoma based on vitrinite reflectance (%R₀) data. Modified from Comer, 1992 and Comer, 2008a.

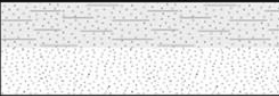
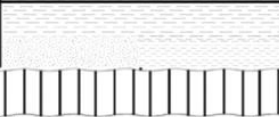
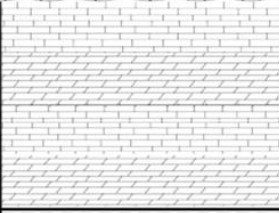
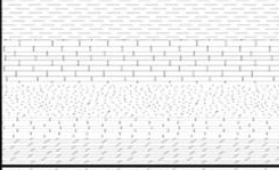
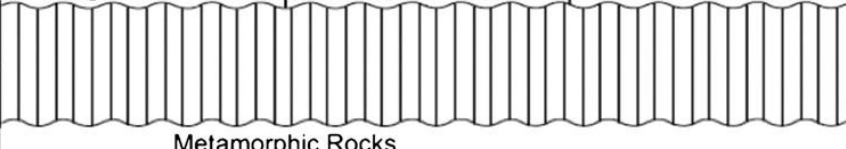
The Woodford Shale in the Anadarko Basin typically yields gamma-ray response of more than 160 API units (Amsden, 1975; Sullivan, 1985). The high gamma-ray response is due to the high organic content of the formation, which has an affinity for uranyl ions (Kirkland et al, 1992; Lambert, 1993). The Woodford is characterized by high gamma ray, high resistivity, and low density readings (Kirkland et al., 1992). A generalized stratigraphic column of the Woodford Shale is shown in Figure 8.

Previous Work

Daniel Ramirez-Caro (2013) analyzed the REE patterns and total concentrations of the organic matter of the Woodford shale. Separation of the organic matter from the Woodford shale was used as an approach to study how diagenesis affects geochemistry of this shale. Ramirez-Caro analyzed both the organic matter fraction and the silicate-carbonate fraction of ten samples

of the Woodford Shale from north-central Oklahoma. He found that the REE concentrations in the organic matter of the Woodford Shale samples ranged from 300 to 800 ppm. These concentrations of the REEs in the Woodford Shale are higher than the average shale, as well as concentrations in modern-day plants. These differences reflect the transformation of buried Woodford Shale organic materials in post-depositional environmental conditions with potential contributions of exchanges of REE coming from associated sediments. Ramirez-Caro normalized the distribution patterns of REEs in the organic materials to the PAAS (post-Archean Australian Shale), and noticed the following significant features: (1) all but two out of the ten samples had a La-Lu trend with HREE enrichment in general, (2) all but two samples showed Ho and Tm positive enrichments, (3) only one sample had positive Eu anomalies, (4) three samples had Ce negative anomalies, although one had a positive Ce anomaly, (5) all but three out of ten had MREE enrichment by varied degrees. Therefore, a reasonable suggestion about the history of the REEs in the organic materials would be that both source and burial transformation effects of the deposited organic materials in association with the inorganic constituents had an influence on the general trend and the specific trends in the distribution patterns of the REEs.

When comparing the distribution patterns of the samples a very different pattern is observed for the organic portion of the Woodford shale in sample WF#10. This was the only sample that when plotted in H/C O/C diagram resulted to have kerogen type 1 from terrestrial origin. This was the only sample to show a positive cerium anomaly and no HREE enrichment among all the samples. REE Distribution patterns show fingerprinting properties when comparing patterns in samples from different provenance or source.

AGE		STRATIGRAPHIC UNIT		
SYSTEM	SERIES	ARKOMA BASIN		
		Formation	Lithology	Depositional Environment
PENNSYLVANIAN	DESMOINES	Boggy Formation ⋮ Hartshorne Sandstone		Fluvial-Deltaic
		Atoka Formation Spiro Sandstone		Channel and Bar
	MORROW	Wapanucka Limestone Game Refuge Sandstone		Shallow-Marine Channel and Bar
MISSISSIPPIAN		Springer Group Caney Shale		Deep Marine
DEVONIAN		Woodford Shale Misener Sandstone /		Deep Marine
SILURIAN		Hunton Group		Shallow Marine
ORDOVICIAN		Sylvan Shale Viola Limestone Simpson Group Arbuckle Group		Shallow Marine Shallow Marine
CAMBRIAN		Honey Creek Formation Reagen Sandstone		Shallow Marine
PRECAMBRIAN		 Metamorphic Rocks		

Vertical dots indicate that numerous stratigraphic unit names were omitted.

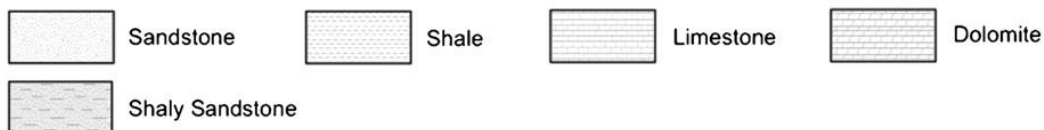


Figure 8. Generalized stratigraphic column for the Anadarko Basin, south-central Oklahoma (<http://aapgbull.geoscienceworld.org/content/96/3/493/F1.expansion.html>).

Chapter 2 - Heavy Minerals in Shales

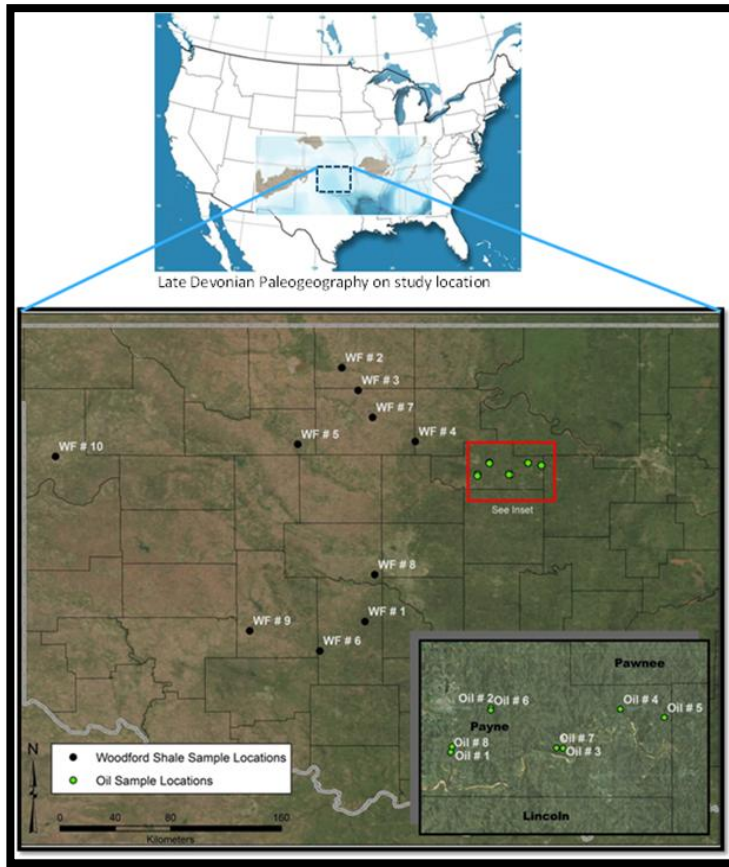
Heavy minerals are minerals with a specific gravity greater than 2.9g/cm^3 . Most heavy mineral studies have been conducted in sandstones even though mudrocks (shales) comprise over 60% of the sedimentary column (Totten and Hanan, 1998). Petrologic studies of mudrocks have focused on the clay-mineral fractions, while the non-clay fraction has received very little attention. Previous studies have focused on the quartz and feldspar fraction of mudrocks (Blatt and Schultz, 1976; Charles and Blatt, 1978; and Blatt and Totten, 1981), and a study by Furlan et al., examined the detrital micas in mudrocks in order to understand trends in whole-rock K/Ar isotopic ratios.

Blatt and Sutherland (1969) proposed that heavy mineral analyses of fine-grained rocks had the potential to broaden our understanding of sedimentary systems. Heavy mineral studies in shales have been ignored for a few reasons: 1) conventional wisdom suggests that there should not be any heavy minerals large enough to separate and work with, or that they are so minor in abundance that they should be ignored and 2) it is very difficult to perform density separations in mudrocks due to their high clay content (Totten and Hanan 2007).

The heavy mineral fraction represents a minor percentage of most clastic sedimentary rocks, but contains the largest possible variation in mineralogy. There have been many studies that have focused on the potential utility of heavy minerals even though the mechanisms by which they were deposited are not fully understood (Totten and Hanan, 2007). The use of the accessory-mineral fraction of sandstones for provenance and tectonic discrimination has employed advanced techniques that could be applied to mudrocks (Totten and Hanan 1998). The low permeability of shales makes them suitable for the preservation of heavy minerals.

Chapter 3 - Methods

Samples for this study were collected during the fall of 2011 by Daniel Ramirez of Kansas State University. Figure 9 shows the location of the samples for both studies. Eight Woodford Shale samples were collected from the Greater Anadarko Basin, obtained from the OPIC (Oklahoma Petroleum Information Center) in the OGS (Oklahoma Geological Survey). The samples were selected from cores in good condition that had the highest organic matter present based on observation. An example of the core plugs from the chosen sections is shown



in Figure 9.

Figure 9. Location of Woodford Shale Samples are indicated by black dots (Ramirez, 2013).

Materials

Lithium metatungstate (LMT) was used to separate the heavy-mineral fraction of mudrocks. LMT has several advantages when applied to mudrock heavy-mineral separations: 1) Clay minerals will not settle with heavy minerals. The large LMT ions are less likely to be absorbed by clay minerals; therefore, they do not increase the specific gravity of the clays as organic molecules do; 2) LMT is water based and non-toxic. Most standard heavy liquids are hazardous, often require special handling and the use of respirators due to their volatile nature and 3) there is no recycling cost other than the cost of filters. The specific gravity of this liquid is very easy to adjust by either evaporation or dilution with distilled water. Distilled water and plastic or stainless steel vessels are necessary when working with LMT because the heavy liquid will precipitate insoluble Ca-metatungstate in the presence of free Ca^{2+} ions and can react with certain metals. The properties of LMT are shown in Table 1. The LMT for this study was adjusted to a specific gravity of 2.95. This allowed for the flotation of quartz, feldspars, and clay minerals, and settling of heavy minerals and some of the iron-rich micas.



Figure 10. Sampling location in blue arrow of WF#5 Mobil Dwyer MT, Plug Depth 17581 ft.

Product Information	LMT
Chemical Name	Lithium Metatungstate
Chemical Formula	Li₆(H₂W₁₂O₄₀)
Formula Weight	2892
% WO₃	96.3
% Li or NH₄	1.4
Specific gravity (max.) in H₂O	3.4
Operating Specific Gravity (max.)	3.2

Table 1. Properties of LMT.

Sample Preparation

The method reported by Hanan and Totten (1996) was used to quantitatively to separate heavy minerals from the Woodford samples, so that they may be studied by the same established methods as applied to sandstones. Samples for this study were prepared by disaggregating the mudrocks with a mortar and pestle. The samples were disaggregated until the sample could pass through 250 um sieve. The weight of the disaggregated samples, the amount of LMT added to each polycarbonate centrifuge tube and the total mass of the tube, sample, and LMT are shown in Table 2.

Sample	Mass of Sample (g)	Mass of LMT (g)	Total Mass (g)
McCalla Ranch 1-12	17.0	18.0	125.3
Chenowetu	15	112.3	125.6
Curtis 2	15.6	112.2	125.2
Dwyer Mt	13.3	110.3	125.2
Guthrie	6.9	102.1	127.9
Ne Tiden	6.6	102.3	128.2
Haunan 2	5.5	103.4	128.0
Sara Kirk	6.7	107.5	133.3
Cement Ord	6.8	107.3	133.1
Lela Rahm	7.6	106.5	133.2

Table 2. Masses of disaggregated mudrock samples, sample and LMT, and total mass (including mass of centrifuge tube).

Procedure

Heavy Mineral Separation

Disaggregated shale samples were placed in 50mL polycarbonate centrifuge tubes and suspended in an amount of LMT sufficient to fill the tube, but with enough space to balance the tubes with LMT prior to centrifuging. The tubes were balanced with LMT until the weight of the

tubes was within 0.5 g of each other. After dispersing the shale and LMT mixture by shaking, the samples were centrifuged for 2 hours at 3000 rpm in an IEC Clinical Centrifuge. A centrifuge is necessary because it decreases the settling time of heavy mineral grains, (especially the smaller grains) and reduces rafting of heavy mineral grains onto lighter grains.

After centrifuging, the heavy mineral fraction was isolated in the bottom of the centrifuge tube by freezing the bottom portion of the tube using liquid nitrogen. The light mineral fraction and the LMT were washed off. The light mineral fraction was caught in a funnel and washed on filter paper. The LMT was filtered and recycled for later use. The light fraction was retained for future work on the Woodford Shale. After removing the light fraction the heavy fraction was caught in a filter funnel and washed on a pre-weighed 0.45 um filter. The filter with the heavy minerals was dried and weighed to determine the weight percent of heavy minerals.

Mineral Identification and Size Analysis

Identification of the mineralogy, composition and size of the heavy mineral fraction was determined by scanning electron microscopy (SEM). For this study, we used the SEM at the Kansas State University Microscopy lab in the Department of Biology. Dr. Dan Boyle operated the SEM. The SEM techniques for mineral identification included: energy dispersive spectra (EDS) on individual grains and backscatter electron imaging. Point counting to quantify heavy mineralogy percentages was done directly on BSE photomicrographs.

Chapter 4 - Results

The results of the heavy mineral separations are presented in Table 3. Many of the samples contained a high percentage of euhedral, Ca-tungstate precipitated grains as identified under SEM. The early work developing the method described this as a possibility (Hanan and

Totten, 1996). These grains were interpreted as precipitating from solution during the separation process, and needed to be removed from the heavy mineral percentages. To normalize the samples to a calcium-tungstate-free percentage, the photomicrographs were point counted (520 points) to determine the percentage of the area that each mineral covered. The percentage of heavy minerals in each sample was calculated by adjusting to a calcium-tungstate-free value. The normalized value of the heavy minerals is shown in column 8 of Table 3. Table 4 contains additional data about the samples including depth, vitrinite reflectance and TOC.

Weight % Heavy Minerals - Woodford Shale Samples							
Sample #	Sample Name	Sample Mass	Mass (sep)	mass filter paper	mass of heavies	% Heavies	Normalized Heavies
WF#1	McCalla Ranch	17.05	0.60	0.07	0.32	1.89	1.03
WF#3	Lela Rahm	7.60	0.16	0.07	0.09	1.14	1.13
WF#5	Dwyer	13.31	0.41	0.07	0.13	0.96	0.88
WF#6	Cement Ord	6.81	0.26	0.07	0.19	2.83	2.76
WF#7	Chenoweth	15.00	0.41	0.07	0.13	0.88	0.68
WF#8	Curtis	15.60	0.52	0.07	0.23	1.50	1.28
WF#9	Aiden Rd	6.62	0.18	0.07	0.11	1.60	1.43
WF#10	Hannah	5.50	0.33	0.07	0.26	4.72	4.72

Table 3. Percentage of heavy minerals in the Woodford Shale samples.

Woodford Samples					
Sample #	Sample Name	Normalized Heavies	Depth	Vitrinite Reflectance	TOC
WF#1	McCalla Ranch	1.03	12309	0.75	1.74
WF#3	Lela Rahm	1.13	6279	0.55	4.62
WF#5	Dwyer	0.88	8717	0.68	6.05
WF#6	Cement Ord	2.76	17581	1.25	6.54
WF#7	Chenoweth	0.68	6513	0.52	3.19
WF#8	Curtis	1.28	8520	0.53	11.5
WF#9	Aiden Rd	1.43	6793	0.47	6.05
WF#10	Hannah	4.72	14323	2.00	0.36

Table 4. Depth, vitrinite reflectance values and Toc data for the Woodford Shale samples.

EDS Spectra

The SEM photomicrographs and associated EDS spectra for Woodford samples 6, 8 and 10 are shown below (Figures 11-25). The rest of the EDS spectra are located in Appendix A. Mineral species were identified based on EDS spectra, elemental data.

WF#6 (Cement Ord)

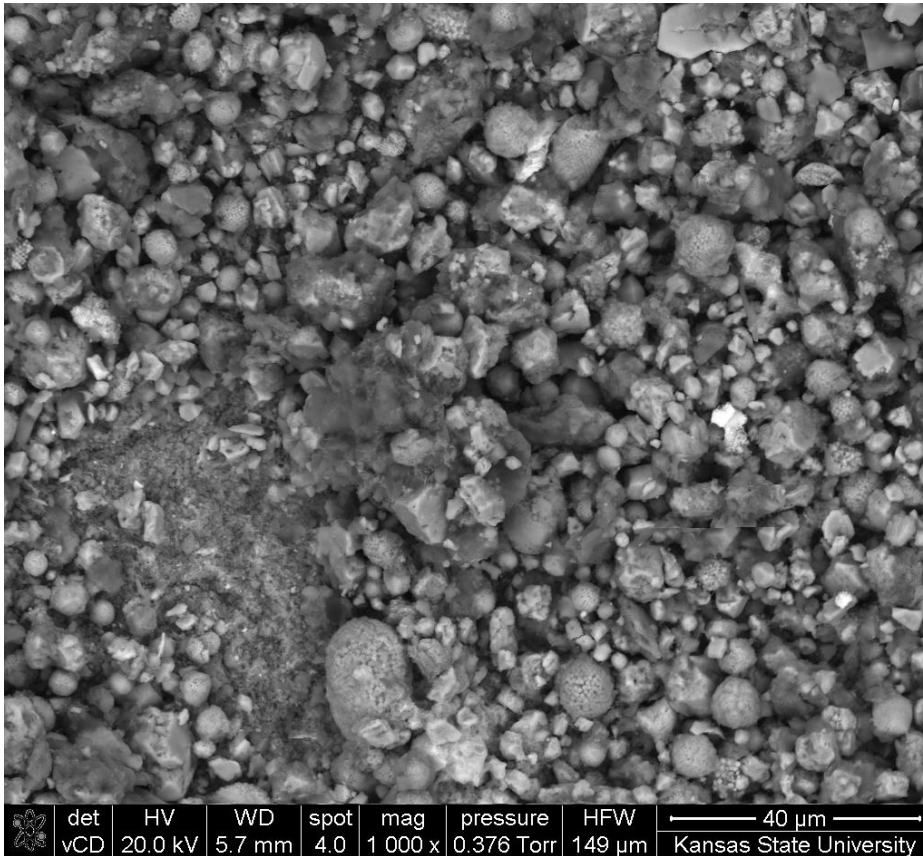


Figure 11. Photomicrograph showing the heavy minerals in WF#6 (Cement Ord). Pyrite framboids are clearly visible throughout this sample and appear as raspberry-like spheres.

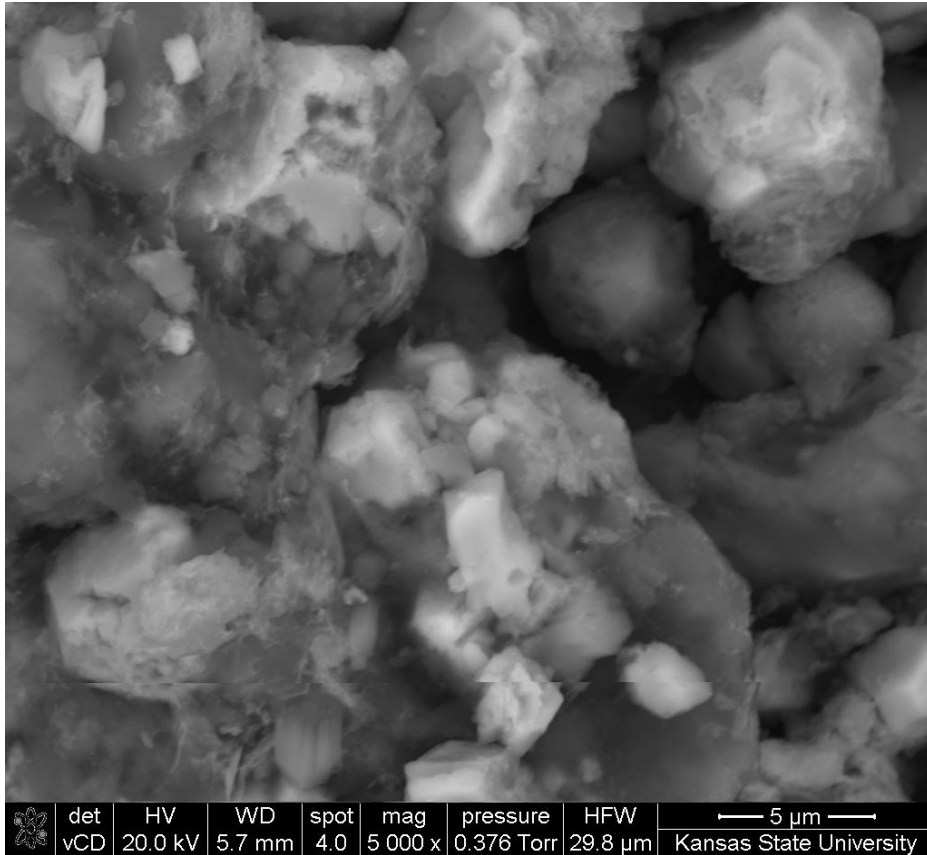


Figure 12. Heavy minerals in sample WF#6 Cement Ord. In this photomicrograph a few euhedral pyrite grains are present, along with W-bearing mineral crystals that are less than 1μm in size. A grain of Fe-mica is visible in the center of the right side.

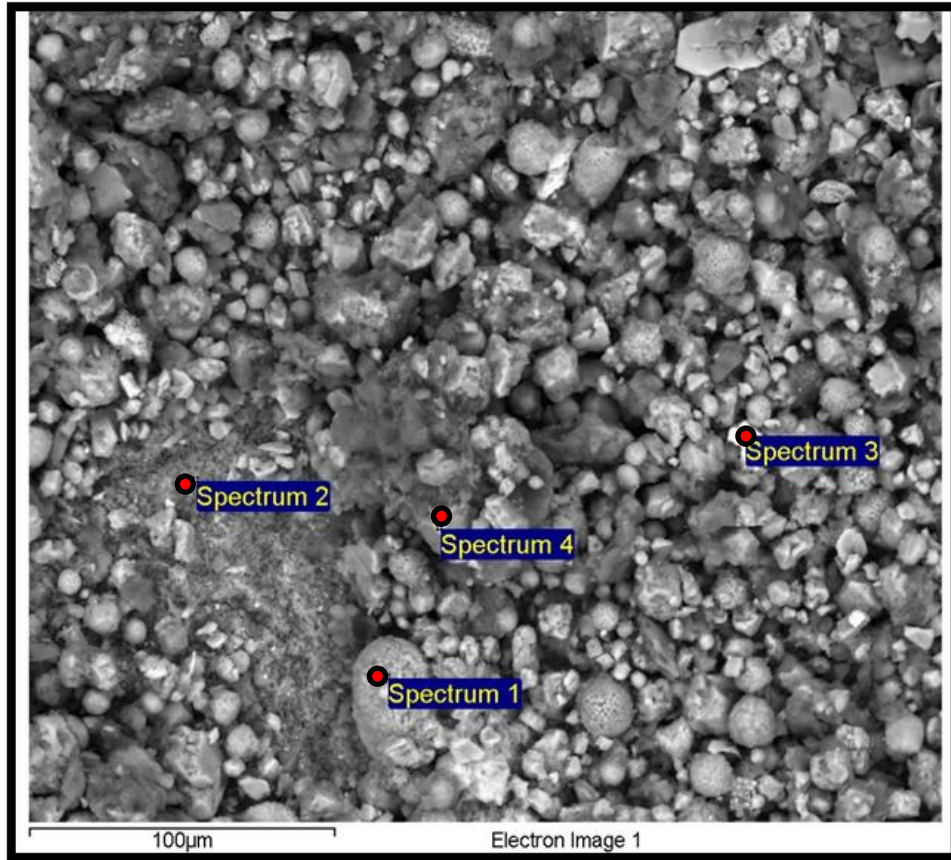


Figure 13. Locations for the EDS spectra shown in Figure 14. Spectrum 1 is located on a framboid, spectrum 2 is located on fine-grained Fe-Mica, Spectrum 3 is located on a grain of scheelite, and Spectrum 4 is located on cubic pyrite.

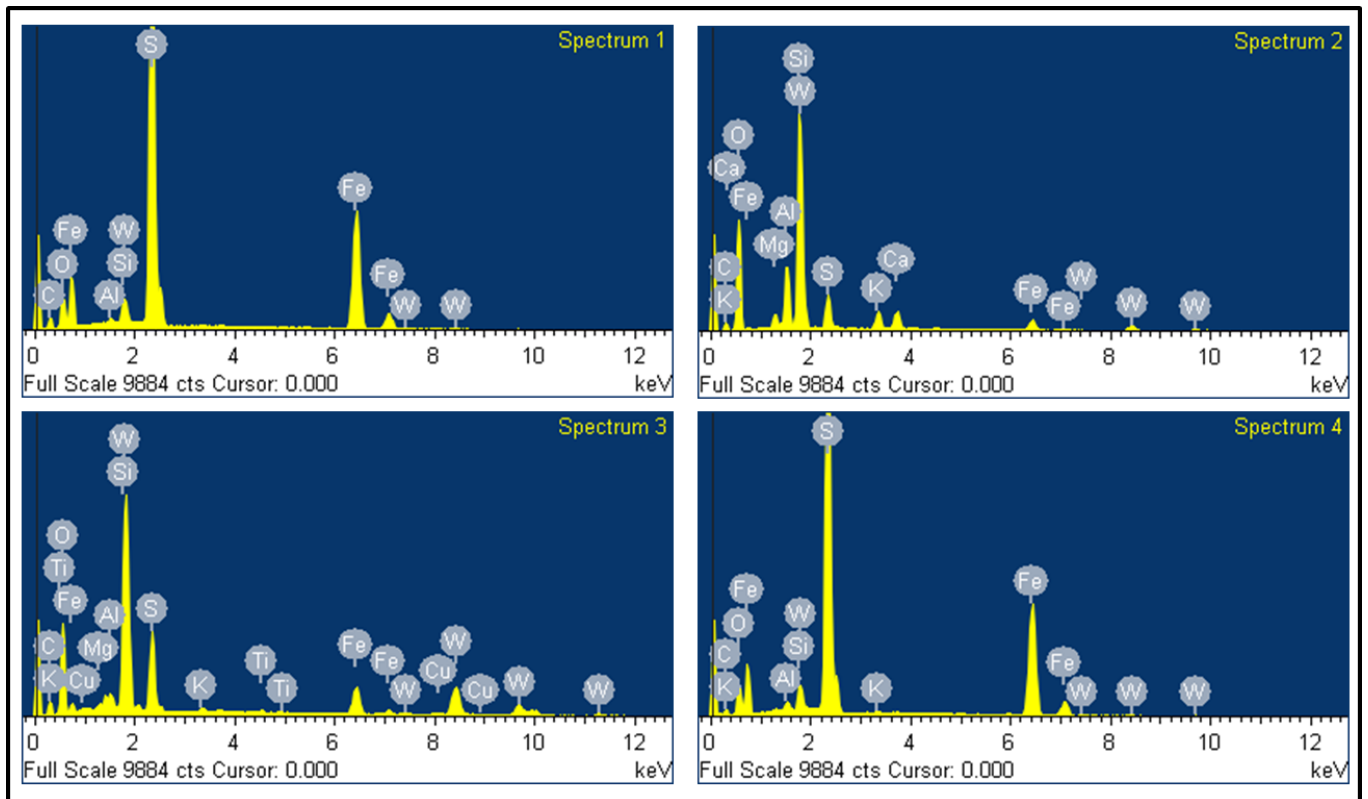


Figure 14. EDS spectra for WF#6 Cement Ord sample locations.

Spectrum 1			Spectrum 2		
Element	Weight%	Atomic%	Element	Weight%	Atomic%
C K	16.77	35.8	C K	10.16	17.59
O K	11.75	18.83	O K	43.92	57.09
Al K	0.3	0.29	Mg K	1.3	1.11
Si K	1.08	0.99	Al K	4.94	3.81
S K	36.6	29.27	Si K	16.78	12.43
Fe K	31.75	14.58	S K	4.25	2.76
W M	1.75	0.24	K K	2.39	1.27
Total	100	100	Ca K	2.64	1.37
			Fe K	3.98	1.48
			W M	9.64	1.09
			Total	100	100
Spectrum 3			Spectrum 4		
Element	Weight%	Atomic%	Element	Weight%	Atomic%
C K	10.92	25.87	C K	12.92	29.32
O K	29.4	52.27	O K	11.03	18.8
Mg K	0.36	0.42	Al K	0.56	0.57
Al K	0.9	0.95	Si K	1.35	1.31
Si K	1.82	1.85	S K	39.36	33.47
S K	8.79	7.8	K K	0.26	0.18
K K	0.44	0.32	Fe K	33.08	16.15
Ti K	0.35	0.21	W M	1.43	0.21
Fe K	7.96	4.05	Total	99.99	100.01
Cu K	0.79	0.35			
W M	38.27	5.92			
Total	100	100.01			

Figure 15. Elemental, weight percent and atomic percent data for WF#6 Cement Ord.

WF#8 (Curtis)

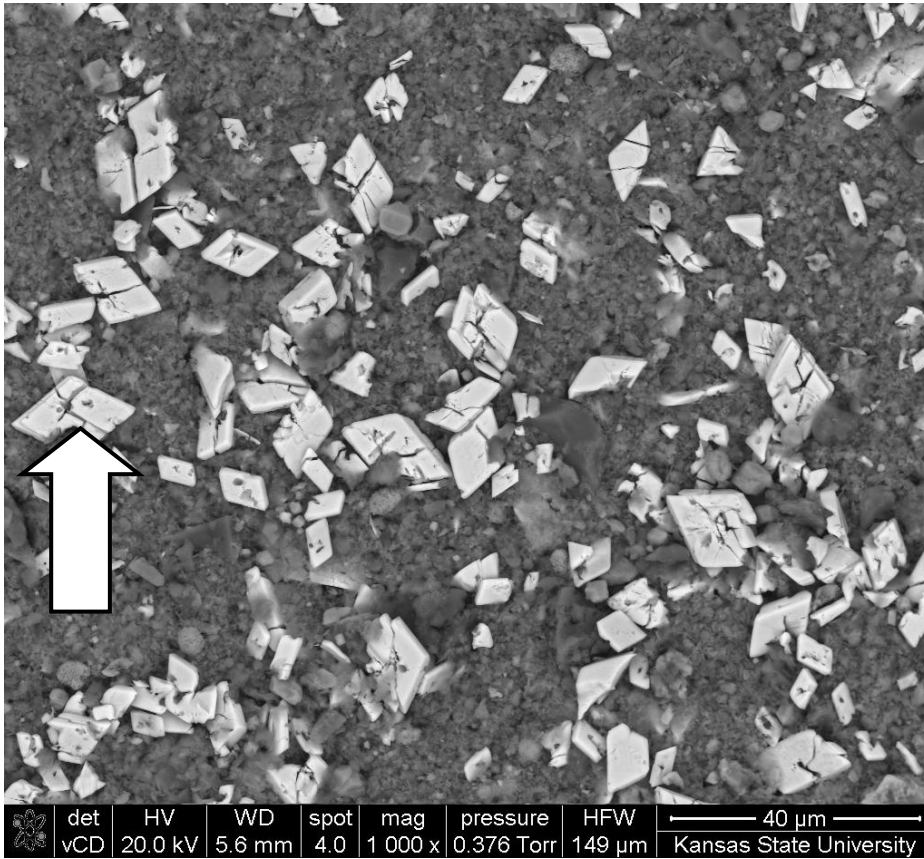


Figure 16. Heavy minerals in sample WF#8 Curtis. BSE image shows W-bearing mineral artifacts as bright grains (arrow).

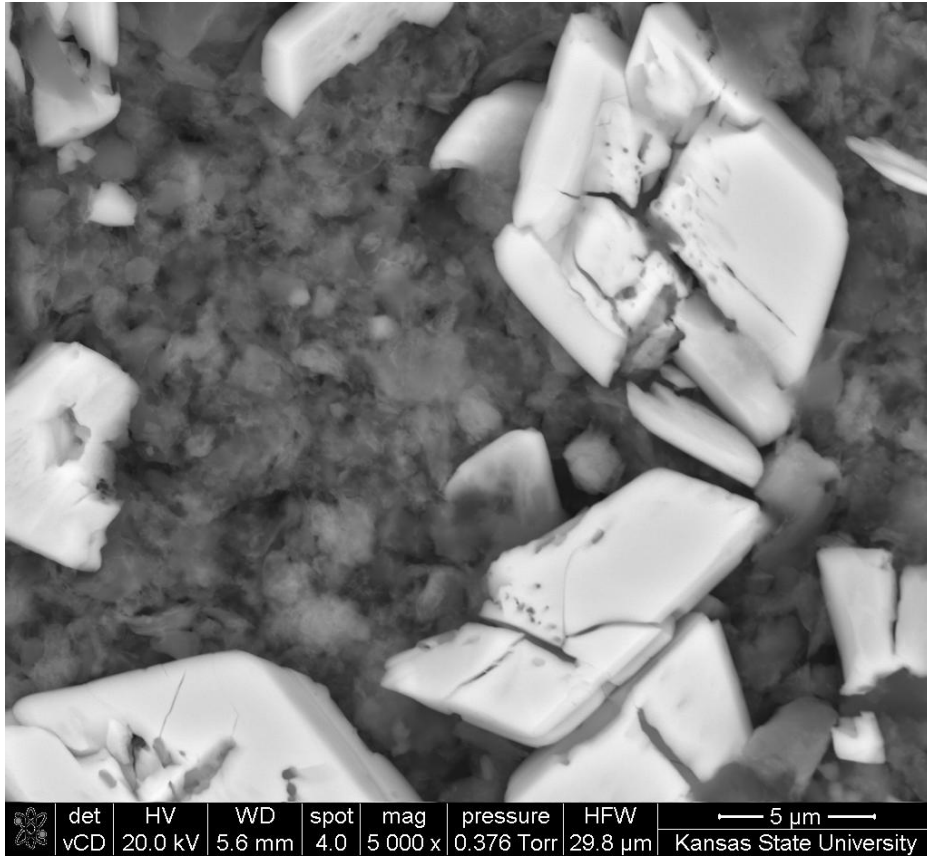


Figure 17. Heavy minerals in sample WF#8 Curtis. W-bearing mineral artifacts are euhedral, bright grains.

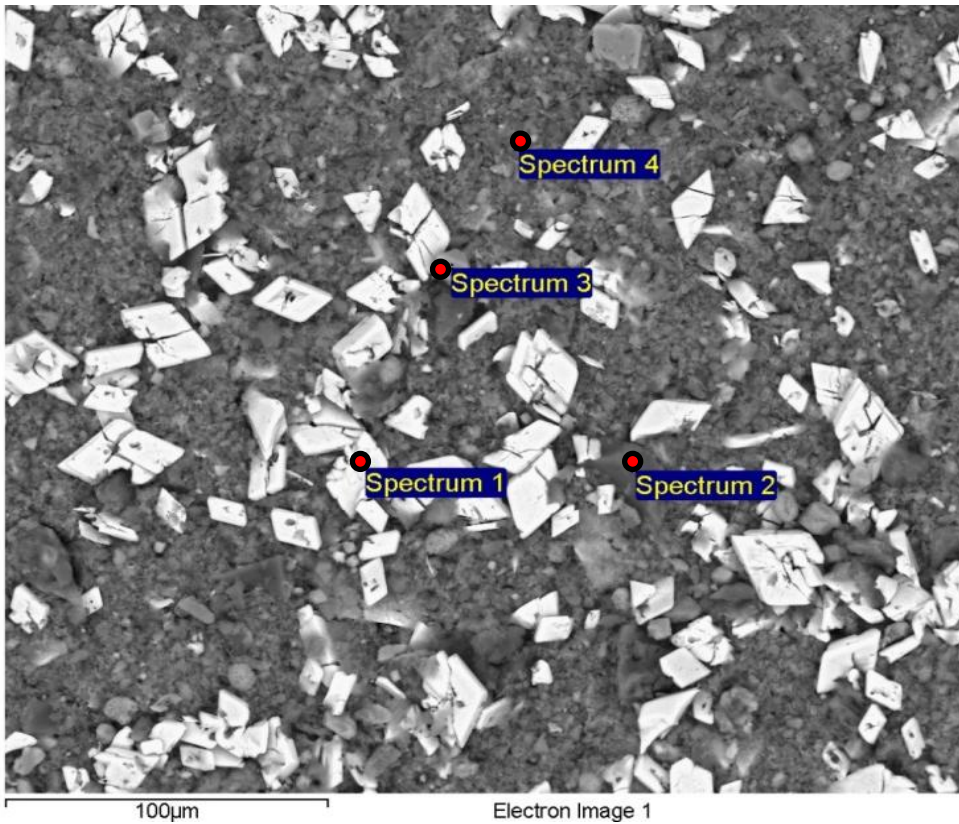


Figure 18. Locations for the EDS spectra shown in figure 19.

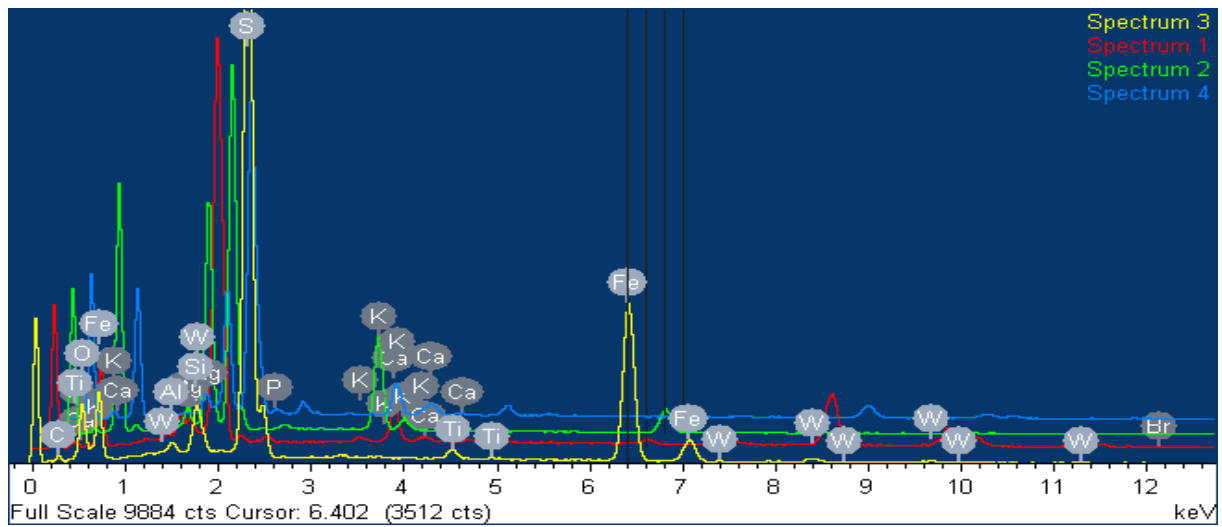


Figure 19. Elemental, weight percent and atomic percent data for WF#8 Curtis.

Spectrum 1			Spectrum 2		
Element	Weight%	Atomic%	Element	Weight%	Atomic%
C K	1.96	7.13	C K	3.2	5.53
O K	25.8	70.33	O K	49.83	64.66
S K	0.41	0.56	Mg K	0.99	0.84
K K	0.5	0.55	Al K	10.82	8.33
Ca K	3.83	4.16	Si K	19.01	14.05
Fe K	1.1	0.86	S K	0.32	0.21
Br L	2.16	1.18	K K	7.39	3.93
W M	64.24	15.24	Ti K	0.48	0.21
Total	100	100.01	Fe K	5.17	1.92
			W M	2.79	0.31
			Total	100	99.99
Spectrum 3			Spectrum 4		
Element	Weight%	Atomic%	Element	Weight%	Atomic%
C K	6.48	15.94	C K	3.13	6.36
O K	14.6	26.96	O K	40	60.99
Al K	0.5	0.55	Mg K	1.4	1.41
Si K	1.25	1.32	Al K	7.53	6.8
S K	40.17	37.01	Si K	17.71	15.38
Ti K	0.92	0.57	P K	0.44	0.35
Fe K	32.23	17.05	S K	1.21	0.92
W M	3.85	0.62	K K	3.64	2.27
Total	100	100.02	Ca K	1.33	0.81
			Ti K	1.68	0.86
			Fe K	3.12	1.36
			W M	18.8	2.49
			Total	99.99	100

Figure 20. Elemental, weight percent and atomic percent data for WF#8 Curtis.

WF#10 (Hannah)

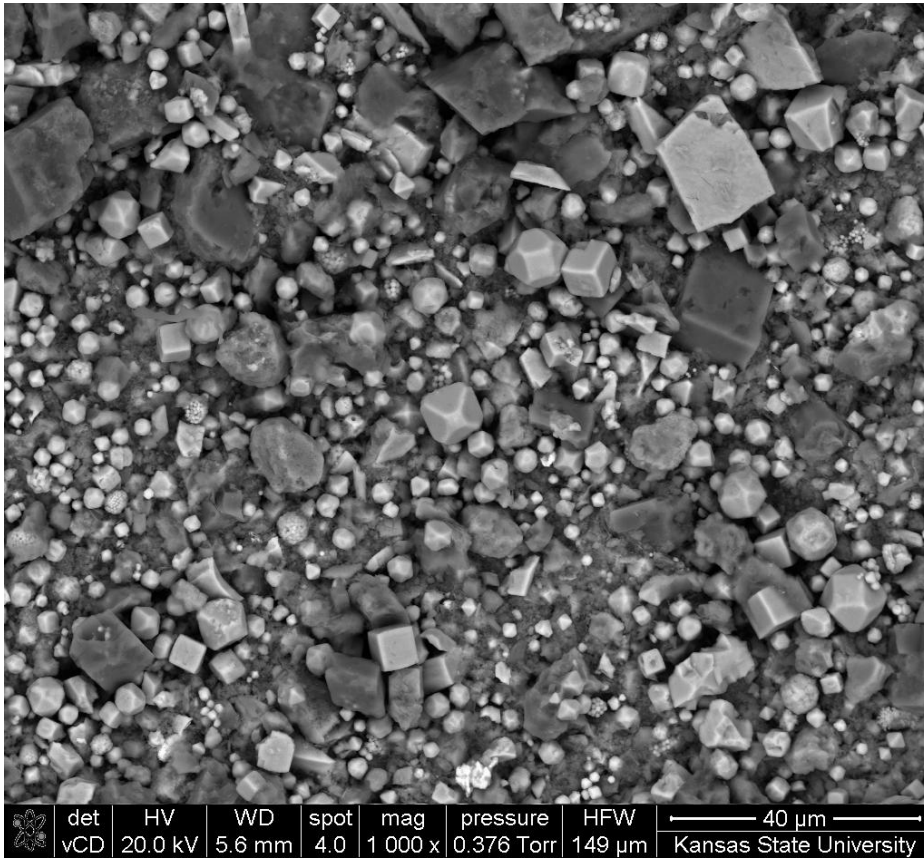


Figure 21. Heavy minerals in sample WF#10 Hannah. This sample is very pyrite rich and has many different forms of pyrite present to include: octahedral pyrite, pyritohedrons, cubic pyrite, framboidal pyrite, as well as euhedral grains of Ankerite.

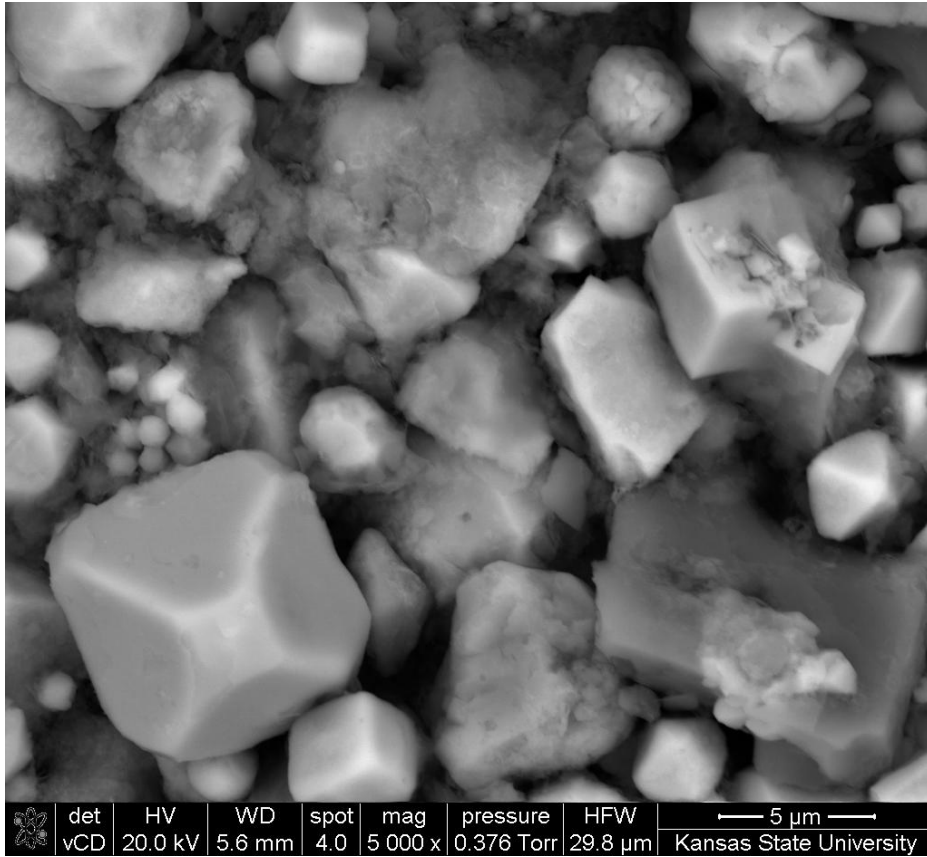


Figure 22. Heavy minerals in sample WF#10 Hannah. In this zoomed in view of WF#10 we can see octahedral and cubic pyrite, a few framboids, some euhedral pyrite and a piece of Ankerite.

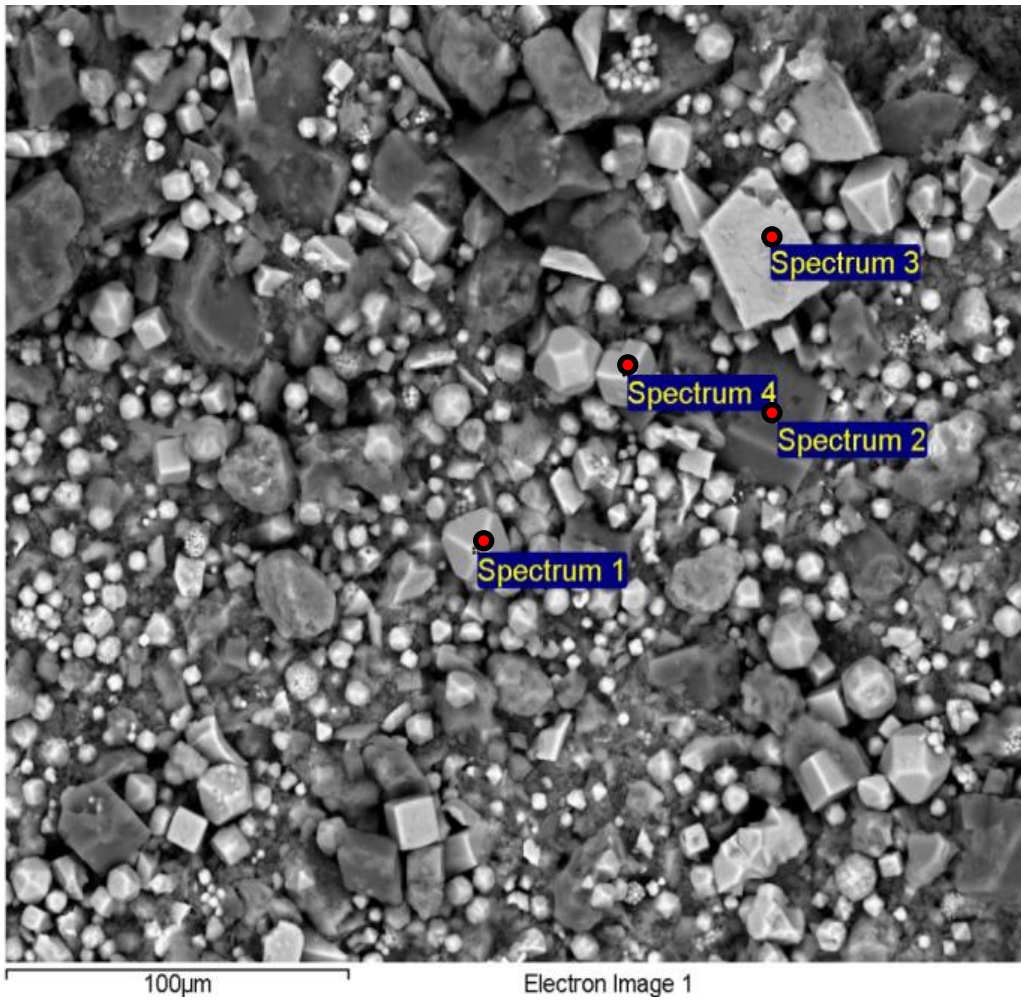


Figure 23. Locations for the EDS spectra shown in figure 24.

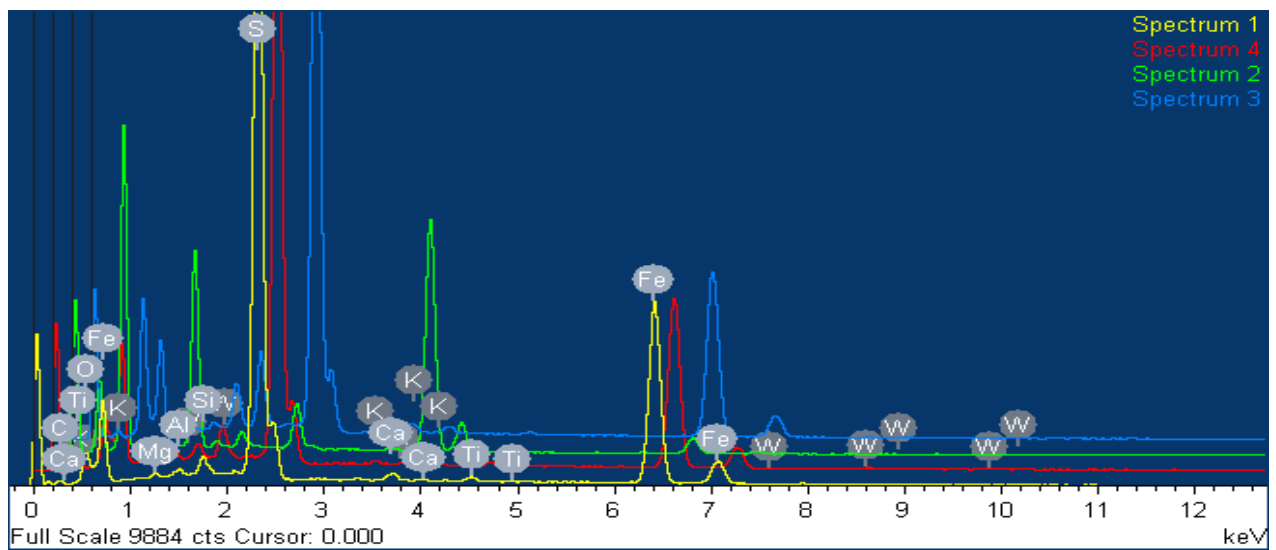


Figure 24. Elemental, weight percent and atomic percent data for WF#10 Hannah.

Spectrum 1			Spectrum 2		
Element	Weight%	Atomic%	Element	Weight%	Atomic%
C K	5.04	13.3	C K	16.91	24.54
O K	8.94	17.72	O K	56.29	61.35
Mg K	0.31	0.41	Mg K	8.56	6.14
Al K	0.33	0.38	Al K	0.22	0.14
Si K	0.84	0.95	Si K	0.54	0.33
S K	45.24	44.74	S K	1.82	0.99
Ca K	0.63	0.5	Ca K	13.15	5.72
Ti K	0.46	0.31	Fe K	2.52	0.79
Fe K	38.21	21.7	Total	100.01	100
Total	100	100.01			
Spectrum 3			Spectrum 4		
Element	Weight%	Atomic%	Element	Weight%	Atomic%
C K	2.22	4.97	C K	10.92	24.69
O K	26.58	44.79	O K	13.64	23.15
Mg K	0.34	0.38	Mg K	0.42	0.46
Al K	1.79	1.79	Al K	0.62	0.63
Si K	2.94	2.82	Si K	1.28	1.23
S K	36.64	30.81	S K	39.66	33.58
K K	0.55	0.38	K K	0.22	0.15
Ca K	0.4	0.27	Ca K	0.71	0.48
Ti K	0.22	0.12	Ti K	0.31	0.17
Fe K	28.31	13.67	Fe K	31.58	15.35
Total	99.99	100	W M	0.64	0.09
			Total	100	99.98

Figure 25. Elemental, weight percent and atomic percent data for WF#10 Hannah.

Point-Counting Results

The eight Woodford samples were point-counted, with a total of 520 points counted for each sample. The results of the point counting are shown for each Woodford sample below in Tables 5-12. It is important to note that any points counted for scheelite or filter paper was subtracted from the total to normalize the actual heavy mineral percentages.

McCalla Ranch				
Mineral	Points	Percent	Grain Size	Grain Shape
Framboidal Pyrite	38	17.35	10-15 μ m	Round
Euhedral Pyrite	65	29.68	10 μ m	Round
Ankerite	48	21.92	10-15 μ m	Orthorhombic
Cubic Pyrite	68	31.05	15 μ m	Cubic
	219	100.00		

Table 5. Point-counting results for WF#1 McCalla Ranch.

Lela Rahm				
Mineral	Points	Percent	Grain Size	Grain Shape
Ankerite	82	15.77	15 μ m	Orthorhombic
Cubic Pyrite	36	6.92	10 μ m	Cubic
Euhedral Pyrite	298	57.31	5-10 μ m	Round
Fe-Mica	67	12.88	50 μ m	Round
Framboidal Pyrite	37	7.12	10 μ m	Round
	520	100.00		

Table 6. Point-counting results for WF#3 Lela Rahm.

Dwyer				
Mineral	Points	Percent	Grain Size	Grain Shape
Ankerite	51	9.66	20µm	Orthorhombic
Cubic Pyrite	169	32.58	15µm	Cubic
Euhedral Pyrite	92	17.80	10µm	Round
Fe-Mica	98	18.75	<1µm	Subrounded
Framboidal Pyrite	110	21.21	10-15µm	Round
	520	100.00		

Table 7. Point-counting results for WF#5 Dwyer.

Cement Ord				
Mineral	Points	Percent	Grain Size	Grain Shape
Framboidal Pyrite	51	10.02	10-20µm	Round and sometimes elongate
Fe-Mica	45	8.84	20µm	Sub-rounded and flakey in appearance
Cubic Pyrite	181	35.56	5-10µm	Cubes
Euhedral Pyrite	165	32.42	5µm	Round
Ankerite	65	12.77	15-20µm	Sub-rounded
Fossil	2	0.39	5-10µm	Fragment
	509	100.00		

Table 8. Point-counting results for WF#6 Cement Ord.

Chenoweth				
Mineral	Points	Percent	Grain Size	Grain Shape
Ankerite	6	1.57	15 µm	Rhombic
Cubic Pyrite	120	31.41	5 µm	Cubes
Euhedral Pyrite	115	30.10	10µm	Round
Fine grained Fe-Mica	51	13.35	<1µm	Round
Fossil	1	0.26	5 µm	Fragment
Framboidal Pyrite	64	16.75	15µm	Round and elongated well developed framboids
Fe-Mica	25	6.54	15 µm	Round w/flakey appearance
	382	99.98		

Table 9. Point-counting results for WF#7 Chenoweth.

Curtis				
Mineral	Points	Percent	Grain Size	Grain Shape
Cubic Pyrite	25	6.16	<5 μm	cubes (a few cubes up 10 μm)
Euhedral Pyrite	60	14.77	<5 μm	Round
Fine grained Fe-Mica	273	67.24	<1 μm	Round
Framboidal Pyrite	10	2.47	<5 μm	Framboids
Fe-Mica	38	9.36	15 μm	Round
	406	100.00		

Table 10. Point-counting results for WF#8 Curtis.

Jones and Pellow				
Mineral	Points	Percent	Grain Size	Grain Shape
Ankerite	179	36.67	15-20 μm	Orthrhombic
Cubic Pyrite	208	42.63	20-25 μm	Cubic and Dodechadedral
Euhedral Pyrite	76	15.57	10 μm	Round
Fe-Mica	25	5.12	15-20 μm	Round
	488	99.99		

Table 11. Point counting results for WF#9 Jones and Pellow.

Hannah				
Mineral	Points	Percent	Grain Size	Grain Shape
Ankerite	136	25.29	15 μm	Rhombic
Cubic Pyrite	101	19.27	5-10 μm	Cubes
Euhedral Pyrite	218	42.47	<5 μm	Round
Fine grained Fe-Mica	20	4.18	1 μm	Sub-rounded
Framboidal Pyrite	21	4.19	<5 μm	Round
Pyritohedrons	24	4.60	10 μm	Dodechaderal
	520	100.00		

Table 12. Point-counting results for WF#10 Hannah.

The heavy mineral fraction of the Woodford Shale showed a surprisingly limited mineralogy. The largest mineral constituent was pyrite. The average amount of pyrite present in

all of the samples is 66%, with all but one sample having pyrite percentages of 58% or higher. Several different forms of Pyrite can be seen in all of the samples. Fe-Mica was the next largest constituent of these samples (16%). Only one sample was Fe-Mica free (McCalla Ranch). Ankerite was present in the samples at an average of 18%. Some samples included fossil fragments. The fossils made up less than 1% of the samples. A pie chart showing the abundances of the minerals in sample WF#7 (Chenoweth) is shown in Figure 26. The rest of the graphs showing the heavy mineral distribution for each of the samples are shown in Appendix B. An example of the Fe-mica found in the samples is shown in Figure 27, and example of the Ankerite is found in Figure 28, and an unidentified mineral is shown in Figure 29.

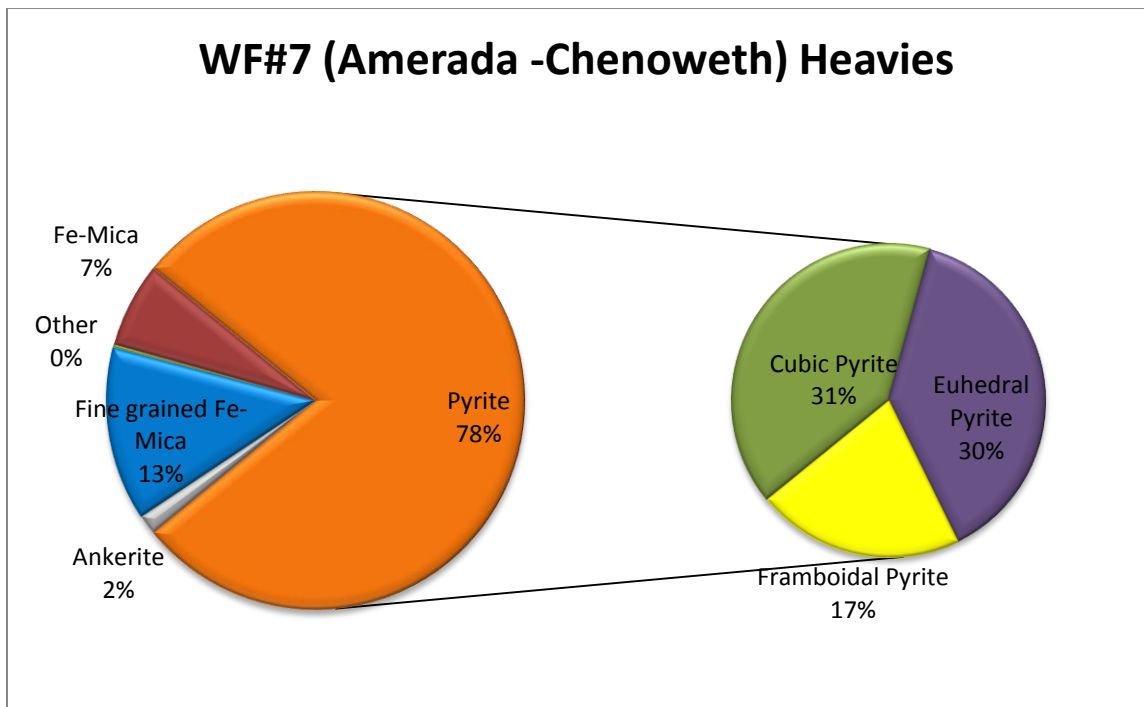


Figure 26. Mineral abundances in sample WF#7 (Amerada-Chenoweth).

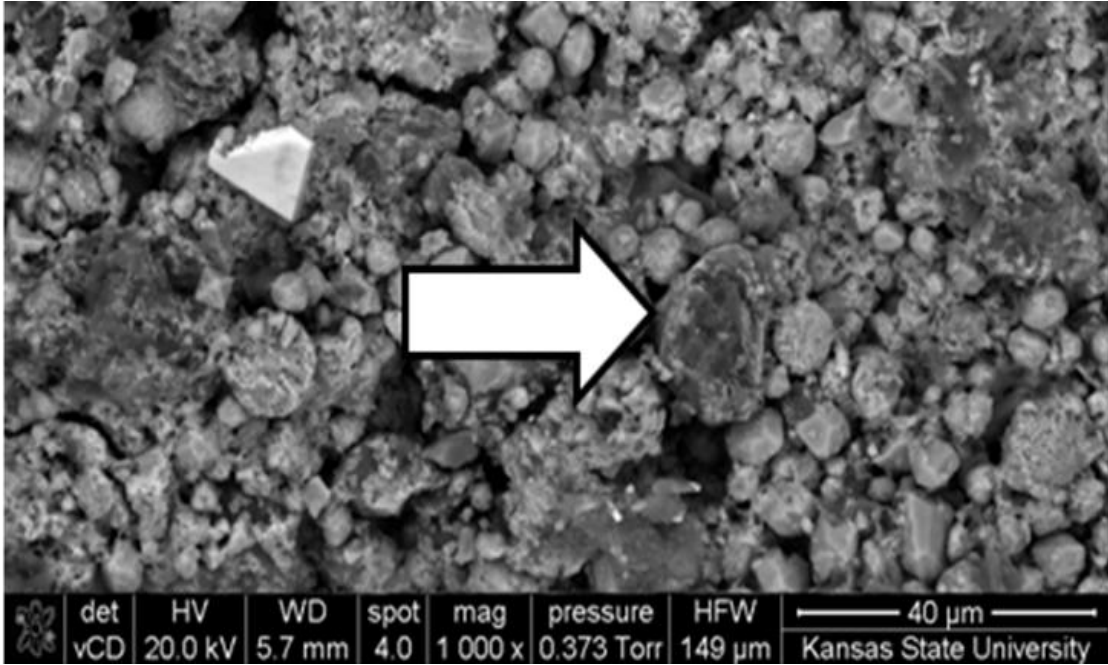


Figure 27. Example of Fe-Mica found in Woodford Shale Samples (WF#3 Lela Rahm).

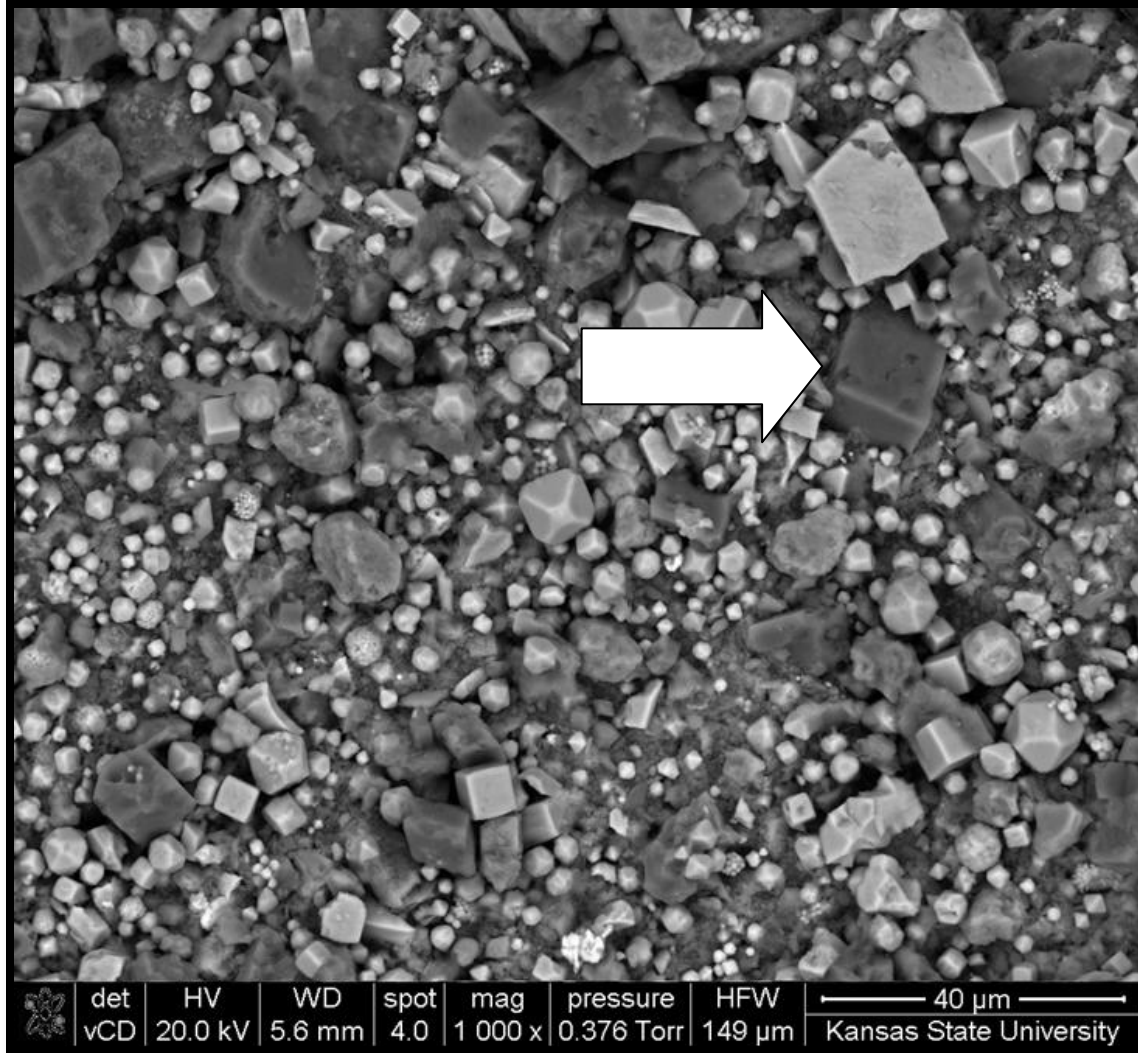


Figure 28. An example of the Ankerite found in the Woodford Shale samples (WF#10 Hannah).

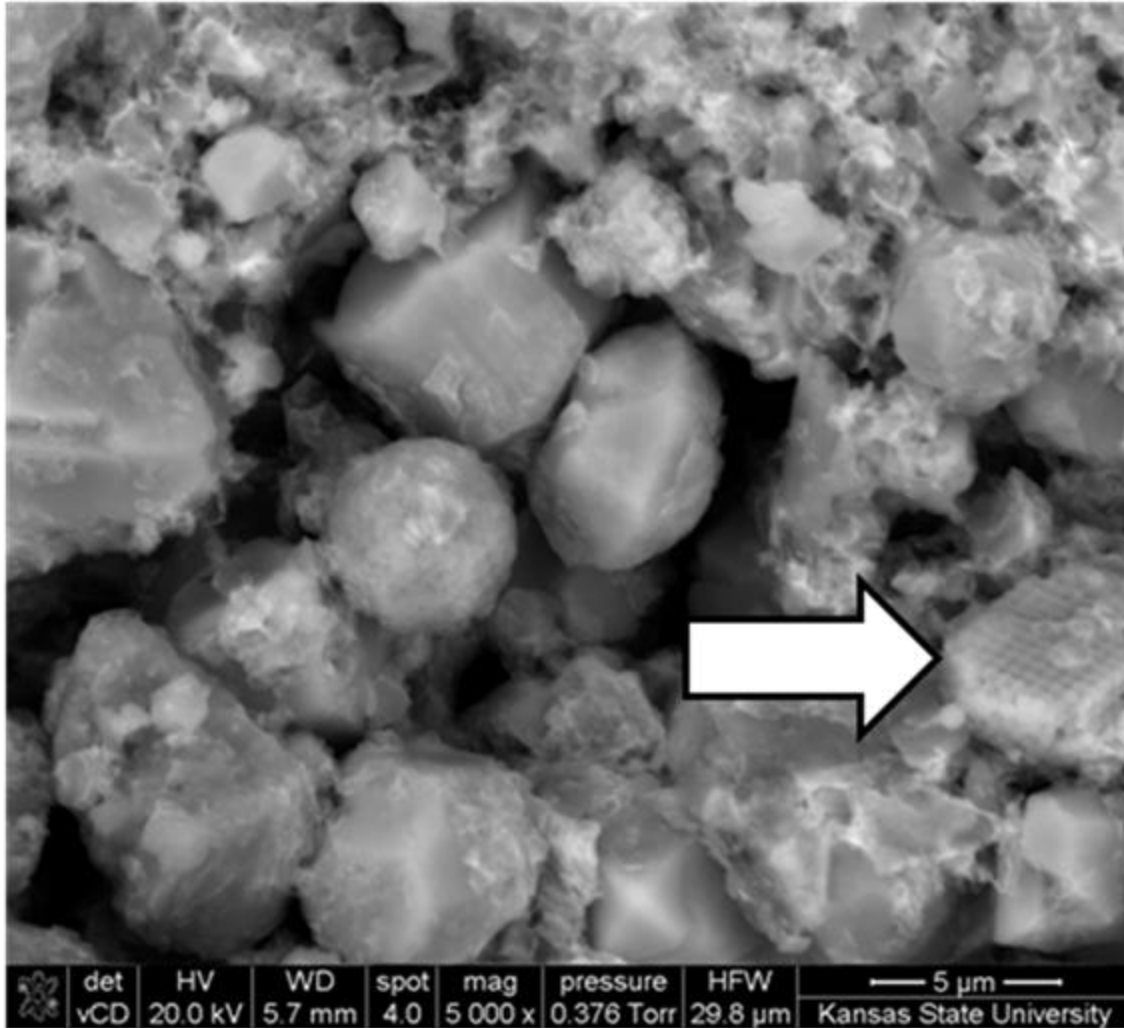


Figure 29. An example of an unidentified fragments found in the Woodford Shale samples (WF#3 Lela Rahm).

Chapter 5 - Discussion

Other Heavy Mineral Studies

Totten and Hannan 1998, looked at heavy minerals in the Stanley Shale formation (Mississippian) from the Oauchita Mountains and Cenozoic shales from the Gulf of Mexico. For the Stanley Shale samples they found that the median grain size of the heavy minerals was 25 μ m and that Fe-oxides, Ti-oxides, and Fe-bearing biotites were the dominant minerals present in

these samples. For the Gulf of Mexico shales, Figure 30 shows the mineral breakdown of the Stanley Shale samples. Figure 31 shows the distribution of the heavy minerals in the average Woodford Shale from this study. There is little variety of heavy minerals in the Woodford when compared to the Stanley and GOM shales. This supports the conclusions of Kirkland et al., 1992, that there was little dilution of quiet water deposition with detrital sediment.

It is very difficult to make any positive correlations between the Stanley and Woodford Shales, because the Woodford is pyrite, carbonate, and Fe-rich, whereas the Stanley Shale has almost no pyrite and carbonates. The Woodford is more comparable to the Average Cenozoic GOM shales. Both the Woodford and the GOM samples have high amounts of both pyrite and carbonate, as well as some Fe-micas. From this, it may be suggested that the diagenetic changes that took place in the GOM shales are more similar to the changes that took place in the Woodford Shale. There is still a significant lack of any detrital heavy minerals in the Woodford compared to GOM shales.

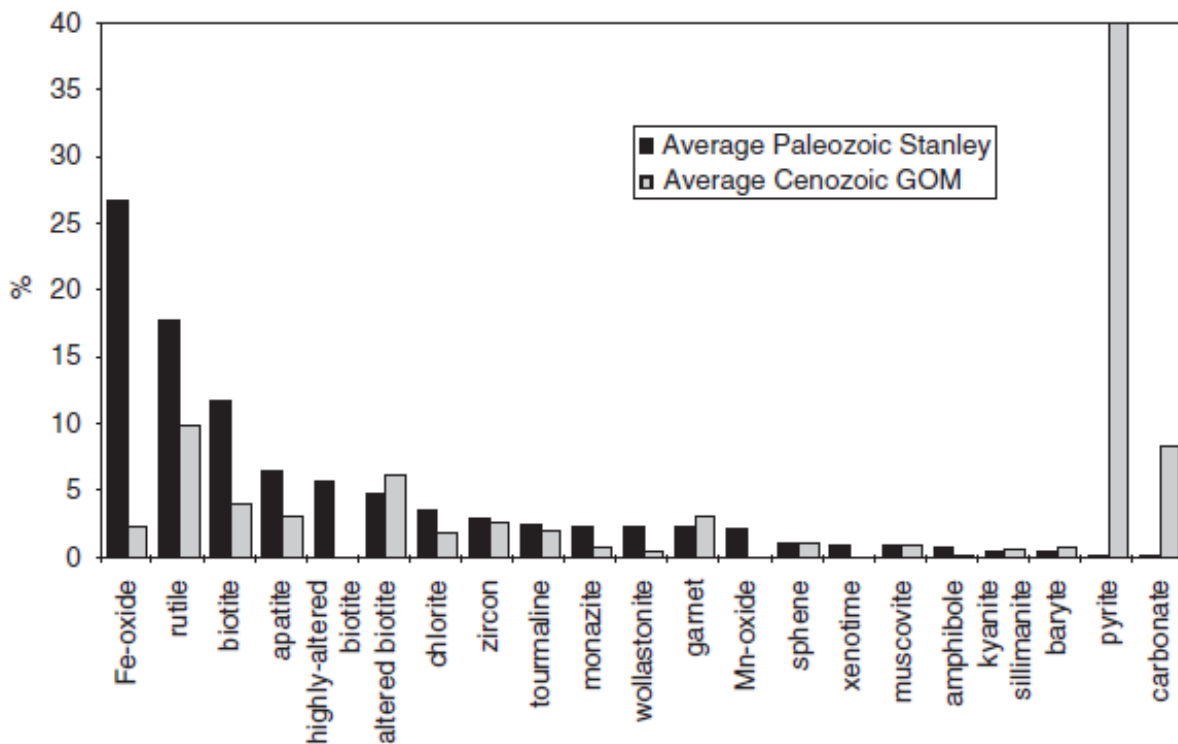


Figure 30 Average distribution of heavy minerals within the Average Stanley Shale (black) and the average Cenozoic Gulf of Mexico Shale (gray) From Totten and Hannan 1998.

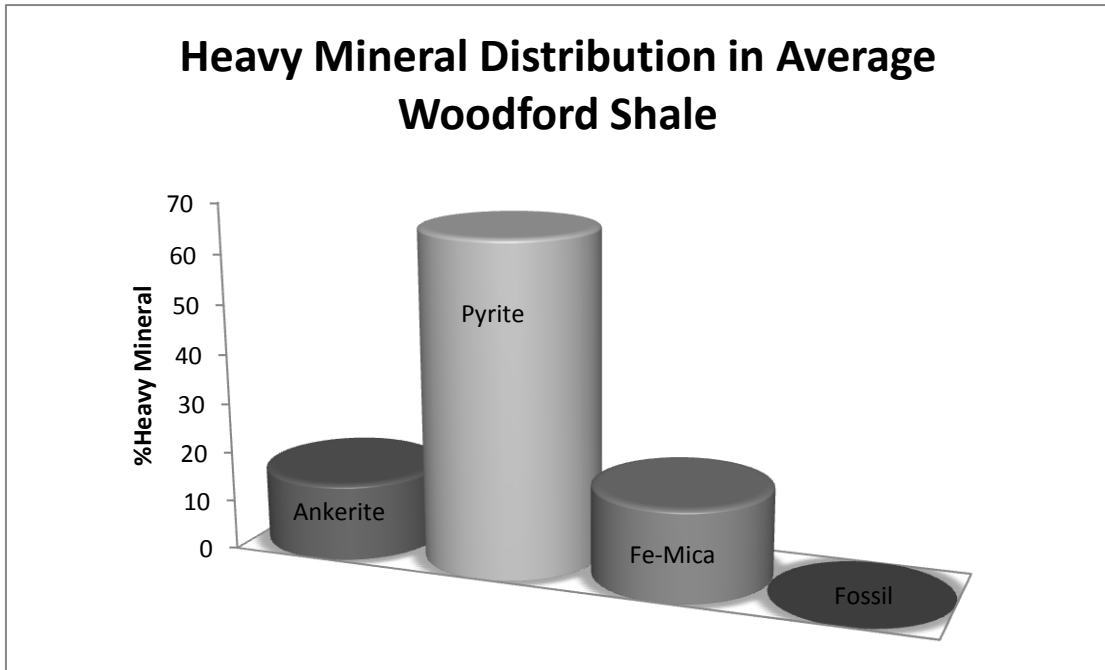


Figure 31. Heavy mineral distribution in the average Woodford Shale.

Pyrite in the Heavy Mineral Fraction of the Woodford Shale

Pyrite (FeS_2) is a sulfide mineral that is common in sedimentary rocks in the crust of the earth. It has a metallic luster and a hardness of 6.5. It belongs to the Isometric Diploidal crystal system and the space group $2/m$. The density of pyrite ranges from 5.0-5.2, and it has a simple cubic face centered structure.

The amount of pyrite in the heavy mineral fraction of the Woodford Shale ranged from 20 - 78% of the heavy minerals present. The form of the pyrite varied considerably, examples from samples 6,8,9, and 10 are shown in Figure 32. The different types of disseminated pyrite found in the Woodford Shale samples are listed below:

- 1) Single crystals of authigenic Pyrite (cubic, octahedral and pyritohedral morphologies). Figure 33 from WF#10 Lonestar-Hannah shows is an example of this type of pyrite. These pyrite crystals are likely authigenic in origin.
- 2) Framboidal Pyrite- aggregates of pyrite crystals <0.5 μm in diameter. Figure 34, from WF#3 Lela Rahm shows this morphology of pyrite.
- 3) Single Framboids of Pyrite as shown in Figure 35.
- 4) Framboidal pyrite transitioning to euhedral pyrite as shown in Figure 36.
- 5) Euhedral pyrite, as shown in Figure 37.

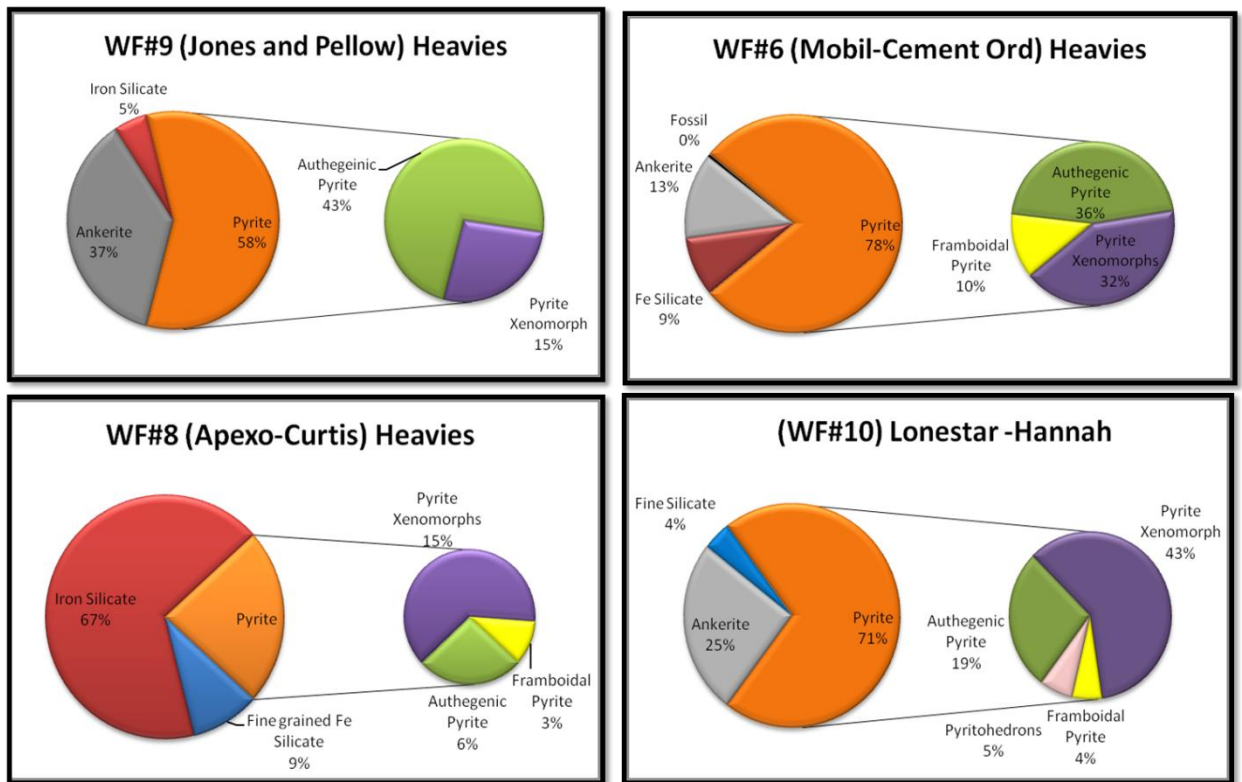


Figure 32. Pyrite distributions for four Woodford samples are shown in the smaller of the two pie charts.

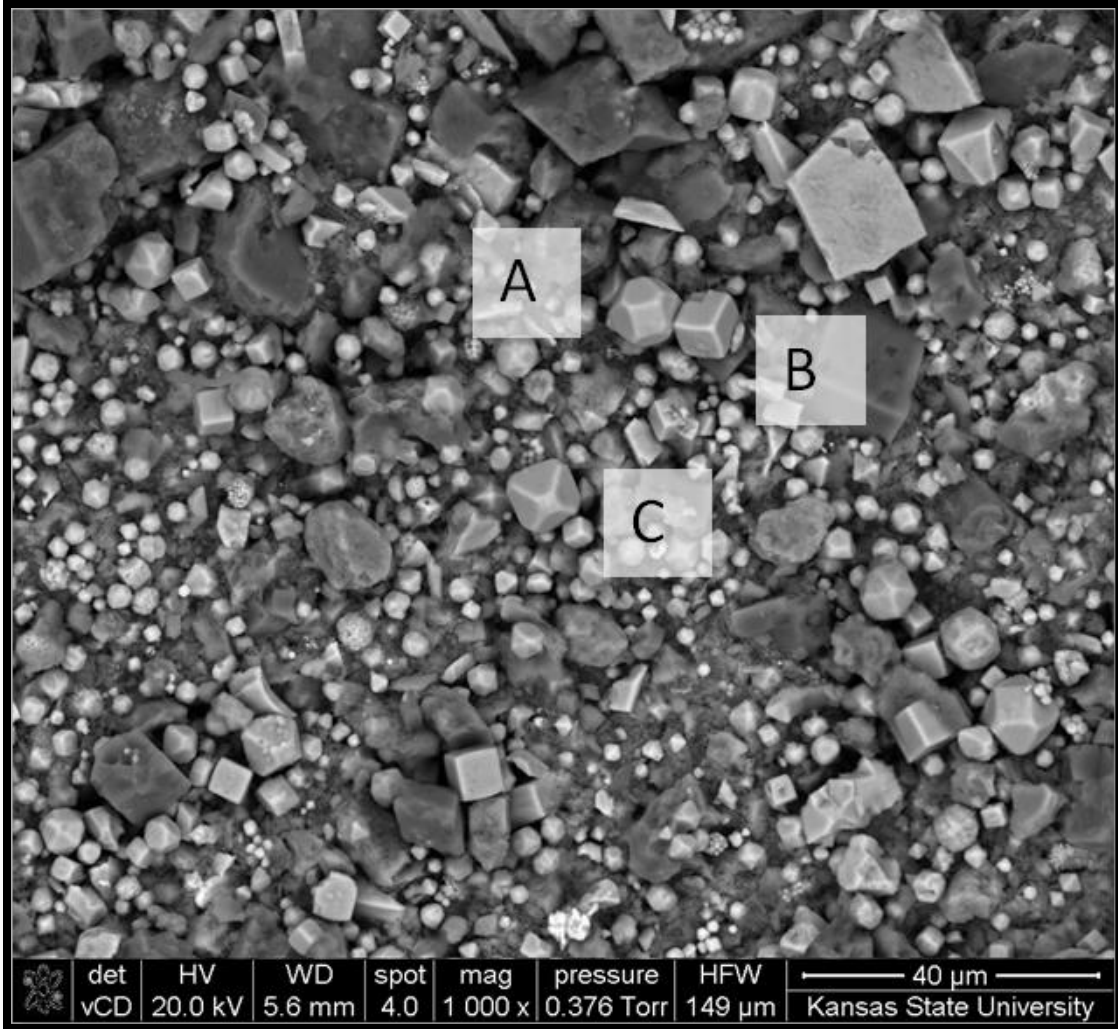


Figure 33. SEM photomicrograph of WF#10 Hannah showing Single euhedral crystals of pyrite. A) is the pyritohedron morphology, B) is cubic morphology, and C) is the octahedral morphology

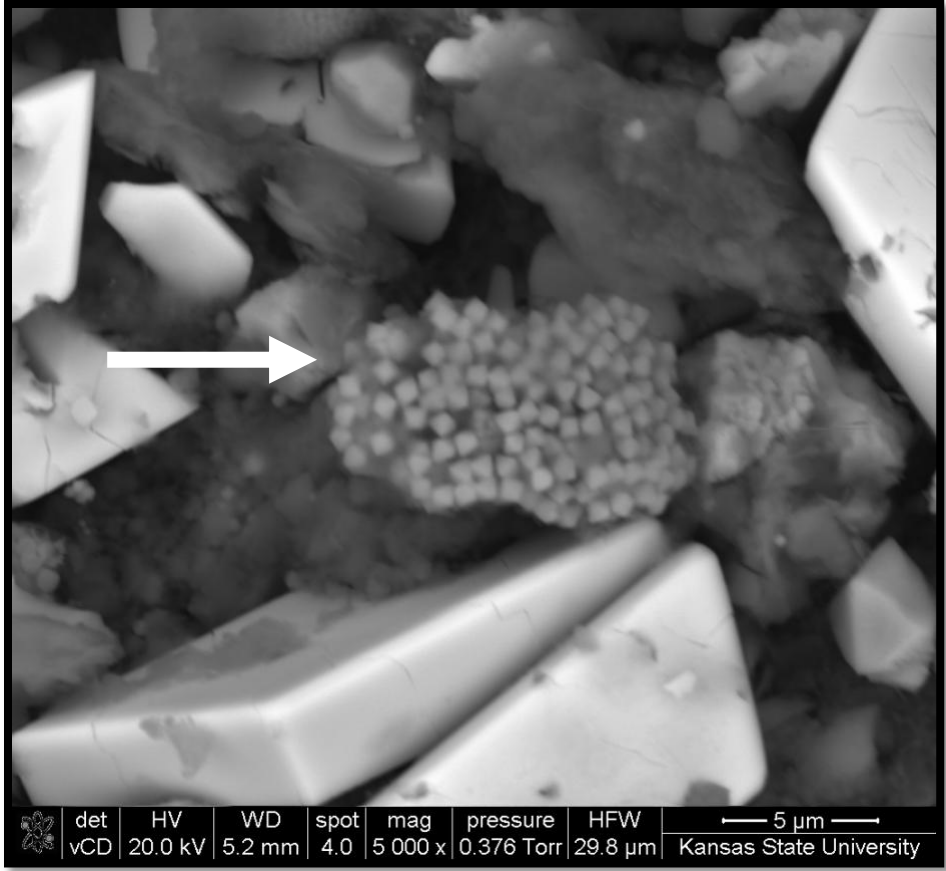


Figure 34. Photomicrograph of WF#3 Lela Rahm. The white arrow indicates the framboidal pyrite present in this sample.

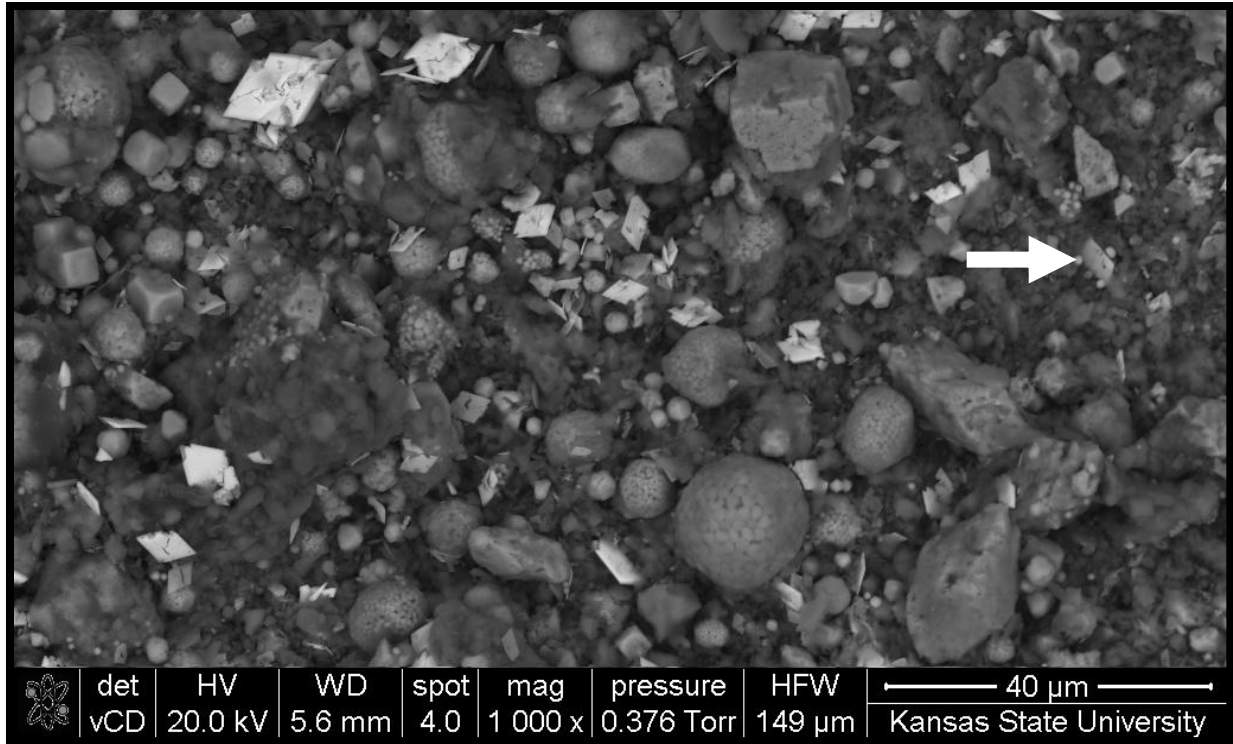


Figure 35. The white arrow in this figure is indicating single framboids of pyrite that are present in the WF#7 (Dwyer) sample.

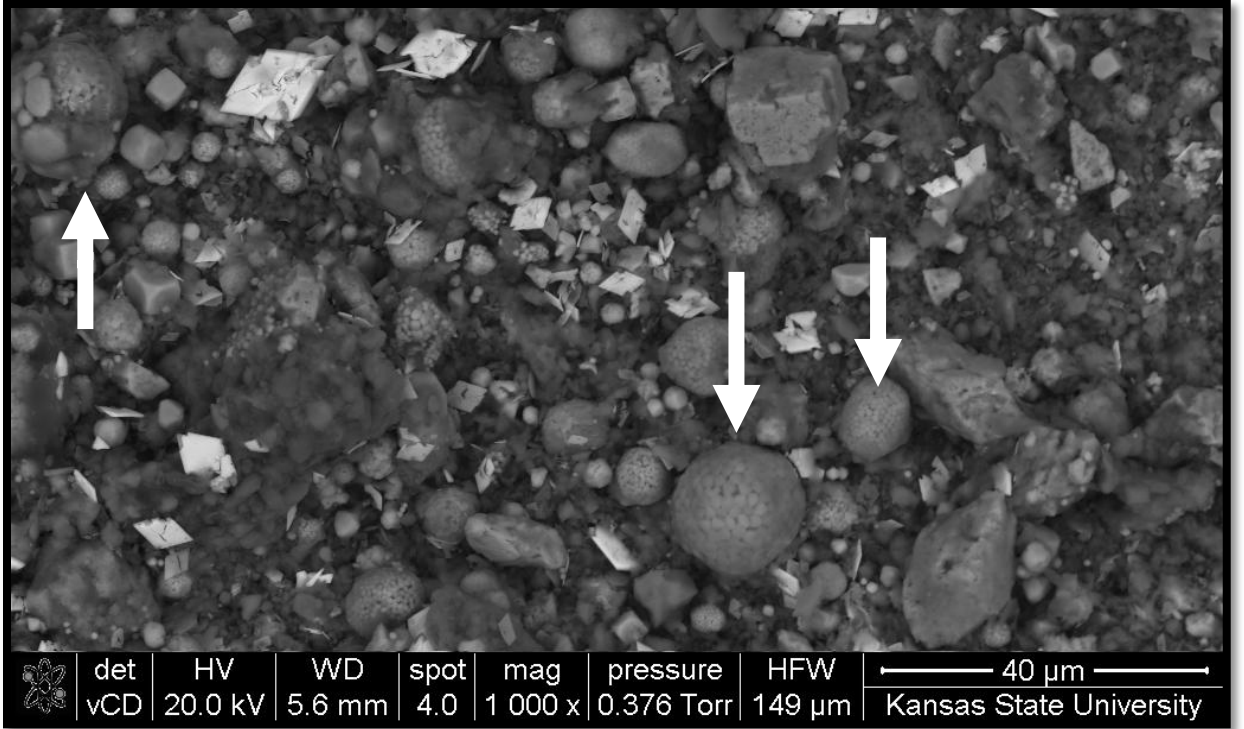


Figure 36. The white arrow in this figure indicates pyrite framboids that are transitioning to euhedral pyrite.

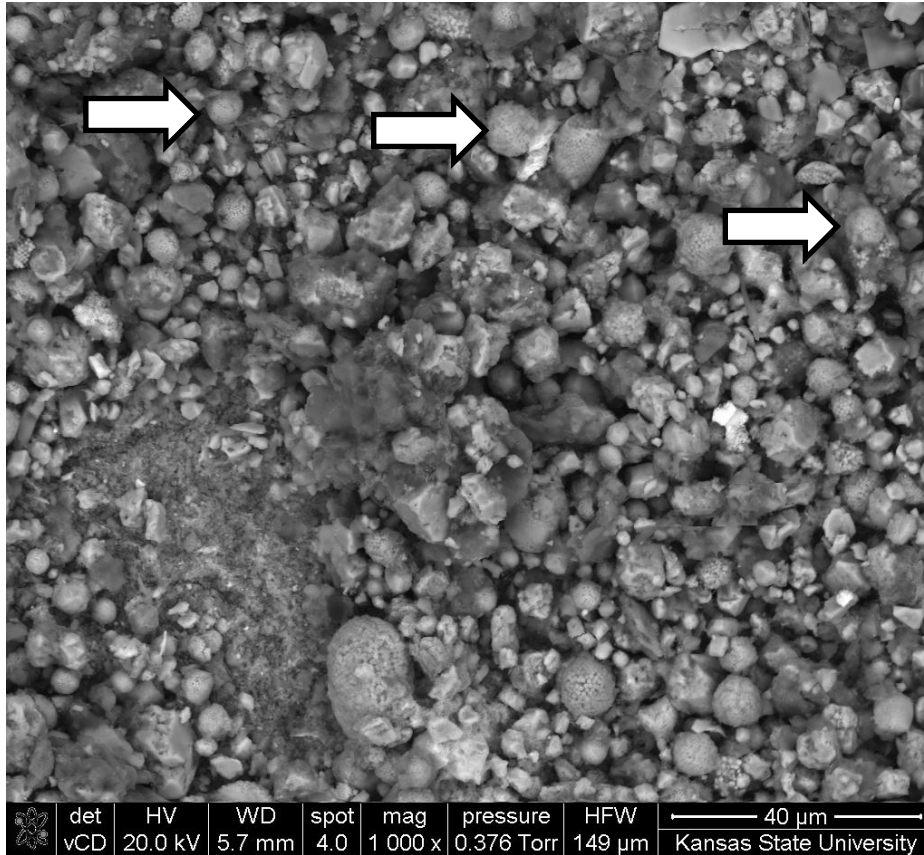


Figure 37. Example of the euhedral pyrite found in the Woodford Shale samples. From WF#6 (Cement Ord).

The Relationship Between Euhedral and Framboidal Pyrite

Love and Amstutz (1966) assumed that euhedral pyrite might represent the conversion of framboidal pyrite precursors. They mentioned the possibility of a complete conversion from framboidal pyrite to euhedral pyrite where no trace of framboids should be preserved. I believe that the pyrite in the Woodford samples show this conversion from framboidal pyrite. In figure 37 above, the framboids appear to have overgrown to the point where it is difficult to observe individual framboids. At first glance the framboid above appears to be a spherical pyrite ball. In this study, we found that euhedral pyrite increases as framboidal pyrite decreases. This is shown

in Figure 38.

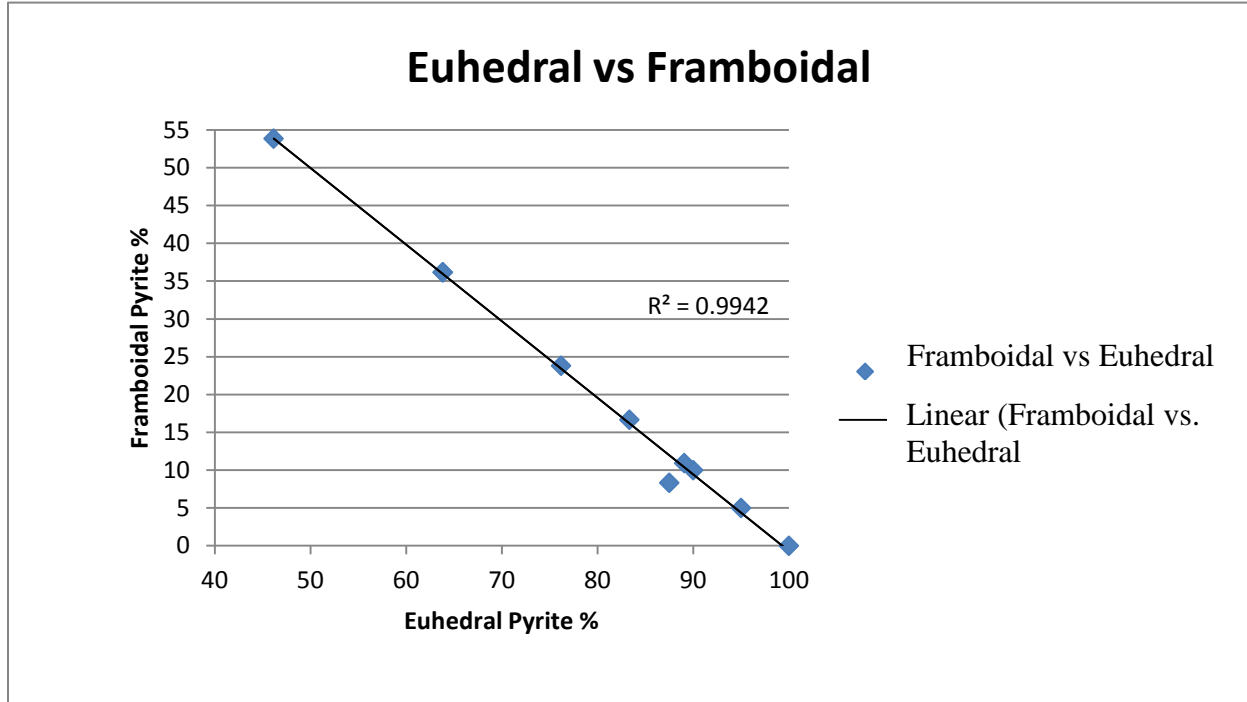


Figure 38. Graph showing the relationship between Euhedral and Framboidal Pyrite in the Woodford Shale samples.

The Sulfur Cycle

The majority of sulfur is found on Earth in rocks as salts or in its elemental form (S_8). Oceans and organic matter are the main sources of sulfur on Earth. Biological organisms play an important role in the formation of sulfur, inorganic forms of sulfur and sulfide minerals. These sulfur compounds change and move from soil, air and water in a process called the sulfur cycle (<http://water.me.vccs.edu/courses/ENV211/lesson17.htm>).

The first step in the sulfur cycle is the mineralization of organic sulfur into inorganic forms such as (H_2S), elemental sulfur (S_8) and sulfide minerals (including pyrite) (Bickle et. Al, 1994). This step occurs when organic-rich plant remains start to decompose and the sulfur

leaches into the soil (<http://water.me.vccs.edu/courses/ENV211/lesson17.htm>). The second occurs when the sulfur reacts with the oxygen and water in the soil and the organic sulfur oxidizes to form sulfate (SO_4^{-2}). The third step is the reduction of sulfate to sulfide. The final step is the incorporation of sulfide in organic compounds containing metal (Bickle et al., 1994).

Dissolved sulfate and hydrocarbons are thermodynamically unstable together in all diagenetic environments. Because of this instability, redox-reactions occur, where sulfate is reduced by hydrocarbons either biologically or thermochemically in a process called Dissimilative sulfate reduction. Biological sulfate reduction is called BSR and Thermochemical sulfate reduction is TSR (Machel, 2005). Thermochemical sulfate reduction (TSR) occurs at high temperature diagenetic environments (160-180 degrees C), and bacterial sulfate reduction (BSR) occurs over longer time periods (Tens of thousands of years) in low-temperature diagenetic environments (Machel, 2005). Figure 38 shows the temperature regimes for BSR and TSR as well as associated vitrinite reflectance values that occur for biodegradation, oil generation on gas generation.

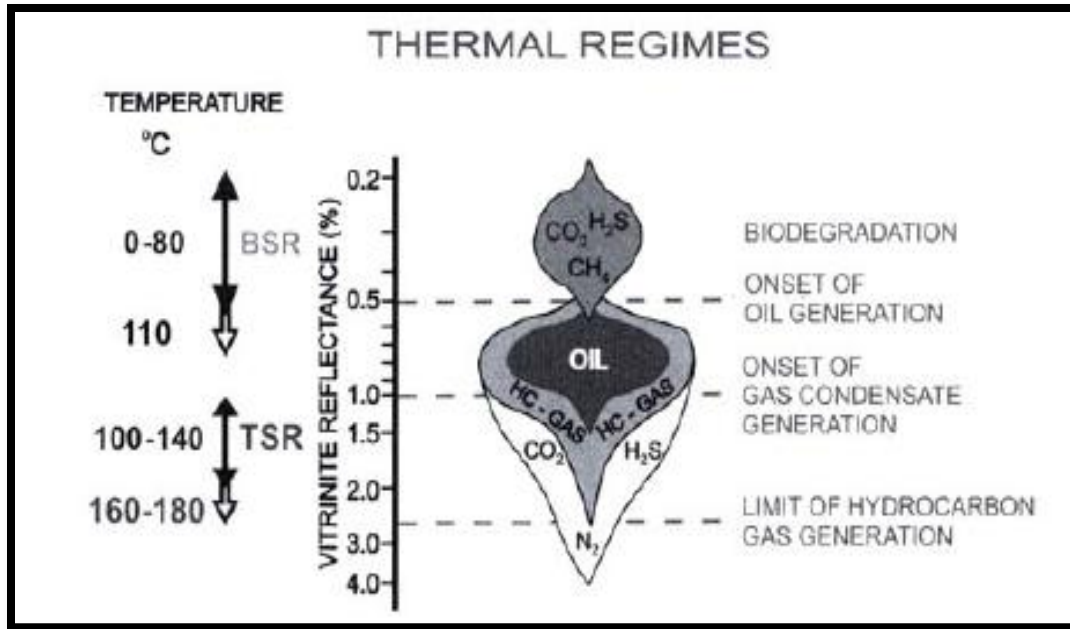


Figure 39. Diagram showing the different thermal regimes (BSR and TSR) and how they relate to vitrinite reflectance and oil and gas generation (Machel, 2005).

Heavy minerals as an Indicator of Thermal Maturity

The percent of heavy minerals present in the samples was compared to total organic carbon (TOC), vitrinite reflectance (Ro), Depth (ft) and location in the Anadarko basin, as well as REE variation from Ramirez. Table 10 shows the TOC values of the 10 Woodford Samples. Figure 40 shows the relationship between vitrinite reflectance (Ro) and the % of heavy minerals present in the Woodford Samples. From the graph it becomes noticeable that samples with higher % of heavy minerals are more thermally mature. WF#10-Hannah has the highest percentage (4.69) of heavy minerals and also has the highest vitrinite reflectance value (2.0). McCalla Ranch and Cement Ord also have higher percentages of heavy minerals and also have a higher thermal maturity than the other samples (1.25). There is an obvious trend apparent where samples with lower amounts of heavy minerals present have a low thermal maturity. It may be

suggested from this study that as a rock becomes over-mature the percentage of heavy minerals in the rock will increase. The R² value for this trend is .92 which makes it statistically probable.

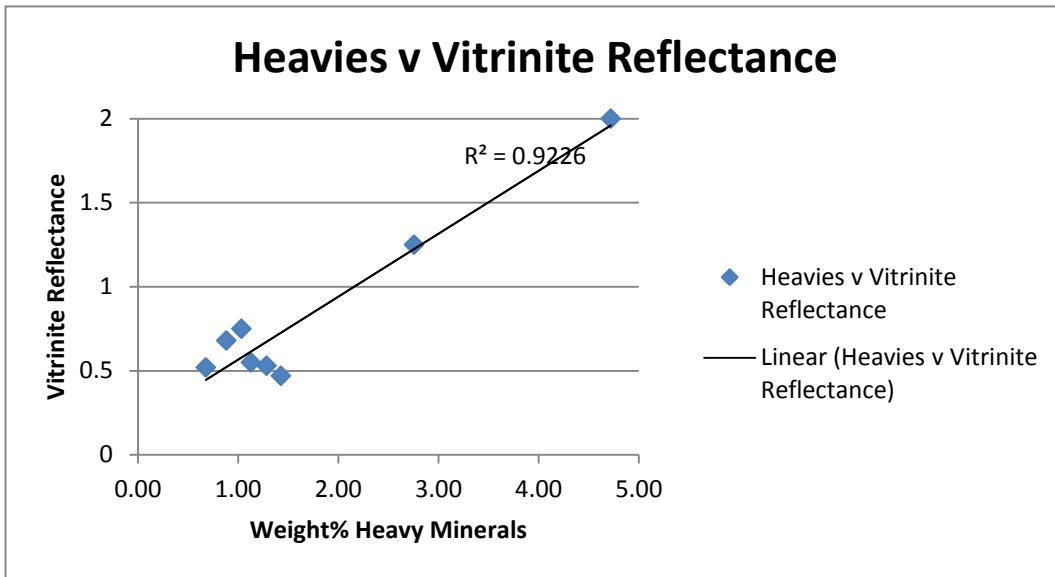


Figure 40. Graph showing the relationship between weight percent heavy minerals and vitrinite reflectance.

WELL NAME	LECO
	TOC
Shell McCalla Ranch WF#1	1.74
Mobil Sara Kirk WF#2	1.09
Mobil Rahm Lela WF#3	4.62
Shell Guthrie WF#4	6.51
Mobil Dwyer Mt WF#5	6.05
Mobil Cement Ord WF#6	6.54
Amerada Chenoweth WF#7	3.19
Apexco Curtis WF #8	11.50
Jones and Pellow WF#9	6.05
Lonestar Hannah WF#10	0.36

Table 13. TOC values for the Woodford Shale samples.

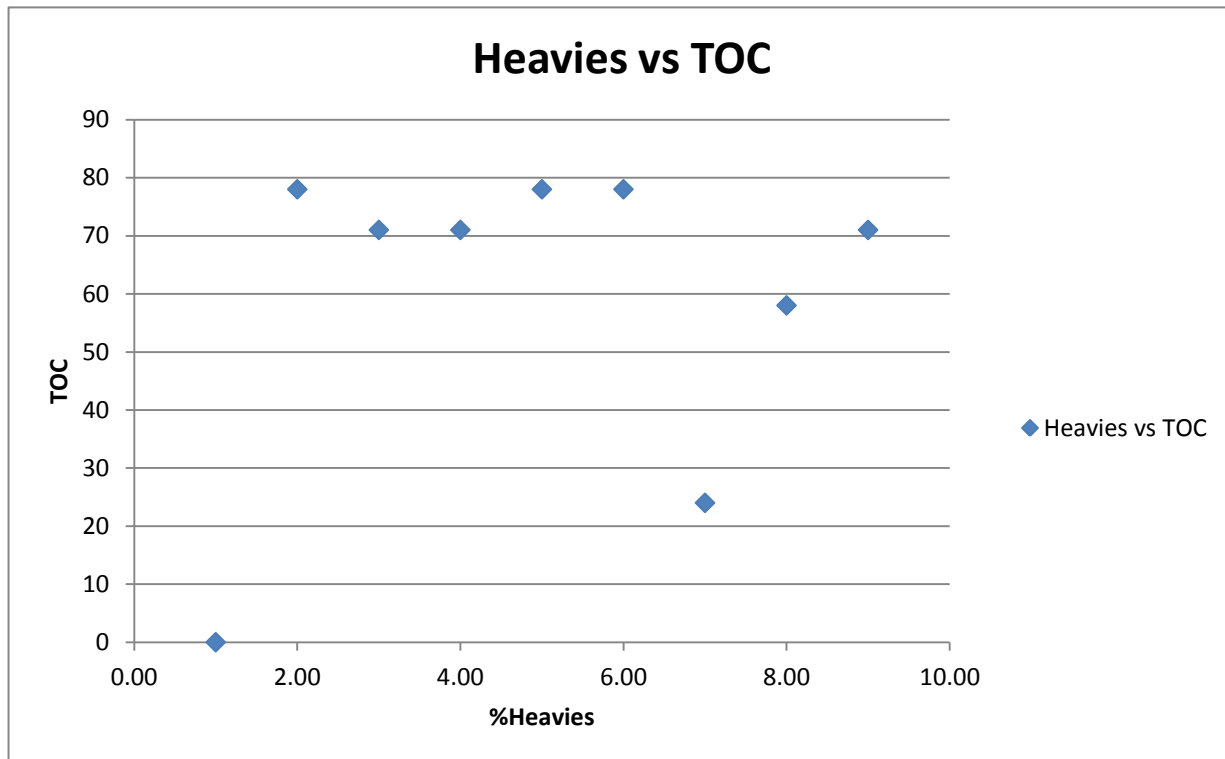


Figure 41. Graph showing the relationship between weight percent heavies and TOC.

The percentage of heavy minerals does not correlate with either depth (Figure 41) or TOC (Figure 42). It would appear that thermal maturity is controlling the release of both iron and sulfur, hence the growth of authigenic pyrite is the major contributor to heavy mineral percentages in the Woodford.

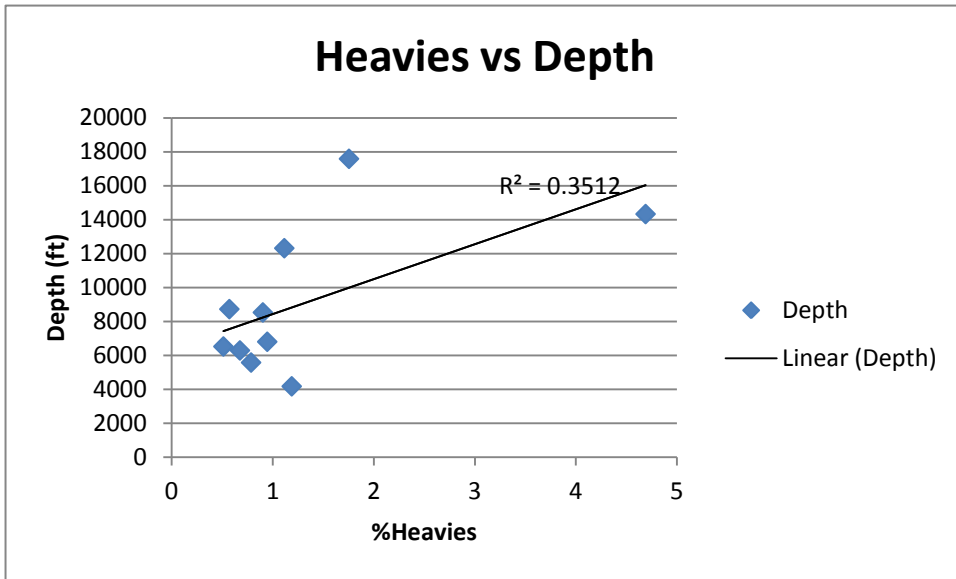


Figure 42. Graph showing the relationship between weight percent heavies and depth.

Chapter 6 - Conclusions

From this work, it may be suggested that a higher weight percent of heavy minerals, may be a sign of the onset of metagenesis, over-maturity and dry-gas generation. This can be concluded from comparing the relationship between vitrinite reflectance and the weight % of heavy minerals present in a sample. Lower weight percents of heavy minerals correspond to samples that have lower vitrinite reflectance values. A decrease in the amount of framboidal pyrite may also be a sign of the onset of metagenesis and over-maturity. As noted by Love and Amstutz (1966) and Soliman and Goresy (2012), framboidal pyrite seems to undergo a transition to rounded grains of euhedral pyrite. This work supports this claim.

References

- Adler, F. J. (1971). Anadarko basin and central Oklahoma area, in Future petroleum provinces of the United States – their geology and potential: AAPG Memoir 15 (2), 1061-1070.
- Amsden, T. W. (1975). Hunton Group (Late Ordovician, Silurian, and Early Devonian) in the Anadarko Basin of Oklahoma: Oklahoma Geological Survey Bulletin 121, 214 .
- (1983). Early and middle Paleozoic history of the Anadarko basin (abs.): Oklahoma Geology Notes, 43, 86.
- Bickle, M. J., Alt, J. C., Teagle, D. A. H., (1994). Sulfur transport and sulfur isotope fractionations in ocean floor hydrothermal systems: Mineralogical Magazine, 58A, 88-89.
- Blatt, Harvey, and B. Sutherland (1969). Intrastratal Solution and Non-opaque Heavy Minerals in Mudrocks. Journal of Sedimentary Petrology 39, 591-600.
- Blatt, Harvey, and Matthew W. Totten (1981). Detrital Quartz as an Indicator of Distance from Shore in Marine Mudrocks. Journal of Sedimentary Petrology, 51.
- Blatt, Harvey and Middleton, G.V., and Murray, R.C (1980). Origin of Sedimentary Rocks, 2, 782.
- Brewer, J. A., R. Good, J. E. Oliver, L. D. Brown, and S. Kaufman (1983). COCORP profiling across the southern Oklahoma aulacogen: overthrusting of the Wichita Mountains and compression within the Anadarko basin: Geology, 11, 109-114.
- Burke, K. (1977). Aulacogens and continental breakup: Annual Review of Earth and Planetary Sciences, 5, 371-396.
- Cardott, B. J. (2009). Overview of Woodford Gas-Shale Play in Oklahoma." *Woodford Gas Shale Conference*. Oklahoma Geological Survey, 23 May 2007.
- Cardott, B. J., and Lambert, M.W., (1985). Thermal Maturation by Vitrinite Reflectance of Woodford Shale, Anadarko Basin, Oklahoma. American Association of Petroleum Geologists Bulletin, 69(11), 1982-2998.
- Comer, J.B., and Hinch, H.H., (1987). Recognizing and quantifying expulsion of oil from the Woodford Formation and age-equivalent rocks in Oklahoma and Arkansas: AAPG Bulletin, v. 71, No. 7, p 844-858.
- Comer, J.B. (2005). Facies Distributions and Hydrocarbon Production Potential of Woodford Shale in the Southern Midcontinent. In Cardott (ed.) Unconventional Energy Resources in the Southern Midcontinent, 2004 Symposium. Oklahoma Geological Survey Circular 110, 51-62.

- Comer, J. B. (2008a). Reservoir Characteristics and Production Potential of the Woodford Shale. *World Oil* 229.
- Comer, J.B. (2008b). Woodford Shale in Southern Midcontinent, USA – Transgressive System Tract Marine Source Rocks on an Arid Passive Continental Margin with Persistent ocean Upwelling. American Association of Petroleum Geologists Annual Convention, San Antonio, Texas. Poster presentation.
- Comer, J. B. (2012). Organic Geochemistry and Paleogeography of Upper Devonian Formations in Oklahoma and Northwestern Arkansas. In Johnson and Cardott (eds.) *Source Rocks in the Southern Midcontinent, 1990 Symposium*. Oklahoma Geological Survey Circular 93, 70-93.
- Conant, L. C., and Swanson, V.E. (1961). Chattanooga Shale and related rocks of central Tennessee and nearby areas: U.S. Geological Survey Professional Paper 357, 91.
- Denison, R. E (1982). Geologic cross section from the Arbuckle Mountains to the Muenster arch, southern Oklahoma and Texas: GSA Map and Chart Series MC-28R, 1 sheet, 8 p.
- Energy Information Administration (EIA) (2011a) Shale Gas is a Global Phenomenon. *Today in Energy*, <http://www.eia.gov/todayinenergy/detail.cfm?id=811>, accessed Jan 24, 2013.
- Feinstein, S. (1981). Subsidence and thermal history of southern Oklahoma aulacogen: implications for petroleum exploration: *AAPG Bulletin*, 65, 2521-2533.
- Fritz, R.D., M.K. Horn, and S.D. Joshi, (1991). *Geological Aspects of Horizontal Drilling*, Tulsa: AAPG, 563 p.
- Garner, D. L., and Turcotte, D.L. (1984). The thermal and mechanical evolution of the Anadarko basin: *Tectonophysics*, 107, 1-24.
- Gaswirth and Higley (2012) in Gaswirth and Higley (2013). Petroleum system analysis of the Hunton Group in West Edmond Field, Oklahoma. *AAPG Bulletin*.
- Gilbert, M. C. (1982). Geologic setting of the eastern Wichita Mountains, with a brief discussion of unresolved problems, in M.C. Gilbert and R. N. Donovan eds., *Geology of the eastern Wichita Mountains, southwestern Oklahoma: Oklahoma Geological Survey Guidebook* 21, 1-30.
- (1983). Timing and chemistry of igneous events associated with the southern Oklahoma aulacogen: *Tectonophysics*, 94, 439-455.
- Goldschmidt, V.M. (1933). *Grundlagen der quantitativen Geochemie. – Fortschr. Miner. Kristallogr. Petrogr.*, 17, 112.

- Ham, W. E., and J. L. Wilson (1967). Paleozoic epeirogeny and orogeny in the central United states: *American Journal of Science*, 265 (5), 332-407.
- R. E. Denison, and C.A. Merrit (1964). Basements rocks and structural evolution of southern Oklahoma: *Oklahoma Geological survey Bulletin* 95, 302.
- Hanan, M.A., and Totten, M.W., (1996). Analytical Techniques For the Separation and SEM Identification of Heavy Minerals in Mudrocks. *Journal of Sedimentary Research* 66.5, 1027-1030.
- Hoffman, P., J. F. Dewey, and K. Burke (1974). Aulacogens and their genetic relation to geosynclines, with a Proterozoic example from Great Slave lake, Canada, in *Modern and ancient geosynclinal sedimentation: SEPM Special Publication* 19, 38-55.
- Johnson, K. S., and B. J. Cardott (1992). Geologic Framework and Hydrocarbon Source Rocks of Oklahoma. *Oklahoma Geological Survey Circular* ,93 (21), 37..
- Johnson, K. S., Amsden, T.W., Denison, R.E., Goldstein, A.G., Dutton, S.P., Rascoe, J.B., Sutherland, P.K., and Thompson, C.M. (1989). *Geology of the Southern Midcontinent. Oklahoma Geological Survey Special Publication*, 89, (2), 1-53.
- Keller, G. R., Lidiak, E.G., Hinze, W.J., and Braile, L.W., (1983). The role of rifting in the tectonic development of the Midcontinent, U.S.A.: *Tectonophysics*, 94, 391 -412.
- Kirkland, D.W., Denison, R.E., Summers, D.M., and Gormly, J.R., (1992). *Geology and Organic Geochemistry of the Woodford Shale in the Criner Hills and Western Arbuckle Mountains, Oklahoma. Oklahoma Geological Survey Circular* 93, 38-69.
- Kuuskräa, V. (2011). *Economic and Market Impacts of Abundant Shale Gas Resources. Advance Resources International*, 2011.
- Lambert, M.W., (1990). Internal Stratigraphy of the Chattanooga Shale in Kansas and Oklahoma, in Johnson, K.S. and B.J. Cardott (eds.) *Source Rocks in the Southern Midcontinent, 1990 symposium: Oklahoma Geological Society Circular* 93, 94-103.
- Love, L.G., and Amstutz, G.C., (1966). Review of Microscopic Pyrite From the Devonian Chattanooga Shale and Rammelsberg Banderz, *Fortschr. Mineral.* 43, 273-309.
- Machel, H.G., (2005). *Investigations of Burial Diagenesis in Carbonate Hydrocarbon Reservoir Rocks. Geoscience Canada*, 32(3).
- Miceli, A. (2010). *Geochemical Characterization of the Woodford Shale, Central and Southeastern Oklahoma. Thesis. University of Oklahoma*, 2010. University of Oklahoma, 2010.

- Soliman, M.F., and Gorse, A.E., (2012). Framboidal and Idiomorphic Pyrite in the Upper Maastrichtian Sedimentary Rocks at Gabel Oweina, Nile Valley, Egypt: Formation Processes, Oxidation Products and Genetic Implications to the Origin of Framboidal Pyrite. *Geochimica et Cosmochimica*, 90, 195-220.
- Northcutt, R.A., and Campbell, J.A., (1995). Abstract: Geologic Provinces of Oklahoma, by R. A. Northcutt and J. A. Campbell; #90957. AAPG.
- Portas, R. (2009). Characterization and Origin of Fracture Patterns in the Woodford Shale in Southeastern Oklahoma for Application to Exploration and Development. Thesis. University of Oklahoma, 2009.
- Potter, P.E., Maynard, J.B., and Pryor, W.A. (1980). *Sedimentology of Shale*. Springer Verlag, New York.
- Powell, B. N., and J. F. Fischer (1976). Plutonic igneous geology of the Wichita magmatic province, Oklahoma: Oklahoma Geological Survey Special Publication 76(1), 35.
- Rankin, D.W. (1976). Appalachian salients and recesses: Late Precambrian continental breakup and the opening of the Iapetus Ocean: *Jour. Geophys. Res.*, 81, 5605-5619.
- Ramirez-Caro, D. (2013). Rare Earth Elements (REE) as Geochemical Clues to Reconstruct Hydrocarbon Generation History. Thesis. Kansas State University Graduate School, 2013. Manhattan. Kansas State University.
- Robert, P. (1980). The optical evolution of kerogen and geothermal histories applied to oil and gas exploration, in B. Durand, ed., *Kerogen insoluble organic matter from sedimentary rocks*. 385-414.
- Shatski, N. S. (1946). The Great Donetz basin and the Wichita System, comparative tectonics of ancient platforms: *Akademiya Nauk SSSR Izvestiya Seriya Geologicheskaya*, 6, 57-90.
- Slatt, R. M., Buckner, N., Abousleiman, Y., Sierra, R., Philp, P., Miceli-Romera, A., Portas, R., O'Brien, N., Tran, M., Davis, R., and Wawrzyniec, T., (2010). Multiscale Characterization of the Woodford Gas Shale, Oklahoma. *Shale Reservoirs—Giant Resources for the 21st Century*, AAPG Memoir 97, 1-21.
- Sorenson R.P., (2005). A dynamic model for the Permian Panhandle and Hugoton fields, Western Anadarko Basin: AAPG bulletin, 89, 921-938
- Sullivan, K.L., (1983). Organic facies variation of the Woodford Shale in western Oklahoma: Master's thesis, University of Oklahoma, Norman, Oklahoma, 101 p.

- Totten, M.W., and Hanan, M.A., (1998). The Accessory-Mineral Fraction of Mudrocks and Its Significance for Whole-rock Trace-element Geochemistry, *Petrography*.
- Totten, M.W., and Hanan, M.A., (2007). Heavy Minerals in Shales. *Developments in Sedimentology*, 58, 323-341.
- Totten, M.W., and Hanan, M.A., (1998). The Accessory-Mineral Fraction of Mudrocks and Its Significance for Whole-rock Trace-element Geochemistry. *Shales and Mudstones II*, 35-53.
- Totten, M.W., Jr. (2011). Electron Probe Micro-Analysis of the Woodford Shale, South Central, Oklahoma. Thesis. University of Oklahoma Graduate College, 2011. Norman: University of Oklahoma.
- Walper, J. L. (1976). The geotectonic evolution of the Wichita aulacogen, Oklahoma, in G. E. Henry, ed. (2011), *Basins of the Southwest, phase 2: North Texas Geological Society*, 192-211.
- Webster, R. E. (1977). Evolution of a major petroleum province: the southern Oklahoma aulacogen: *Compass of Sigma Gamma Epsilon*, 54, 59-71.

Appendix A - Photomicrographs and EDS Spectra

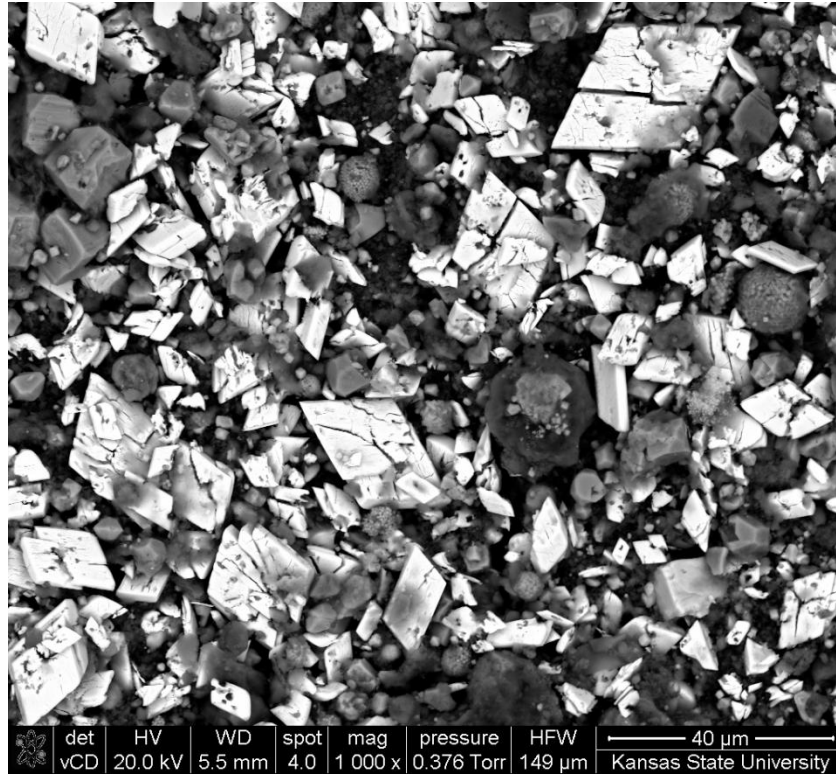


Figure A.1. Heavy minerals in sample WF#1 McCalla Ranch.

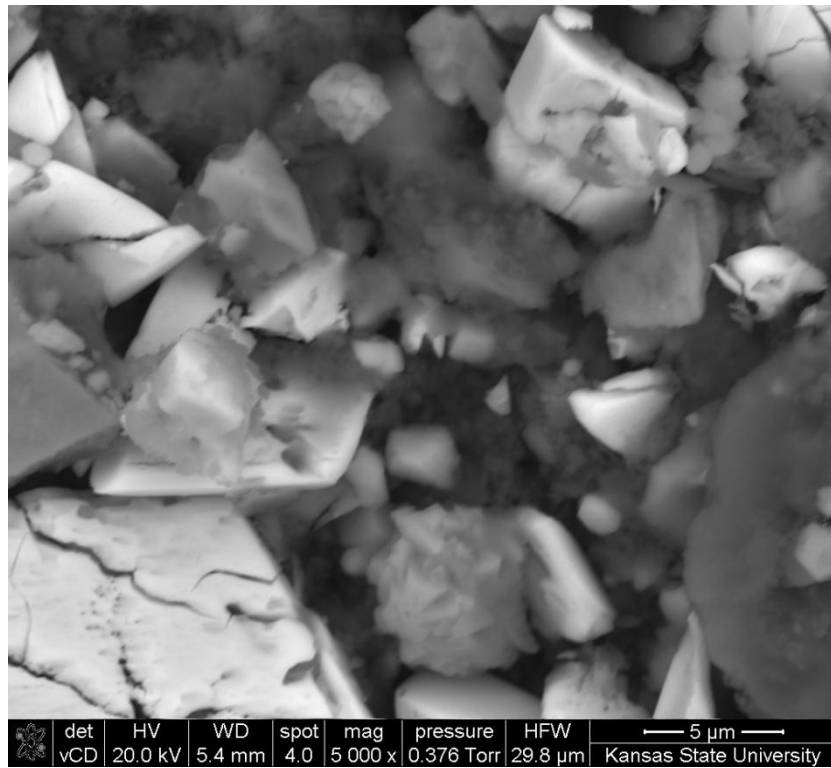


Figure A.2. Heavy minerals in sample WF#1 McCalla Ranch.

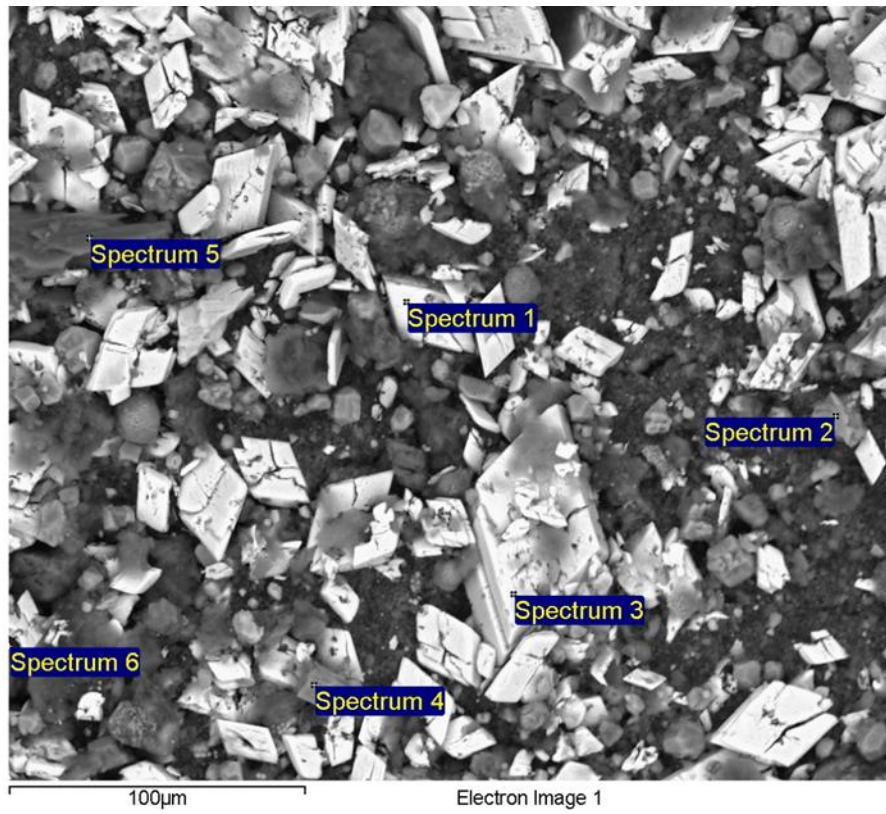


Figure A.3. Locations for the EDS spectra shown in Figure A.4.

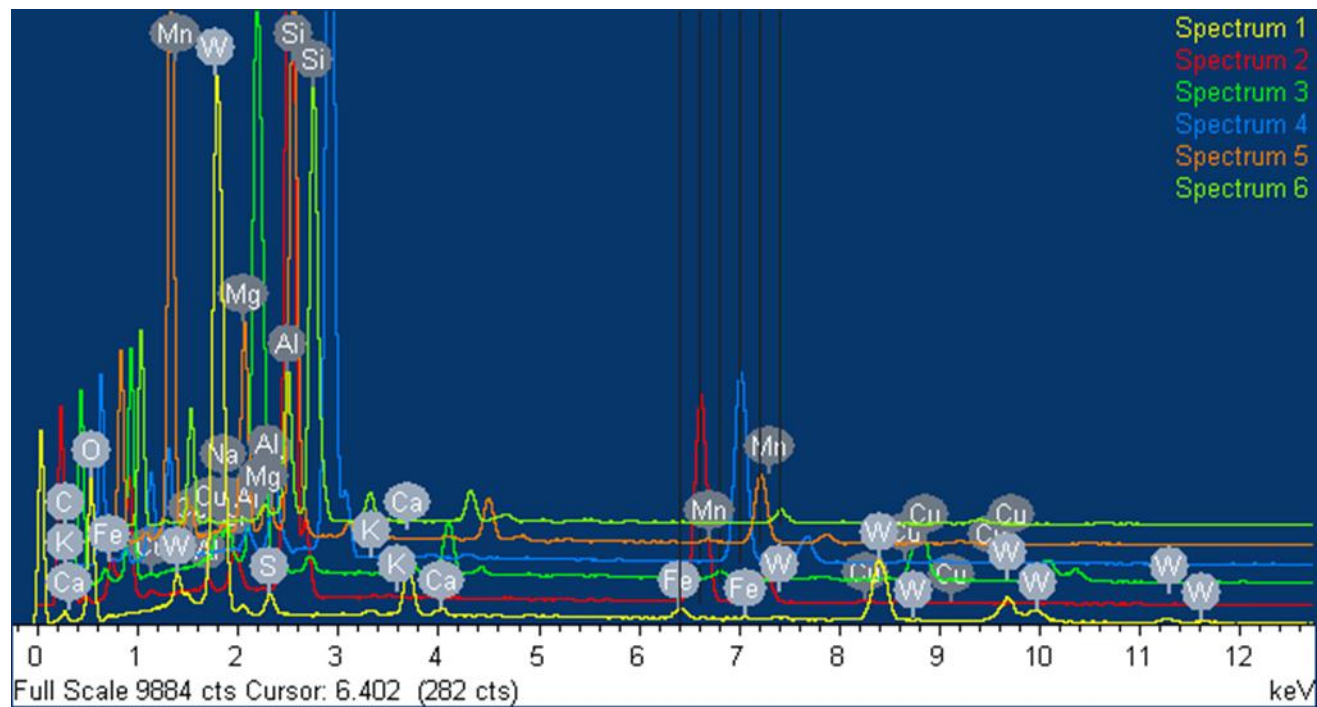


Figure A.4. EDS spectra for WF#1 McCalla Ranch sample locations.

Spectrum 1			Spectrum 2			Spectrum 3		
Element	Weight%	Atomic%	Element	Weight%	Atomic%	Element	Weight%	Atomic%
C K	2.63	8.61	C K	8.07	20.13	C K	3.5	9.75
O K	29.03	71.28	O K	9.76	18.29	O K	35.45	74.2
S K	1.28	1.57	Al K	0.51	0.57	Al K	1.14	1.42
K K	0.36	0.36	Si K	1.01	1.08	S K	0.79	0.82
Ca K	3.97	3.89	S K	44.05	41.16	K K	0.51	0.44
Fe K	1.79	1.23	Fe K	33.64	18.05	Ca K	3.49	2.92
W M	60.94	13.02	Cu K	0.76	0.36	Fe K	1	0.6
Total	100	99.96	W M	2.2	0.36	W M	54.13	9.86
			Total	100	100	Total	100.01	100.01

Spectrum 4			Spectrum 5			Spectrum 6		
Element	Weight%	Atomic%	Element	Weight%	Atomic%	Element	Weight%	Atomic%
C K	12.58	27.13	C K	4.72	7.78	C K	6.63	12.61
O K	16.83	27.26	O K	54.61	67.5	O K	35.21	50.3
Al K	0.82	0.78	Na K	0.47	0.4	Mg K	0.9	0.85
Si K	1.87	1.72	Mg K	7.3	5.93	Al K	8.47	7.17
S K	36.28	29.32	Al K	1.88	1.38	Si K	26.57	21.62
Fe K	28.44	13.19	Si K	17.23	12.13	S K	2.9	2.07
Cu K	0.53	0.22	S K	0.52	0.32	K K	3.47	2.03
W M	2.66	0.38	K K	0.14	0.07	Ca K	0.68	0.39
Total	100.01	100	Ca K	1.98	0.98	Fe K	3.81	1.56
			Mn K	0.32	0.12	W M	11.36	1.41
			Fe K	8.68	3.08	Total	100	100.01
			Cu K	0.41	0.13			
			W M	1.74	0.19			
			Total	100	100.01			

Figure A.5. Elemental, weight percent and atomic percent data for WF#1 McCalla Ranch.

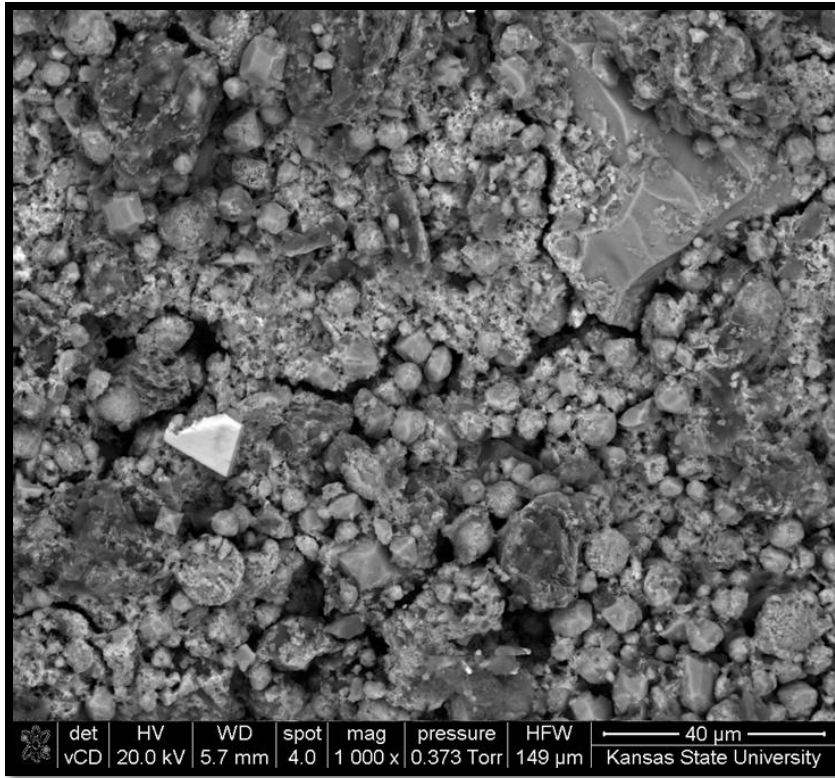


Figure A.6. Heavy minerals in sample WF#3 Lela Rahm.

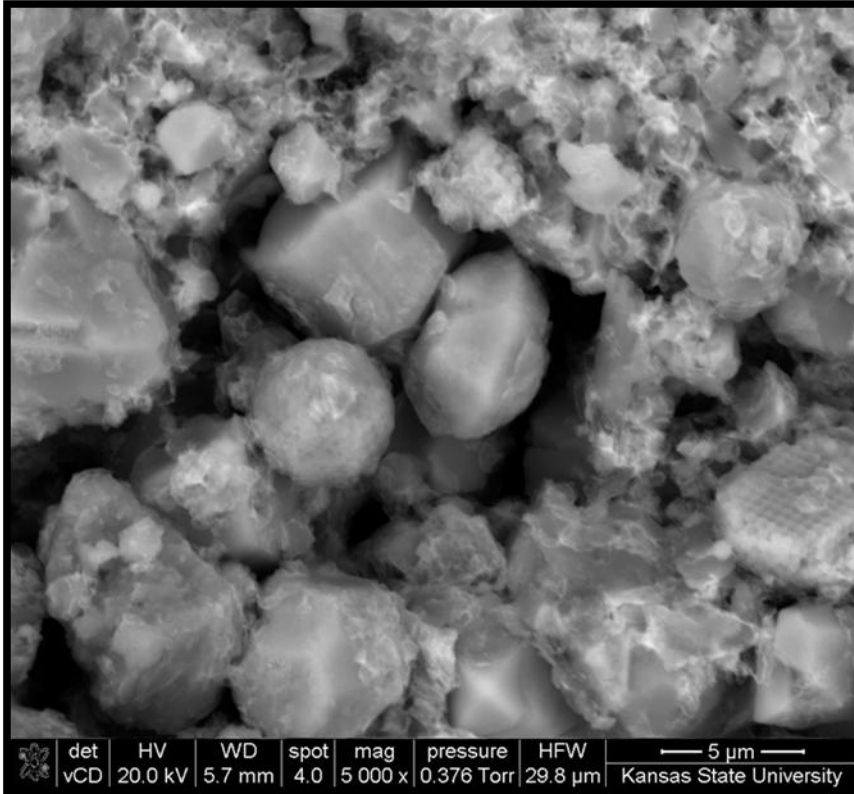


Figure A.7. Heavy minerals in sample WF#3 Lela Rahm.

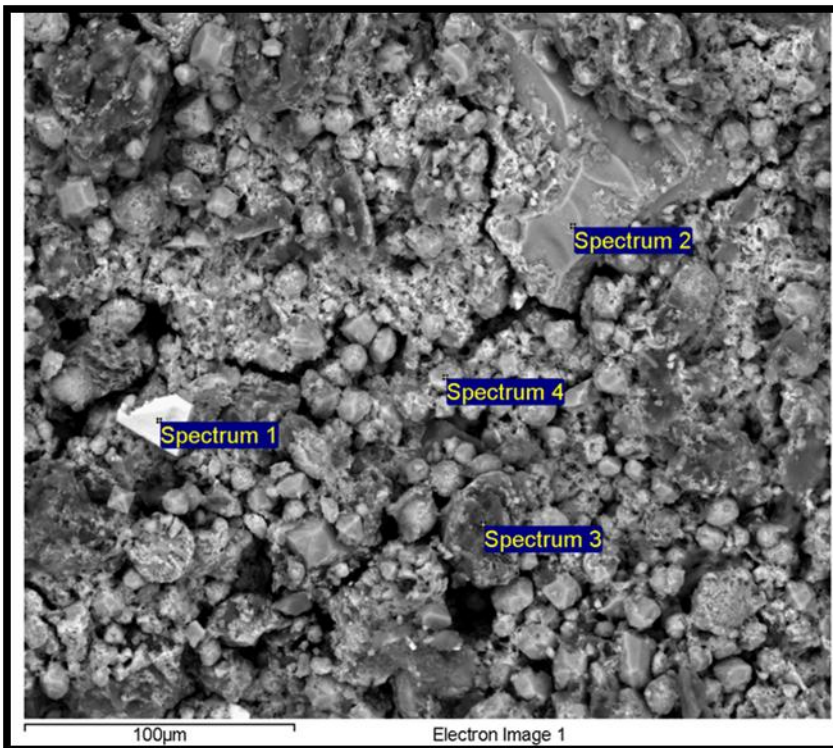


Figure A.8. Locations for the EDS spectra shown in Figure A.9.

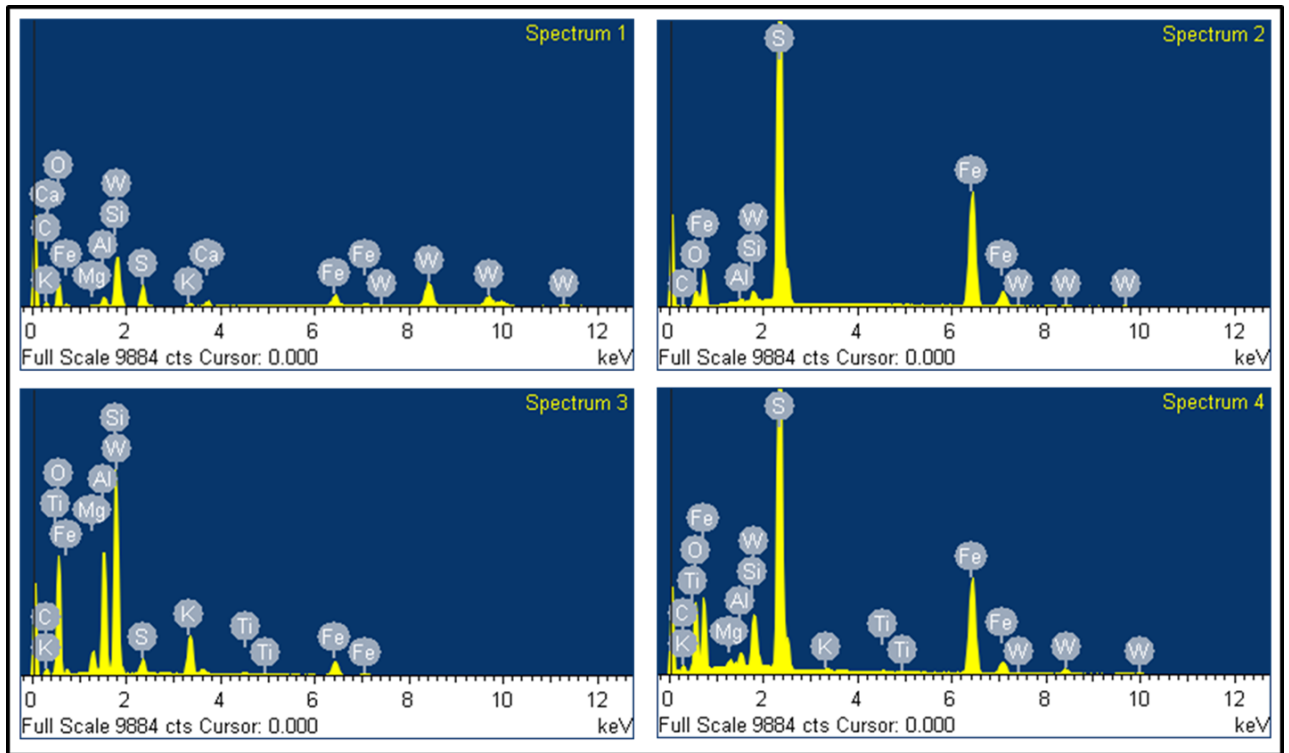


Figure A.9. EDS spectra for WF#3 Lela Rahm sample locations.

Spectrum 1			Spectrum 2		
Element	Weight%	Atomic%	Element	Weight%	Atomic%
C K	14.93	30.33	C K	5.08	13.93
O K	30.27	46.14	O K	6.79	13.98
Mg K	0.6	0.6	Al K	0.36	0.44
Al K	2.39	2.16	Si K	0.65	0.77
Si K	5.15	4.47	S K	45.5	46.73
S K	8.16	6.2	Fe K	40.69	23.99
K K	1.01	0.63	W M	0.92	0.17
Ca K	2.39	1.46	Total	99.99	100.01
Fe K	11.06	4.83			
W M	24.06	3.19			
Total	100.02	100.01			

Spectrum 3			Spectrum 4		
Element	Weight%	Atomic%	Element	Weight%	Atomic%
C K	9.69	15.91	C K	8.81	19.4
O K	45.19	55.7	O K	22.27	36.81
Mg K	2.15	1.74	Mg K	0.51	0.55
Al K	10.22	7.47	Al K	0.81	0.79
Si K	18.82	13.21	Si K	1.36	1.29
S K	1.72	1.06	S K	33.88	27.95
K K	5.34	2.69	K K	0.27	0.18
Ti K	0.32	0.13	Ti K	0.22	0.12
Fe K	5.67	2	Fe K	25.26	11.96
W M	0.89	0.1	W M	6.61	0.95
Total	100.01	100.01	Total	100	100

Figure A.10. Elemental, weight percent and atomic percent data for WF#3 Lela Rahm.

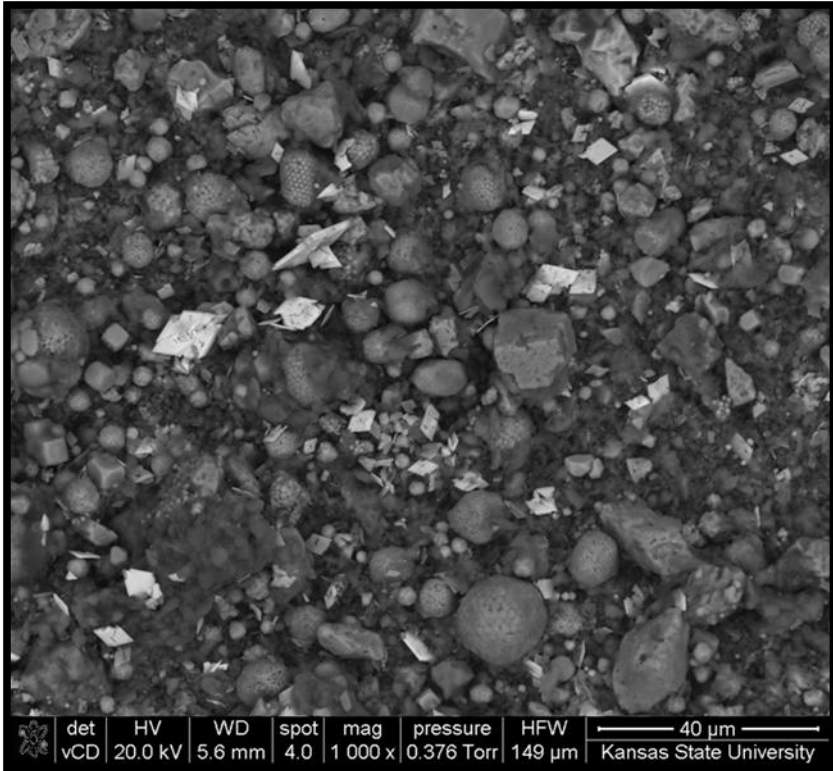


Figure A.11. Heavy minerals in sample WF#5 Dwyer.

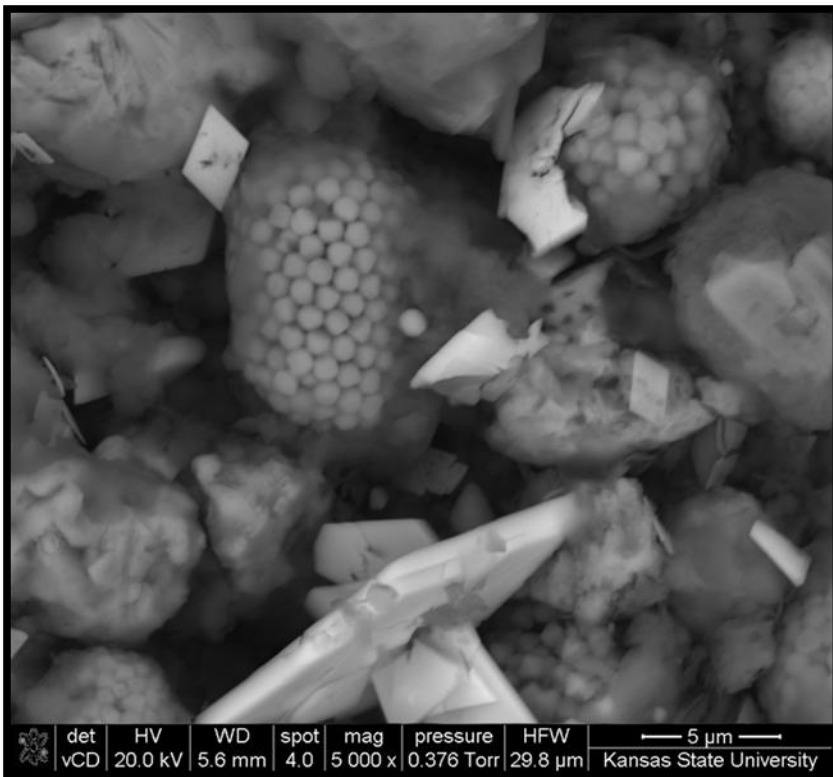


Figure A.12. Heavy minerals in sample WF#5 Dwyer.

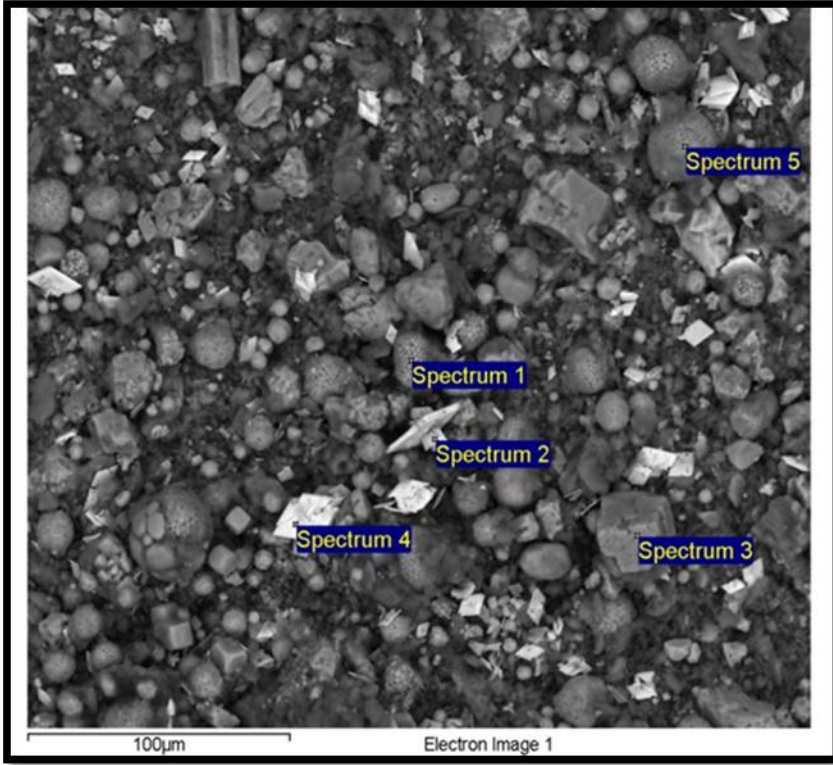


Figure A.13. Locations for the EDS spectra shown in Figure A.14.

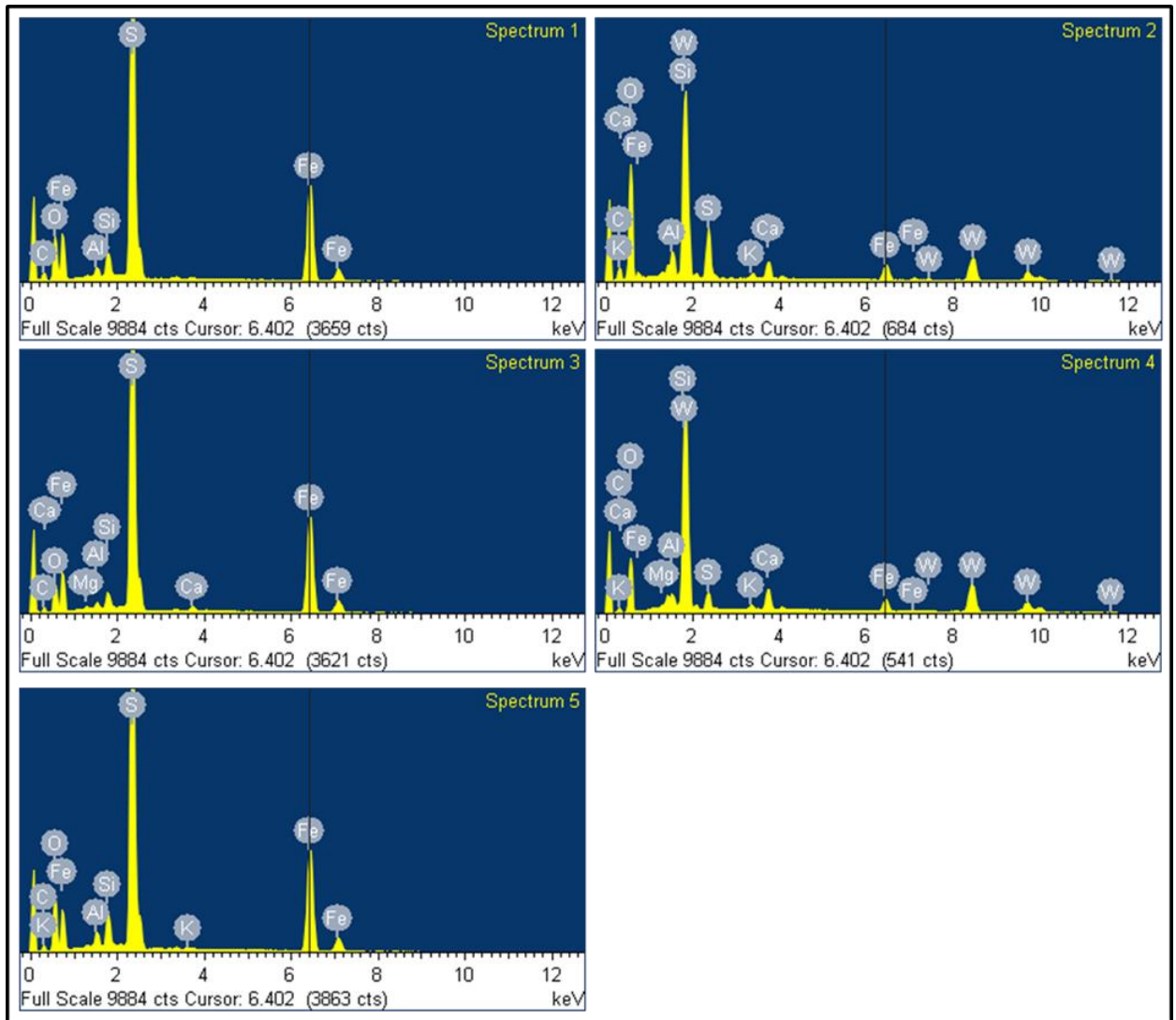


Figure A.14. EDS spectra for WF#5 Dwyer sample locations.

Spectrum 1			Spectrum 2			Spectrum 3		
Element	Weight%	Atomic%	Element	Weight%	Atomic%	Element	Weight%	Atomic%
C K	14.28	29.57	C K	9.77	20.82	C K	10.81	24.53
O K	17.52	27.24	O K	38.3	61.27	O K	13.64	23.24
Al K	0.69	0.63	Al K	1.58	1.5	Mg K	0.35	0.4
Si K	1.72	1.52	Si K	3.26	2.97	Al K	0.42	0.43
S K	35.48	27.53	S K	5.75	4.59	Si K	1.3	1.26
Fe K	30.31	13.5	K K	0.64	0.42	S K	39.05	33.21
Total	100	99.99	Ca K	2.25	1.44	Ca K	0.68	0.46
			Fe K	5.12	2.35	Fe K	33.75	16.48
			W M	33.32	4.64	Total	100	100.01
			Total	99.99	100			

Spectrum 4			Spectrum 5		
Element	Weight%	Atomic%	Element	Weight%	Atomic%
C K	3.87	12.07	C K	10.29	22.08
O K	26.21	61.36	O K	19.56	31.53
Mg K	0.38	0.59	Al K	1	0.96
Al K	1.07	1.49	Si K	2.31	2.12
Si K	1.96	2.62	S K	36.22	29.13
S K	3.07	3.59	K K	0.22	0.14
K K	0.65	0.62	Fe K	30.41	14.04
Ca K	3.68	3.44	Total	100.01	100
Fe K	4.68	3.14			
W M	54.42	11.09			
Total	99.99	100.01			

Figure A.15. Elemental, weight percent and atomic percent data for WF#5 Dwyer.

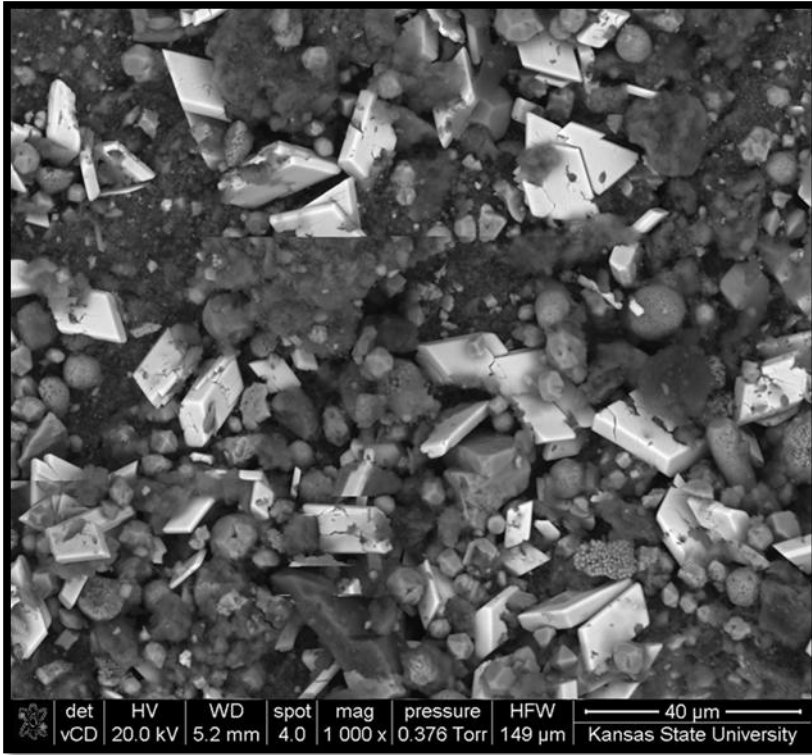


Figure A.16. Heavy minerals in sample WF#7 Chenoweth.

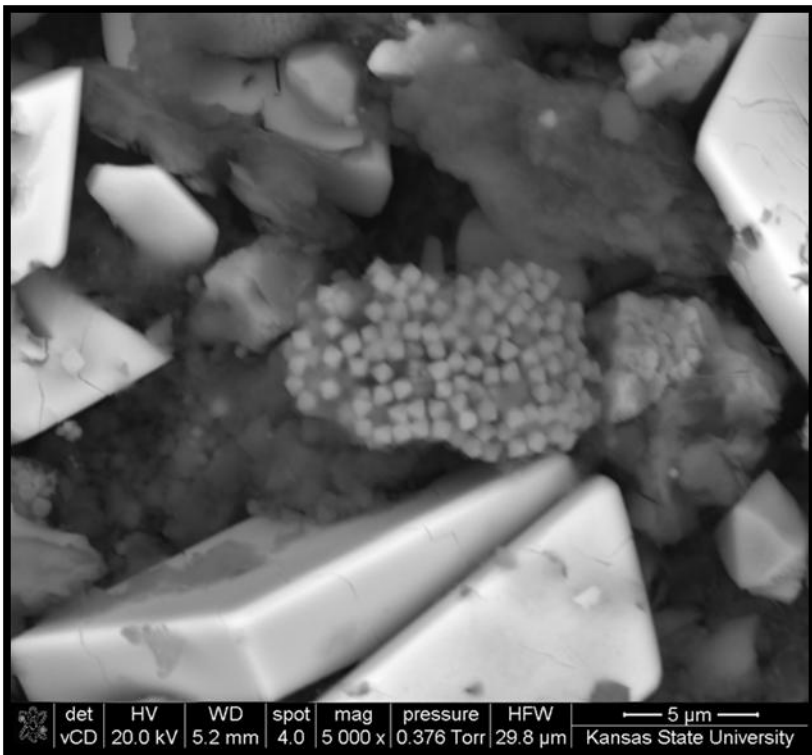


Figure A.17. Heavy minerals in sample WF#7 Chenoweth.

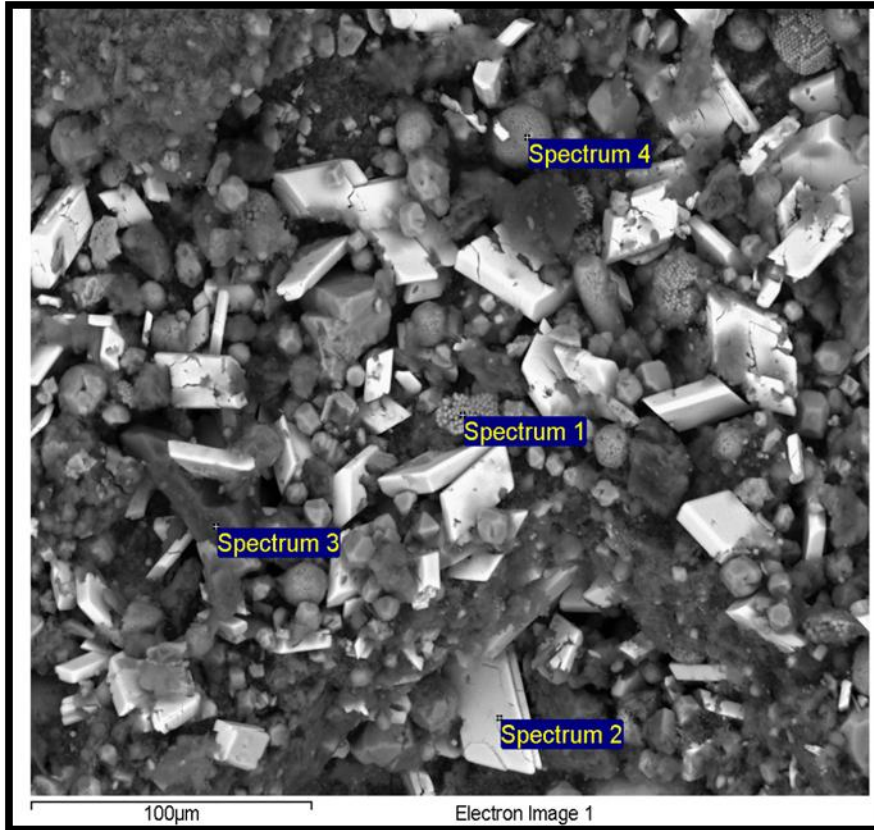


Figure A.18. Locations for the EDS spectra shown in Figure A.19.

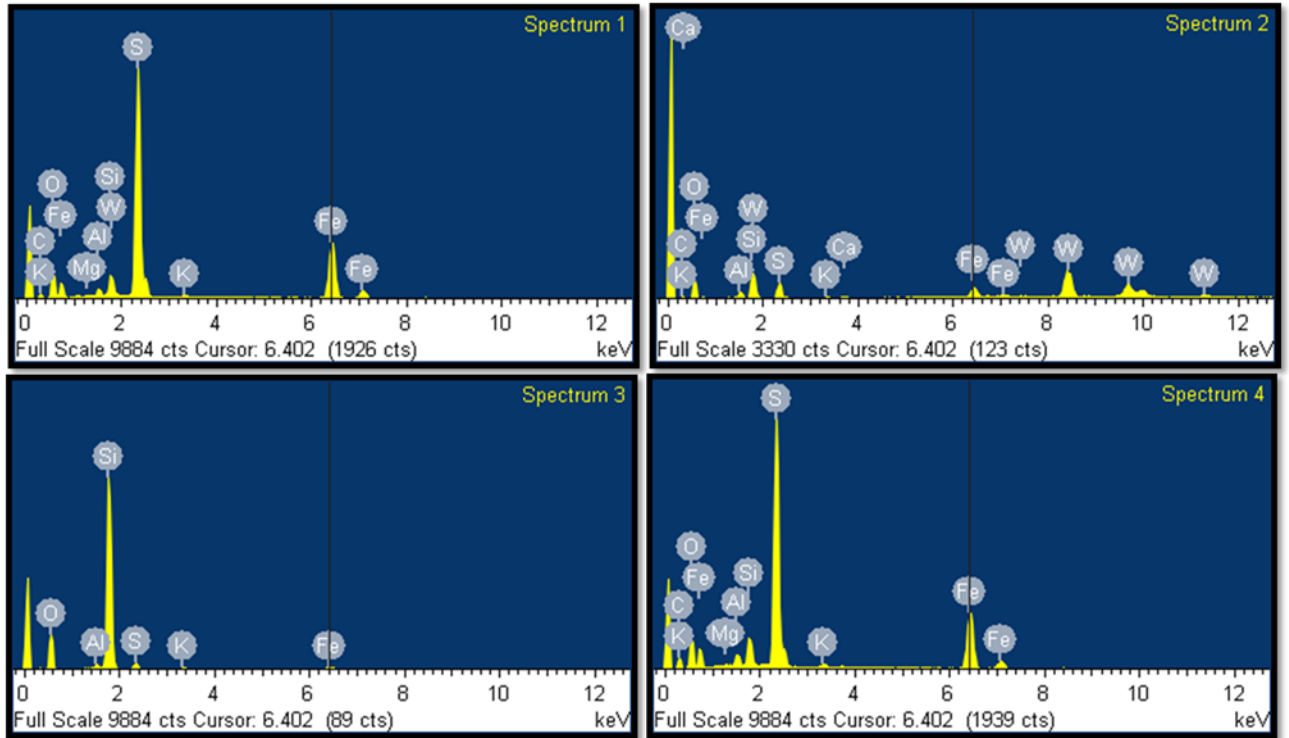


Figure A.19. EDS spectra for WF#7 Chenoweth sample locations.

Spectrum 1			Spectrum 2		
Element	Weight%	Atomic%	Element	Weight%	Atomic%
C K	14.56	30.33	C K	15.7	28.38
O K	17.29	27.05	O K	35.06	47.58
Mg K	0.27	0.27	Al K	2.53	2.03
Al K	0.95	0.88	Si K	8.59	6.64
Si K	2.18	1.95	S K	9.13	6.18
S K	32.92	25.69	K K	1.67	0.93
K K	0.38	0.24	Ca K	1.09	0.59
Fe K	29.83	13.37	Fe K	16.84	6.55
W M	1.63	0.22	W M	9.39	1.11
Total	100	100	Total	100	100

Spectrum 3			Spectrum 4		
Element	Weight%	Atomic%	Element	Weight%	Atomic%
C K	7.97	13.31	C K	25.42	45.21
O K	41.04	51.44	O K	17.35	23.16
Al K	0.75	0.56	Mg K	0.29	0.26
Si K	44.88	32.04	Al K	1.07	0.85
S K	2.52	1.57	Si K	2.66	2.03
K K	0.31	0.16	S K	28.43	18.94
Fe K	2.53	0.91	K K	0.52	0.28
Total	100	99.99	Fe K	24.25	9.28
			Total	99.99	100.01

Figure A.20. Elemental, weight percent and atomic percent data for WF#7 Chenoweth.

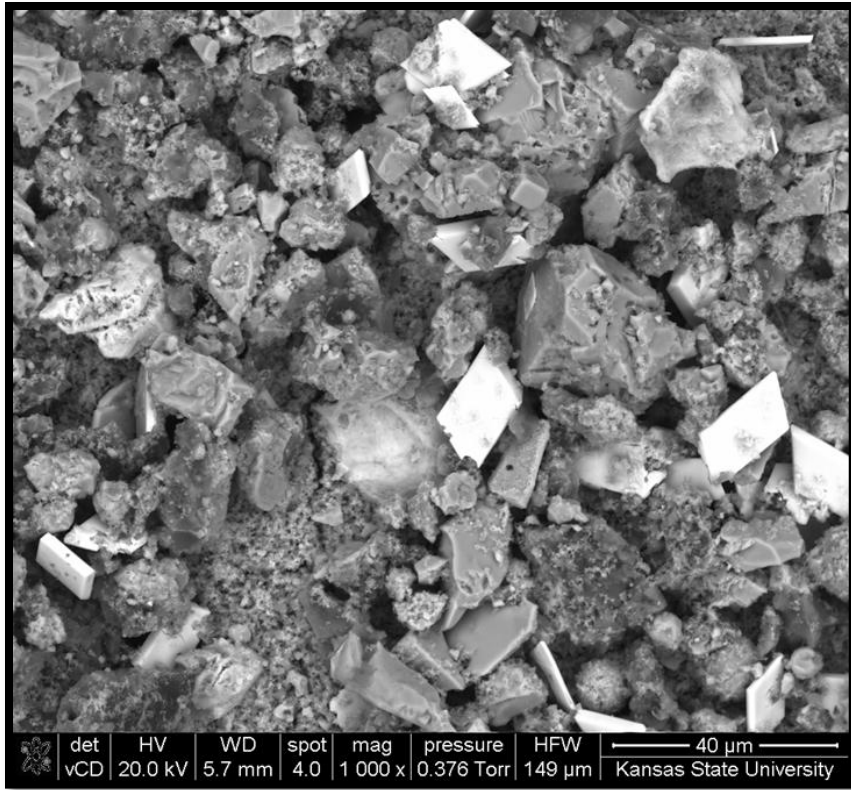


Figure A.21. Heavy minerals in sample WF#9 Jones and Pellow.

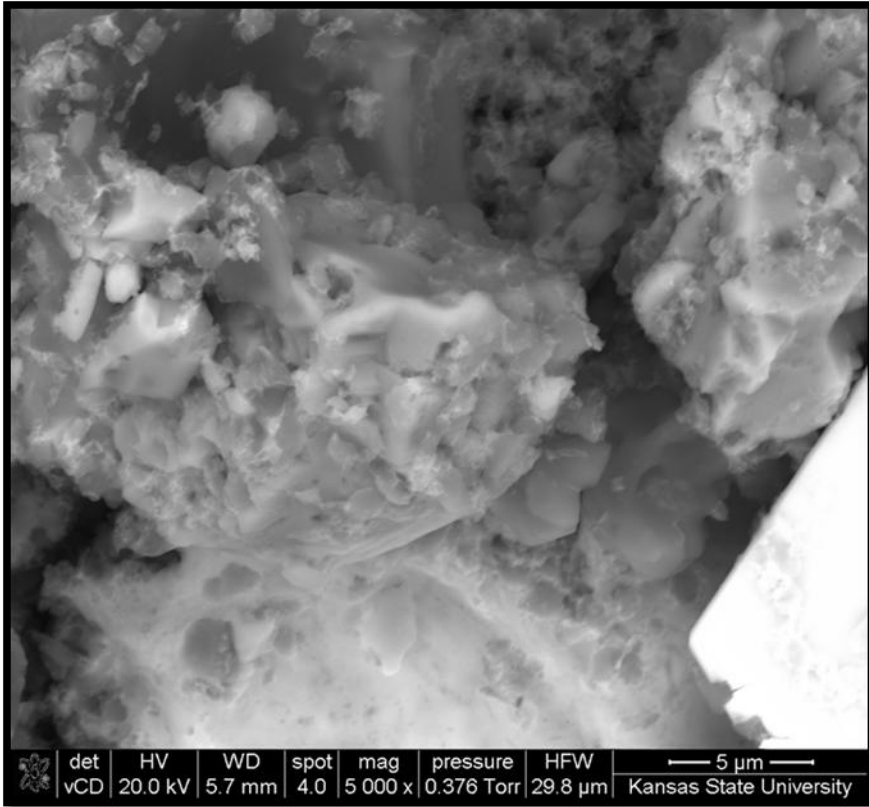


Figure A.22. Heavy minerals in sample WF#9 Jones and Pellow.

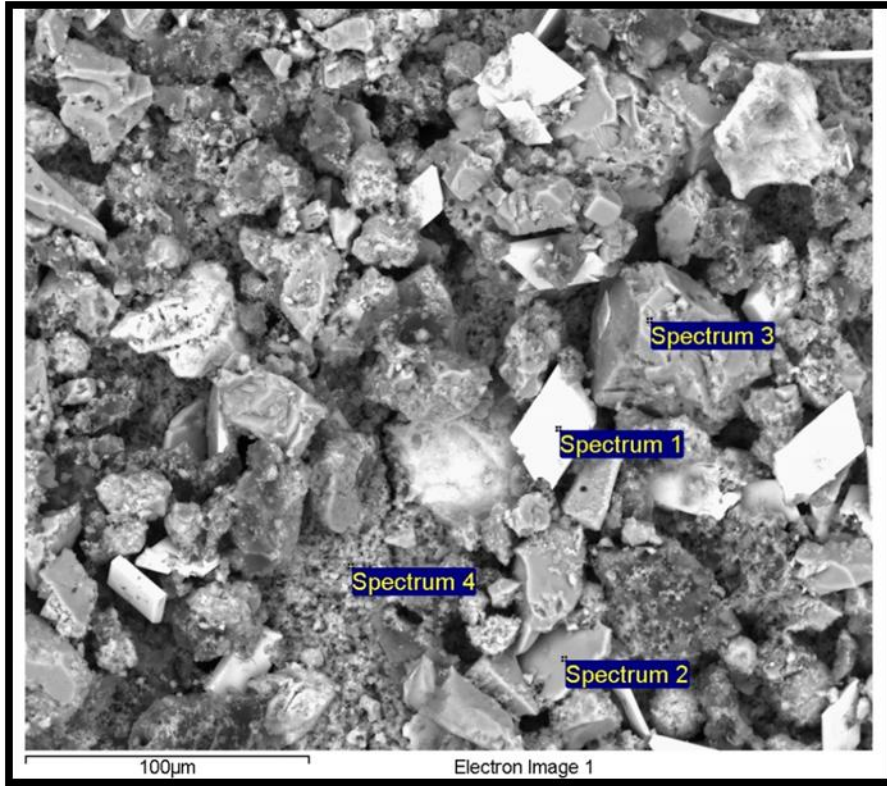


Figure A.23. Locations for the EDS spectra shown in Figure A.24.

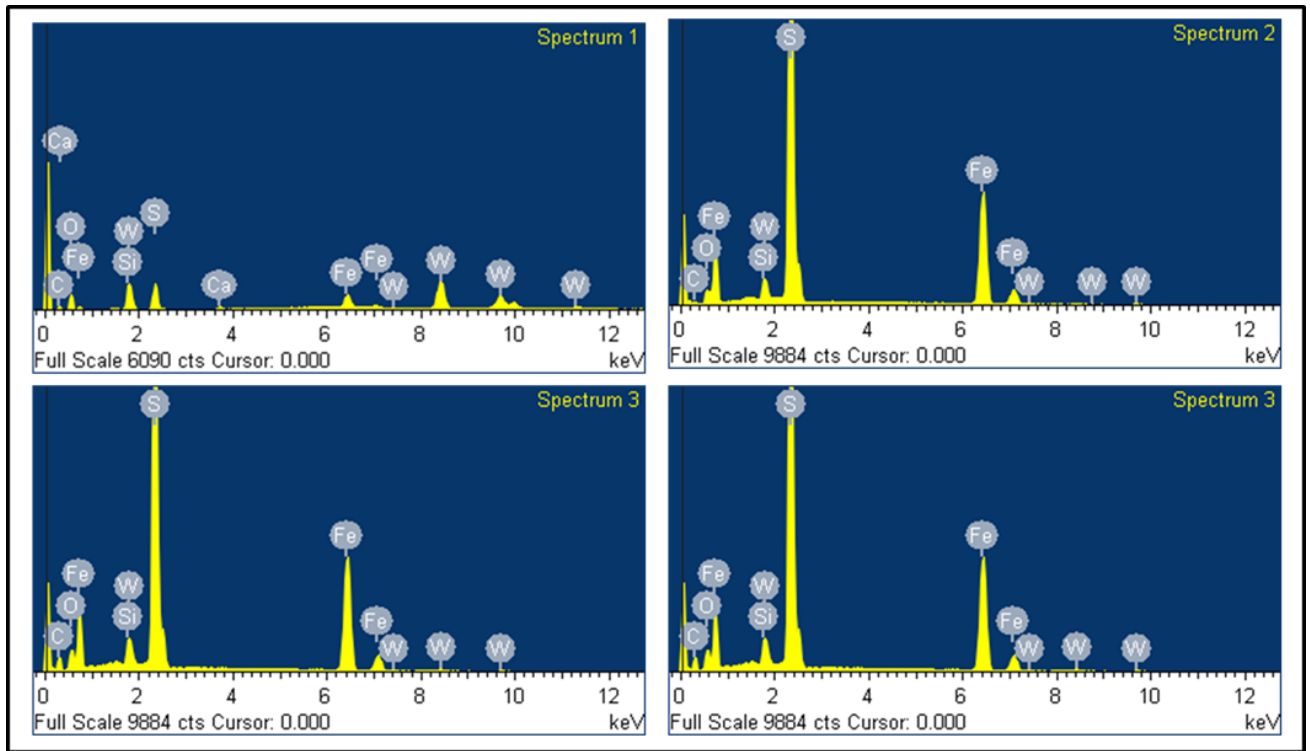


Figure A.24. EDS spectra for WF#9 Jones and Pellow sample locations.

Spectrum 1			Spectrum 2			Spectrum 3			Spectrum 4		
Element	Weight%	Atomic%									
C K	15.04	30.07	C K	6.59	17.6	C K	20	42.25	C K	20	42.25
O K	28.07	42.12	O K	6.32	12.66	O K	8.01	12.71	O K	8.01	12.71
Si K	6.79	5.8	Si K	1.3	1.48	Si K	0.99	0.9	Si K	0.99	0.9
S K	13.36	10	S K	45.95	45.94	S K	37.5	29.67	S K	37.5	29.67
Ca K	1.91	1.14	Fe K	38.47	22.08	Fe K	31.18	14.16	Fe K	31.18	14.16
Fe K	21.12	9.08	W M	1.36	0.24	W M	2.32	0.32	W M	2.32	0.32
W M	13.72	1.79		99.99	100		100	100.01		100	100.01
	100.01	100									

Figure A.25. Elemental, weight percent and atomic percent data for WF#9 Jones and Pellow.

Appendix B - Heavy Mineral Distribution

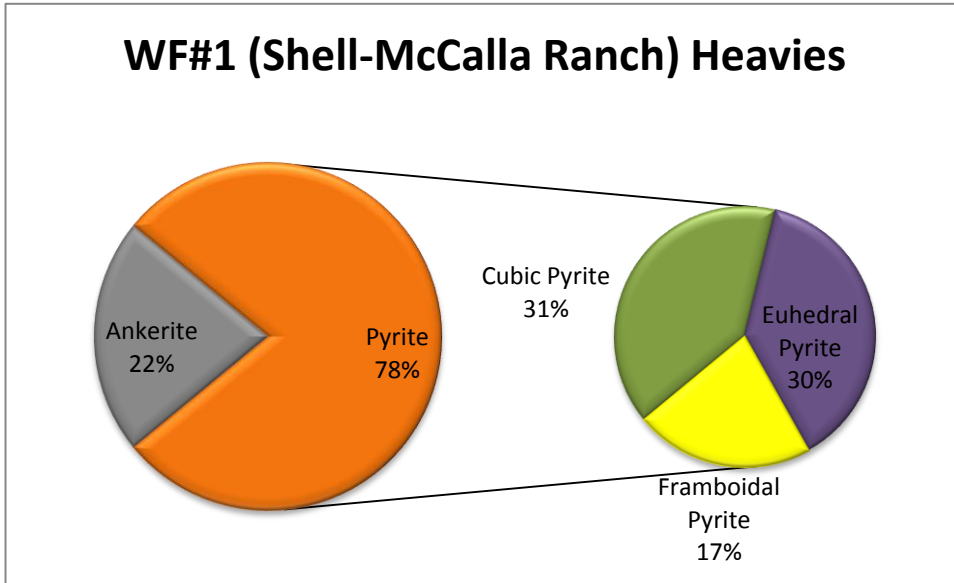


Figure B.1. Heavy mineral distribution for WF#1 McCalla Ranch.

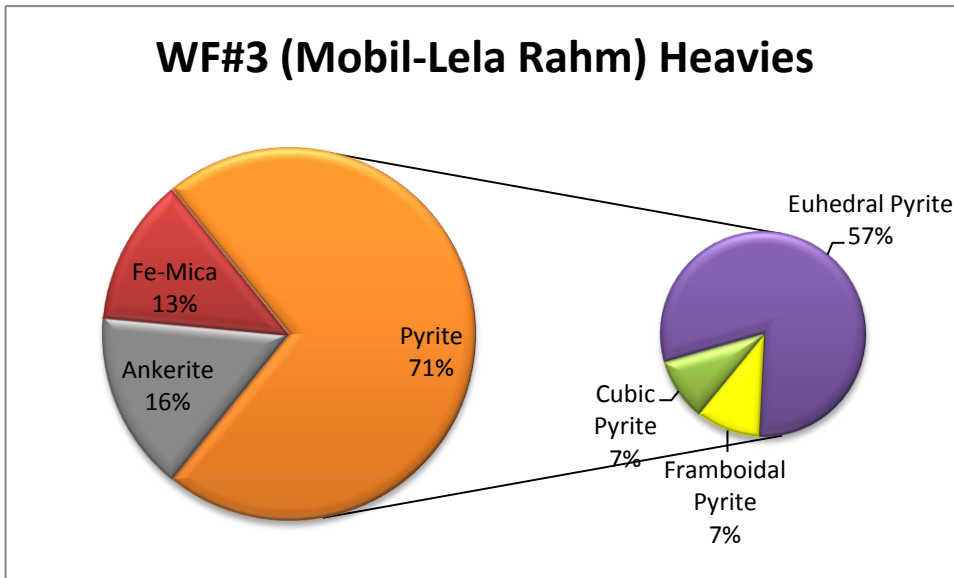


Figure B.2. Heavy mineral distribution for WF#3 Lela Rahm.

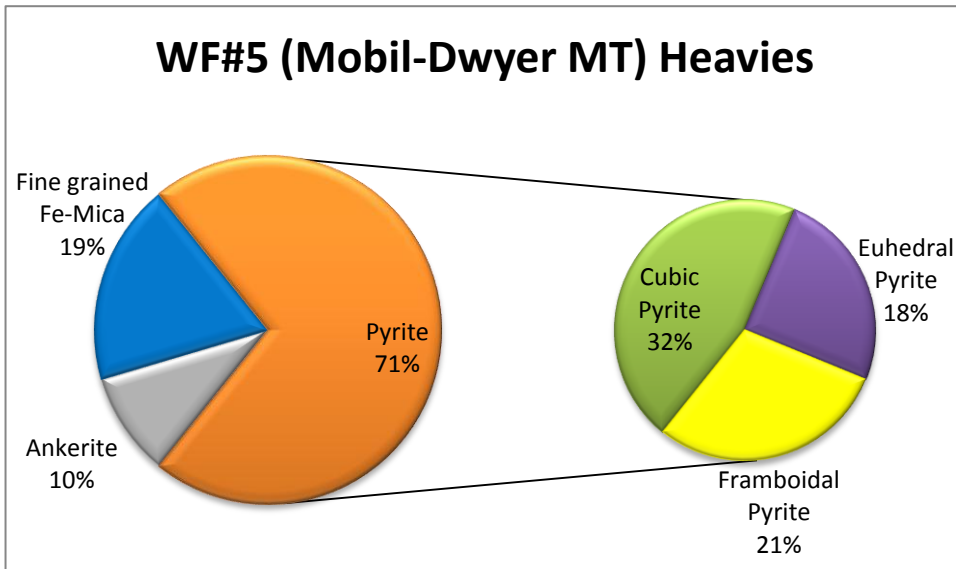


Figure B.3. Heavy mineral distribution for WF#5 Dwyer.

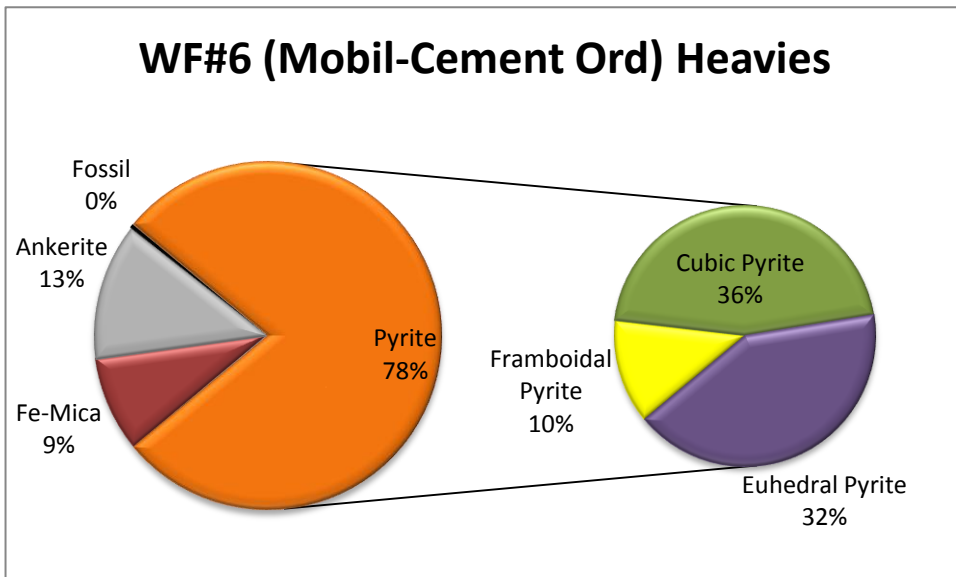


Figure B.4. Heavy mineral distribution for WF#6 Cement Ord.

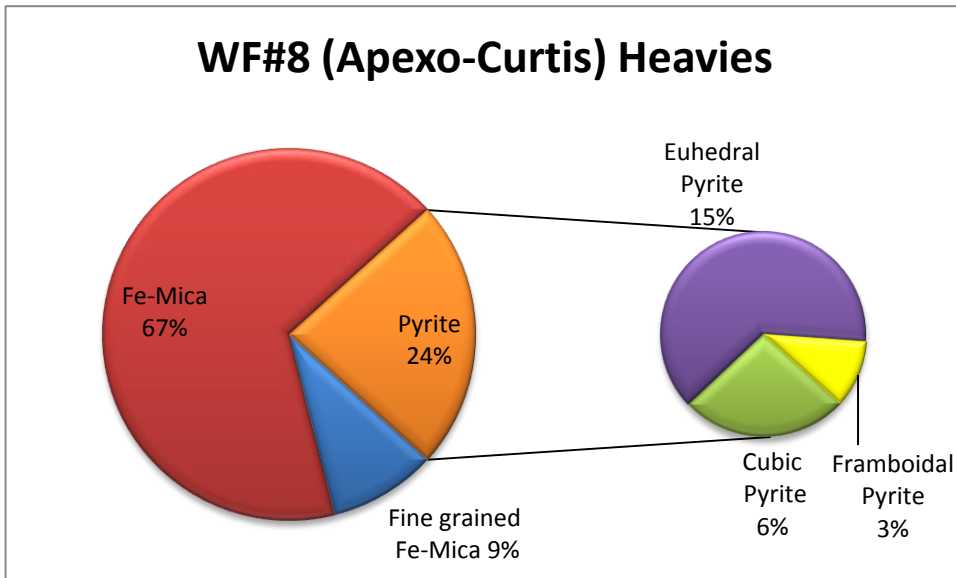


Figure B.5. Heavy mineral distribution for WF#8 Curtis.

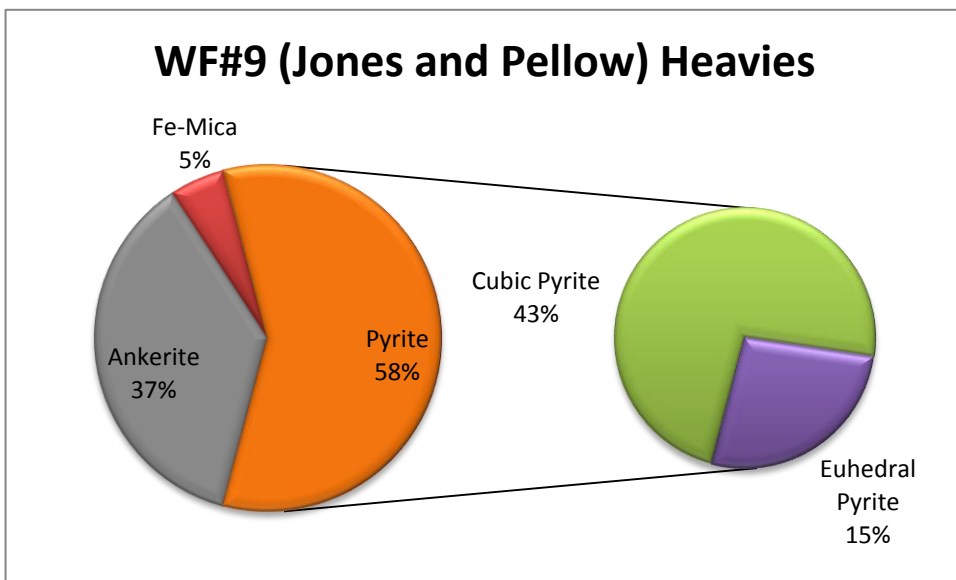


Figure B.6. Heavy mineral distribution for WF#9 Jones and Pellow.

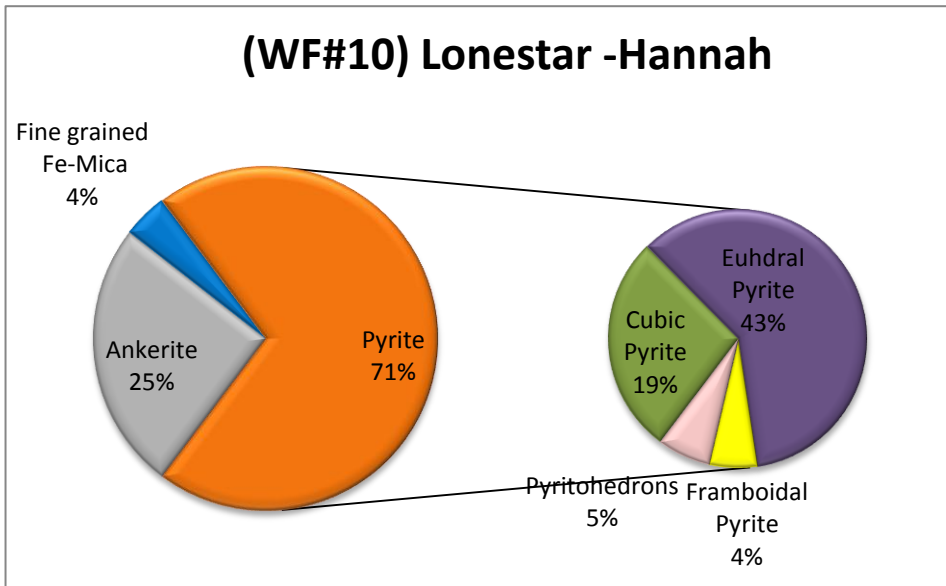


Figure B.7. Heavy mineral distribution for WF#10 Hannah.